

THEORETICAL INTERPRETATION
OF PROTON-PROTON SCATTERING

by

JOHN DAVID JACKSON
B.Sc., University of Western Ontario
(1946)

SUBMITTED IN PARTIAL FULFILLMENT OF THE
REQUIREMENTS FOR THE DEGREE OF
DOCTOR OF PHILOSOPHY
at the
MASSACHUSETTS INSTITUTE OF TECHNOLOGY
(1949)

Signature of Author .
Department of Physics, May 13, 1949

Certified by Thesis Supervisor

Chairman, Department Committee on Graduate Students





Room 14-0551
77 Massachusetts Avenue
Cambridge, MA 02139
Ph: 617.253.5668 Fax: 617.253.1690
Email: docs@mit.edu
<http://libraries.mit.edu/docs>

DISCLAIMER OF QUALITY

Due to the condition of the original material, there are unavoidable flaws in this reproduction. We have made every effort possible to provide you with the best copy available. If you are dissatisfied with this product and find it unusable, please contact Document Services as soon as possible.

Thank you.

Due to the poor quality of the original document, there is some spotting or background shading in this document.

Phys -
Thesis
1949

CONTENTS

Acknowledgements	-----	i
Abstract	-----	ii
(1) Introduction	-----	1
(2) Essentials of the phase shift analysis of scattering	-----	10
(3) Qualitative considerations of proton- proton scattering	-----	20
(4) Determination of the phase shifts from the experimental cross sections	-----	32
(5) Determination of the variational parameters from the experimental data	-----	56
(6) Landau-Smorodinsky result and an approximate relation between the neutron-proton and proton-proton scattering lengths	-----	68
(7) Variational principle for scattering and the expansion (1.3)	-----	76
(8) Effects of small changes in the potentials on the variational parameters	-----	89
(9) Numerical results for various potential shapes and comparison with experiment	-----	95
(10) Rough estimates of the phase shifts for higher angular momenta	-----	110

APPENDICES

(1) Formulae relating phase shifts to experimental cross sections	-----	A1.1
--	-------	------

(2) Formulae and tables for the determination of higher phase shifts -----	A2.1
(3) Apparent S-wave phase shifts from experiment -	A3.1
(4) S-state Coulomb wave functions in the continuum -----	A4.1
References -----	R.1
Biography -----	

ACKNOWLEDGEMENTS

The author is pleased to express his gratitude for being allowed to work under the stimulating guidance of Professor V. F. Weisskopf who, as thesis supervisor, displayed a continued interest in the progress of this research. He is especially indebted to Dr. J. M. Blatt who originally suggested the problem, and aided considerably in its completion through his constant help and guidance. He wishes to thank Mrs. Barbara (Siegle) Levine and Miss Hannah Paul for their excellent computing work. Finally, he is glad to acknowledge his debt to Miss M. Barbara Cook for her important contribution in typing and preparing the final manuscript.

ABSTRACT

The problem of the theoretical interpretation of proton-proton scattering data is considered. Simplified formulae for the determination of the phase shifts from the experimental cross sections are given, along with the numerical expansions and tables necessary for their use. The concept of an "apparent S-wave phase shift" δ_a is introduced to facilitate the analysis of the experimental data for P-wave and D-wave anomalies in addition to the S-wave scattering. The auxiliary functions needed in conjunction with the apparent S-wave phase shift are presented in tabular and graphical form.

The phase shifts are determined from the experimental data, and are analyzed in terms of the apparent S-wave phase shift for P-wave (and/or D-wave) effects wherever the accuracy warrants it. It is not unreasonable to expect a detectable P-wave anomaly in the scattering for energies above 2 or 3 Mev. However, the Van de Graaff data available at present in the energy range 2.5 to 3.5 Mev give only a uncertain indication of a repulsive interaction in the 3P state, and are not inconsistent with no interaction, or a small attraction in the 3P state. The data above 4 Mev (up to 14.5 Mev), taken with cyclotrons as sources of high energy protons, are relatively inaccurate. They point to a slightly repulsive 3P interaction (or an attractive 1D interaction), but again are not inconsistent with purely S-wave

scattering.

The S-wave nuclear scattering is analyzed by means of the expression:

$$K \equiv \frac{\pi \cot \delta_0}{2\pi\eta - 1} + k(\eta) = R \left[-a^{-1} + \frac{1}{2} r_0 k^2 - P r_0^3 k^4 + \dots \right]$$

which is a function of the nuclear phase shift δ_0 and the energy (through η), and allows a representation as a power series in the energy (k^2). The coefficients in the expansion have a simple physical meaning: a is the proton-proton Fermi scattering length; r_0 is the effective range of the nuclear force; P measures the compactness of the nuclear potential (it is negative for a square well, positive for a Yukawa well). The form of K predicts that the experimental data when plotted against k^2 should lie approximately on a straight line, the intercept of which determines the scattering length a and the slope of which determines the effective range of the interaction. The data below 4 Mev do fall very closely along a straight line on such a plot, and determine the values $a \approx -7.67 \times 10^{-13}$ cm., $r_0 \approx 2.65 \times 10^{-13}$ cm., assuming P and higher coefficients are zero.

The quantities $\sigma \left(\frac{\partial K}{\partial \sigma} \right)_E$ and $E \left(\frac{\partial K}{\partial E} \right)_\sigma$ are evaluated for the energy range zero to 10 Mev., and are used to discuss the feasibility and usefulness of measurements near

the interference minimum in the 90 degree scattering at 400 Kev. It is recommended that careful measurements be made on the scattering at $\theta = 90$ degrees in the energy range 420 - 450 Kev.

An approximate relation between the proton-proton scattering length and the corresponding neutron-proton quantity is obtained, and used to examine the hypothesis of the charge-independence of nuclear forces, as determined from proton-proton scattering and singlet neutron-proton scattering.

The derivation of the expansion of K by variational methods, first done by Schwinger⁽⁴⁾, is extended to obtain expressions for the coefficients of the k^4 and k^6 terms in the expansion. The effects of small changes in the potential on the variational parameters is considered, in particular the effects of changes in range and strength of the interaction.

Numerical results of calculations carried out for the four usually assumed potentials are presented, along with formulae allowing one to determine the well parameters which will give closest agreement with the experimental scattering, or, alternatively, the variational parameters implied by a particular choice of well parameters. It is found that all four potential shapes give equally good fits to the experimental data, provided the proper range and strength of interaction are chosen. The well parameters

and variational parameters giving the best least squares fit to the data for a given potential shape are tabulated. The earlier results of Breit et al. ^(1,38) are, in general, confirmed, although more recent experimental data have modified (and narrowed down) the numerical values somewhat.

The experimental accuracy necessary to distinguish between the extremes in well shapes (the square and Yukawa wells) at 10 Mev is examined. It is found that by careful use of existing equipment measurements with the necessary accuracy could be made; such measurements are recommended.

Estimates are given for the phase shifts of higher angular momenta for the four usual well shapes. The S-state Coulomb wave functions are discussed in some detail in an appendix, particular emphasis being placed on the irregular solution $G(r)$. An expansion for $G(r)$ in powers of the energy (k^2) in terms of modified Bessel functions of argument $2(r/R)^{\frac{1}{2}}$ is obtained, to terms in k^4 inclusive.

(1) Introduction

The scattering of protons by protons is, at present, one of the important sources of quantitative information about nuclear forces. The accuracy of proton - proton scattering experiments is comparatively high, due to the fact that the energy control and detection of charged particles is more precise than for neutral particles (for example, the neutrons in neutron - proton scattering). The theoretical interpretation of such scattering experiments is at once easier and more difficult than the corresponding analysis of neutron - proton scattering experiments. For both neutron - proton and proton - proton scattering at low energies (below 10 Mev) the deBroglie wavelength of the nucleons is large compared to the range of nuclear forces, and the nuclear interaction can be assumed, to a very good approximation, to act only in the S ($l = 0$) state of the system of two protons. However proton - proton scattering is easier because the Pauli exclusion principle allows the protons to be only in the 1S state because they are identical particles (the $l = 0$ scattering of neutrons and protons has contributions from both singlet and triplet states because of the non-identity of the particles). The interpretation is more difficult because of the Coulomb scattering which is present in addition to the nuclear effects. However, the fact that the Coulomb field complicates the analysis of the experiments is counterbalanced to some extent by the fact that its presence allows the

J. D. Jackson, Thesis Report

Insert on page 2; ~~at the~~ ^{in place of lines 12, 13, 14:}

The first detailed theoretical ~~analysis~~ ^{treatment} of the scattering of protons by protons was given by Breit, Cordon, and Present ⁽¹⁾ in 1936.

The first quantitative experiments were done in 1936-39 by Heydenburg, ~~the~~ Hofstad, and Tuve ⁽¹⁹⁾ over an energy range ~~of~~ from 200 Kev to 400. Kev. Since that

comparison of the unknown nuclear scattering with the known Coulomb scattering.

It might be pointed out that while the analysis of the low energy scattering experiments is simplified because the nuclear interaction is only in the 1S state, the amount of information about nuclear forces is correspondingly reduced. No information on the effective triplet interaction is obtained until the energy is such that higher angular momenta contribute appreciably to the scattering. The 1S interaction between two protons is purely central in nature (the tensor force does not act in singlet states).

The first quantitative experiments on proton-proton scattering were done in 1936-39 by Heydenburg, Hafstad, and Tuve over an energy range from 200 Kev to 900 Kev. Since that time experiments using Van de Graaff generators as the source of fast protons have been made over the energy range from 200 Kev to 3.5 Mev. Protons from cyclotrons have been used in the energy range from 4 Mev to 14.5 Mev. These experimental data will be discussed in detail in Section 4. No experimental results are available for energies in excess of 14.5 Mev at present. Indeed, it will be seen (see Sections 4 and 5) that the cyclotron data are very inaccurate for the most part, and that present information on the 1S interaction is based predominantly on the data below 4 Mev.

The methods of analyzing the experimental data in terms of phase shifts have been described, and applied to the data, by Breit and his collaborators.⁽¹⁾ For reference purposes a brief discussion of the phase shift method of

analysis, together with some elementary considerations of the qualitative aspects of proton-proton scattering will be given in Sections 2 and 3.

It has been shown ⁽²⁾ that the low energy data on the neutron-proton interaction can be analyzed profitably by means of an expansion for the phase shift δ in powers of the energy $E = \frac{1}{2} \hbar^2 k^2 / m$ (E is the energy in the centre of mass system, k is the relative wavenumber, $m = M/2$ is the reduced mass):

$$k \cot \delta = -a^{-1} + \frac{1}{2} r k^2 - P r^3 k^4 + \dots \quad (1.1)$$

The parameters a , r , P describe the effect of the nuclear interaction on the scattering. The physical meaning of the parameter a is apparent when one examines the scattering cross section at zero energy. In general the cross section for S scattering is:

$$\sigma = \frac{4\pi}{k^2} \sin^2 \delta = \frac{4\pi}{k^2 + k^2 \cot^2 \delta}$$

In the limit of very small k , σ is seen to approach (using (1.1)):

$$\sigma = 4\pi a^2$$

so that the coefficient a is just the Fermi scattering length ⁽³⁾ evaluated at zero energy. The parameter r is a measure of the range of the nuclear interaction, while the coefficient P is the first shape-dependent parameter in the expansion (1.1). P is a measure of the "tail" of the nuclear potential: P is negative for a square well potential,

positive for a Yukawa potential.

Every assumed type of interaction determines a set of coefficients a , r , F , --- . In principle, the experimental data can be analyzed to find the dependence of the phase shift δ on energy, the coefficients of the power series (1.1) thus being determined. In practice, the uncertainties of experiment allow the determination of only a few of the parameters. If the first two terms of (1.1) give an adequate fit to the experimental data, no information can be obtained about the detailed shape of the potential responsible for the scattering; only the strength and the range of the interaction can be determined. The approximation to $k \cot \delta$ afforded by the first two terms of (1.1) is therefore called the "shape-independent" approximation.

The series (1.1) was first derived by Schwinger ⁽⁴⁾ using variational methods. The same approach can be applied to proton-proton scattering. The result, derived by Schwinger in this way, involves the expression:

$$K = \frac{\pi \cot \delta}{e^{2\pi\eta} - 1} + h(\eta) \quad (1.2)$$

Here δ is the phase shift for the S-wave nuclear scattering (this quantity is denoted by K_0 by Breit ⁽¹⁾ ; a subscript 0 will be attached to δ wherever there is possibility of confusion with phase shifts for the waves of higher angular momentum); $\eta = e^2/hv$, where v is the relative velocity of the two protons; the slowly varying function $h(\eta)$ will be defined in Section 5 (formula (5.1)). It is found that K allows a power series expansion similar to (1.1):

Insert on page 5, after line 20 :

$$(f = 2K + 4\gamma - 2 = 2K + 0.30886...)$$

ie it should read like this :

----- quantity f introduced by Breit, Condon,
and Present ⁽¹⁾ $(f = 2K + 4\gamma - 2 = 2K + 0.30886...)$

Breit, Condon, and Present have shown -----

$$K = R(-a^{-1} + \frac{1}{2}r_0k^2 - Pr_0^3k^4 + Qr_0^5k^6 \dots) \quad (1.3)$$

$R = \hbar^2/Me^2 = 2.88(15) \times 10^{-12}$ cm. is a characteristic length for proton-proton scattering; it is the Bohr radius of a proton bound to a fixed centre of electrostatic attraction. The parameters a , r_0 , P , Q are quantities related to the range, depth and detailed shape of the nuclear potential responsible for the deviations from purely Coulombian scattering, in complete analogy to the coefficients of (1.1).

For large energies the first term in the definition of K approaches $Rk \cot \delta$. However, the second term, $h(\eta)$, does not vanish at high energies; rather it increases logarithmically with energy. The fact that (1.3) does not quite reduce to (1.1) even at high energies where the protons can be considered as essentially "free" except for the nuclear interaction is related to the fact that the Coulomb field has an "infinite range" i.e. the wave function of the system does not approach a plane wave plus a spherical scattered wave even at very large distances from the scattering centre.

The quantity K defined by (1.2) is closely related to the quantity f introduced by Breit, Condon, and Present.⁽¹⁾ Breit, Condon, and Present have shown that retaining only the leading term in the series (1.3) does not give an adequate fit to the data. This shows that the force between two protons has a non-vanishing range, since keeping only the first term of (1.3) is equivalent to assuming zero range for the proton-proton interaction.

Landau and Smorodinsky⁽⁵⁾ have given a semi-quantitative

derivation for the leading term of (1.3). They made a plot of K vs. k^2 and found that it led to a straight line, but not of zero slope. They interpreted this correctly to mean that a range correction has to be included. However, their method of derivation did not enable them to relate the coefficient a precisely to the quantum-mechanical properties of the system, nor determine the precise form of the range correction necessary. The advantage of the Landau-Smorodinsky approach is that a qualitative understanding of the problem is readily obtained. An extension of their method to determine an approximate relation between the proton-proton singlet scattering length a and the corresponding neutron-proton quantity is given in Section 6.

Breit and Bouricius⁽⁶⁾ have shown that the experimental data can also be fitted quite well by a "boundary condition" on the logarithmic derivative of the wavefunction at a definite (small) distance. They point out that this is closely related to the possibility of obtaining an adequate fit to the data in terms of the "shape-independent" approximation to the series (1.3).

Lately, several investigators have succeeded in deriving the expansion (1.3) without the use of the variational method. Bethe⁽⁷⁾ has given a discussion of the third parameter P , showing why it is expected to be small compared to unity for most reasonable well shapes. Chew and Goldberger⁽⁸⁾ have used the fact that the Coulomb field can be treated as a small perturbation within the nuclear range to show that the

effective range r_0 , the well shape parameter P , and higher coefficients in (1.3) will not differ very much from the corresponding parameters in the neutron-proton series (1.1). A preliminary discussion of some of the results of this thesis has already been given⁽⁹⁾.

The analysis of proton-proton scattering data by the variational method proceeds in three distinct steps:

- (1) The experimental cross sections are analyzed to find the nuclear phase shifts for the various angular momenta involved in the nuclear scattering. This step is common to all methods of analyzing the data.
- (2) The S-wave phase shift is used to compute the quantity K defined in (1.2). Then K is plotted vs. k^2 (i.e. vs. energy). The expansion (1.3) shows that such a plot should be a straight line at low energies. At higher energies the term quadratic in the energy (the term in k^4) will start to contribute; the plot will become curved, and so on. It should be emphasized that the plot of K vs. k^2 involves the S-wave anomaly only. At higher energies, waves of higher angular momentum will in general contribute to the observed scattering. The phase shifts for those waves must be evaluated separately and put on a different plot; the presence of these higher phase shifts has nothing to do with the curvature of the K vs. k^2 diagram. From this latter plot the "experimental" values of the coefficients in the power series (1.3) are found, that is, as many of them as the accuracy of the data allows.
- (3) The final step of the analysis is the fitting of theoretical potential wells to the observed values of the variational

parameters. If only the first two parameters, a and r_0 , are known (the "shape-independent" approximation), a well of any shape can be made to fit the data, just by choosing the proper depth and range. If the coefficient Pr_0^3 of the k^4 term is also known, some well shapes will be excluded, but there still will be a large number of wells which can be made to fit the data. In general, the more coefficients that are known, the more the shape of the nuclear potential is delimited.

Sections 2 and 3 deal with the general aspects of the usual scattering theory and the peculiarities of proton-proton scattering. In Section 4 the techniques of determining phase shifts from the experimental data are discussed. Convenient formulae are developed for such work and applied to the analysis of existing experimental data. The concept of an "apparent S-wave phase shift" is introduced, and applied to the problem of analyzing the experimental data for possible P-wave and D-wave scattering in addition to the usual S-scattering. Section 5 considers the determination of the parameters in the expansion (1.3) from the experimental data, and examines the sensitivity of K (1.2) to errors in cross section and energy measurements as a function of energy and scattering angle with a view to planning future experiments. It is found that careful measurements near the interference minimum in the scattering at 400 Kev (see Figure (3.3)) would be extremely valuable. The Landau-Smorodinsky result is presented in Section 6, as well as an extension of it giving a relation between the neutron-proton singlet scattering length and the

corresponding proton-proton quantity. The derivation of the expansion (1.3) by variational methods is given in Section 7. Section 8 outlines the effect of small changes in the potential on the variational parameters, while Section 9 deals with the numerical results for the variational parameters for the four usual choices of potential shape, and the comparison with experiment. The experimental accuracy necessary at 10 Mev to distinguish between extremes in well-shapes is also discussed in Section 9. Section 10 gives rough estimates of the phase shifts for higher angular momenta to be expected for the four potential shapes considered. The various appendices discuss in more detail certain formulae and numerical results obtained. In particular, Appendix 4 presents the expansion of the irregular Coulomb wave function $G(r)$ in powers of the energy.

(2) Essentials of the phase shift analysis of scattering

For reference purposes it is worthwhile to outline briefly the usual treatment of scattering problems as given in Mott and Massey⁽¹⁰⁾, and to discuss in a general way the peculiarities of proton-proton scattering. The physical problem of the scattering of a beam of particles incident upon a central field of force is represented quantum-mechanically by an incident plane wave plus a scattered wave diverging from the scattering center. Asymptotically the wave function has the form:

$$\psi \sim e^{ikz} + f(\theta) \frac{e^{ikr}}{r} \quad (2.1)$$

where the plane wave is incident along the z-axis (and normalized to one particle per unit volume); $f(\theta)$ is the scattering amplitude which describes the angular distribution of the scattering. The differential cross section (the ratio of the number of particles scattered into the solid angle element $d\Omega$ per second to the number of particles incident on the scattering center per second) is given by:

$$\sigma(\theta) d\Omega = |f(\theta)|^2 d\Omega \quad (2.2)$$

If the deBroglie wavelength of the incident particles is large compared to the range of the scattering field of force, it is advantageous to decompose the scattering process into component processes, each with relative angular momentum $l\hbar$. Then the main contribution to the scattering will come from those collisions which classically are described as head-on (i.e. zero impact parameter), that is, the $l=0$ or S-wave

collisions. Waves of higher angular momenta (particles with larger impact parameters) will make little or no contribution to the scattering except at higher energies where the deBroglie wavelength of the particles becomes of the same order as, or smaller than, the range of the field of force. In the usual way⁽¹¹⁾ the plane wave e^{ikz} is expanded in terms of the angular momentum eigenfunctions i.e.

$$e^{ikz} = \sum_{l=0}^{\infty} i^l (2l+1) P_l(\cos\theta) \frac{f_l(r)}{kr} \quad (2.3)$$

where $f_l(r) = \sqrt{\frac{\pi}{2}} kr J_{l+\frac{1}{2}}(kr) \rightarrow \sin(kr - \frac{l\pi}{2})$

Similarly the complete wavefunction ψ is written as:

$$\psi = \sum_{l=0}^{\infty} A_l P_l(\cos\theta) \frac{\chi_l(r)}{kr} \quad (2.4)$$

where $\chi_l(r)/r$ must be square integrable at the origin.

Asymptotically, $\chi_l(r)$ is written in the form:

$$\chi_l(r) \rightarrow \sin(kr - l\frac{\pi}{2} + \delta_l)$$

This defines the phase shift δ_l which describes the effect of the scattering field on the component of the incident wave with angular momentum lk . From the above considerations it is expected that δ_0 will be appreciable even at low energies, while δ_l will become rapidly negligible as l increases, except at high energies.

From (2.1) it is seen that asymptotically the difference of (2.4) and (2.3) (i.e. $\psi - e^{ikz}$) must represent an out-

going wave only. This condition determines the constants A_l in (2.4); the scattering amplitude $f(\theta)$ is:

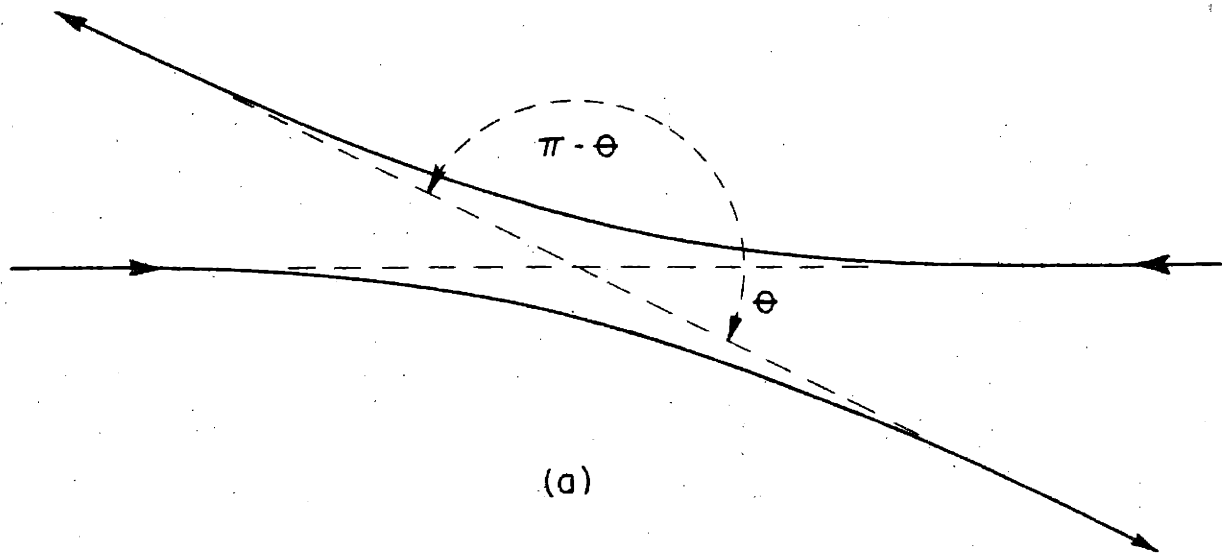
$$f(\theta) = \frac{1}{2ik} \sum_{l=0}^{\infty} (2l+1) \left[e^{2i\delta_l} - 1 \right] P_l(\cos\theta) \quad (2.5)$$

If all δ_l 's except δ_0 vanish, $f(\theta)$ is spherically symmetric in the center of mass system. Deviations from the spherical symmetry indicate the presence of scattering by waves of higher angular momenta.

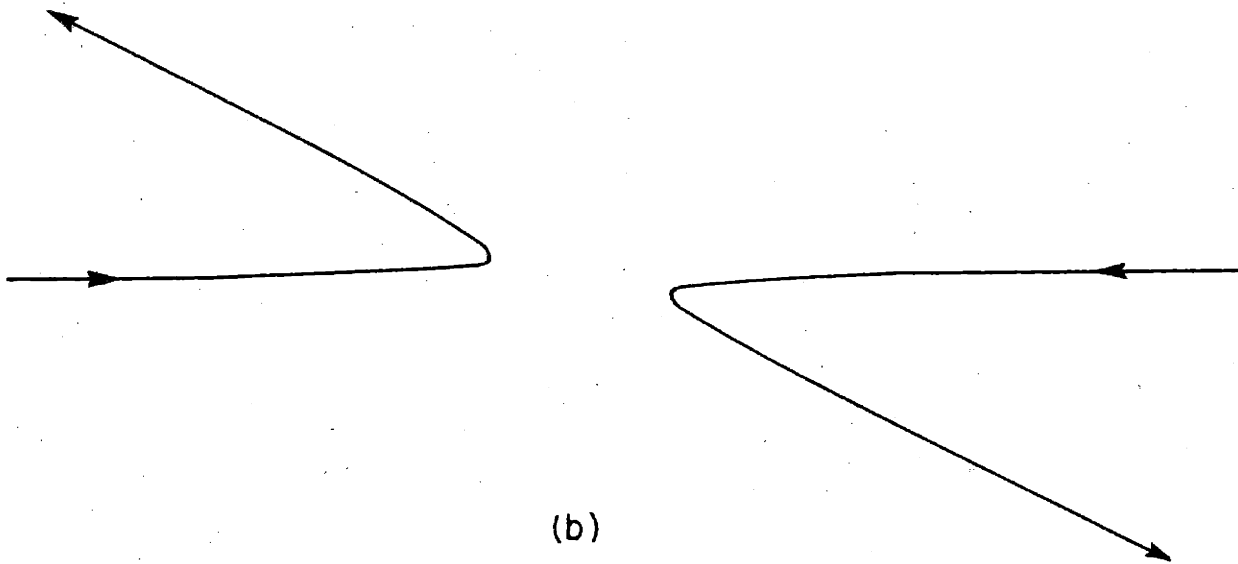
The problem of the scattering of protons by protons is somewhat more complicated than the simple picture outlined above. The first complication which arises is due to the identical nature of the particles. The obvious modification which this identity of particles makes on the scattering process can be seen in Figure (2.1). A typical collision between two protons is shown in the center of mass system, where the two particles move initially with equal and opposite velocities $v/2$. The two apparently different collisions shown in Figure (2.1a) and (2.1b) are experimentally indistinguishable because of the identity of the two particles. Thus one would expect that the effective cross section in which either particle is deflected into the solid angle $d\Omega$ to be:

$$\left\{ |f(\theta)|^2 + |f(\pi-\theta)|^2 \right\} d\Omega$$

This is the so-called "classical" result which consists of



(a)



(b)

Figure 2.1: Two seemingly different identical particle collisions that are experimentally indistinguishable.

an incoherent superposition of the two possible scattering processes. It will now be shown that an additional term involving quantum-mechanical interference effects must be added to the above result.

Protons are identical particles possessing spin 1/2, and obeying Fermi-Dirac statistics and Pauli exclusion principle. Therefore the wave function describing two protons must be anti-symmetric in the exchange of all their coordinates (both spin and space) i.e. $\Psi(q_1, q_2) = -\Psi(q_2, q_1)$, the q 's denoting all coordinates. Ψ can be written as a product of a space part $\psi(r_1, r_2)$ and a spin part $\chi(s_1, s_2)$ i.e. $\Psi = \psi(r_1, r_2) \chi(s_1, s_2)$. If $\chi(s_1, s_2)$ is symmetric under the exchange of the spin coordinates of the two protons, $\psi(r_1, r_2)$ must be anti-symmetric under the exchange of the space coordinates of the two protons, and vice versa.

Assuming for a moment that the protons shown in Figure (2.1) have their spins parallel (i.e. $\chi(s_1, s_2)$ is symmetric (the triplet state)), the space part of the wave function must be anti-symmetric. The appropriate wave function is:

$\psi(r_1, r_2) - \psi(r_2, r_1)$. The interchange of r_1 and r_2 changes \vec{r} into $-\vec{r}$ (\vec{r} being the relative coordinate in the center of mass system), and θ into $\pi - \theta$. Therefore the proper anti-symmetrical wave function corresponding to (2.1) is:

$$\psi = e^{ikz} - e^{-ikz} + \frac{e^{ikr}}{r} [f(\theta) - f(\pi - \theta)]$$

It should be noted that the incident wave may be written

as $2i \sin kz = 2i \sin k (z_1 - z_2)$, showing that the average value of $|\Psi|^2$ incident is 2, and that the wave represents one particle per unit volume in each beam. It follows that the effective cross section for a collision in which either particle is deflected into the solid angle $d\Omega$ is:

$$\sigma_x(\theta) d\Omega = |f(\theta) - f(\pi - \theta)|^2 d\Omega \quad (2.6)$$

provided the particles are in a triplet state (spins parallel).

Similar considerations for the case in which the protons are in the singlet state (spins opposed, space wave function symmetric) leads to the result for the singlet differential cross section:

$$\sigma_s(\theta) d\Omega = |f(\theta) + f(\pi - \theta)|^2 d\Omega \quad (2.7)$$

With unpolarized protons, on the average the probability of having spins parallel (triplet state) is three times as likely as having spins opposed (singlet state) so that the statistical spin weights are $3/4$ and $1/4$ respectively. Hence the observed cross section in which both incident and recoil protons are counted will be:

$$\begin{aligned} \sigma(\theta) d\Omega &= \left[\frac{3}{4} \sigma_x(\theta) + \frac{1}{4} \sigma_s(\theta) \right] d\Omega \\ &= \left\{ |f(\theta)|^2 + |f(\pi - \theta)|^2 \right. \\ &\quad \left. - \frac{1}{2} [f^*(\theta) f(\pi - \theta) + f(\theta) f^*(\pi - \theta)] \right\} d\Omega \quad (2.8) \end{aligned}$$

It is seen that this result which includes the effects of the Pauli principle differs from the "classical" result by the addition of interference terms arising from the coherent superposition of scattering amplitudes. One obvious conclusion of (2.8) which can also be seen from Figure (2.1) is that the scattering of protons by protons is symmetrical about $\theta = 90$ degrees in the center of mass system regardless of the details of the actual angular distribution.

The cross sections given by (2.6) - (2.8) are the differential cross sections in the center of mass coordinates in which the protons move towards each other with velocities $1/2 v$ each. To transform to the laboratory frame of reference in which one of the protons is at rest and the other is incident with the velocity v it is necessary to recall that the differential scattering cross sections are equal in the two systems (just because of conservation of particles).

$$\sigma(\theta) d\Omega = \sigma_{lab}(\Theta) d\Omega_{lab}$$

where θ is the scattering angle in the center of mass system, Θ is the scattering angle in the laboratory system, and $d\Omega = 2\pi \sin \theta d\theta$, $d\Omega_{lab} = 2\pi \sin \Theta d\Theta$

If the particles have equal masses, then $\Theta = \theta/2$, and it follows that:

$$\sigma_{lab}(\Theta) = 4 \cos \Theta \sigma(2\Theta) \quad (2.9)$$

Note that because of the recoil of the struck proton no scattering is observed for angles greater than $\Theta = 90$ degrees in the laboratory system of reference, and that, aside from the $\cos \Theta$ factor, the scattering is now symmetrical about $\Theta = 45$ degrees.

The treatment used to obtain the expression (2.5) for the scattering amplitude was based on the assumption that the form (2.1) for the incident plus scattered waves is valid asymptotically. That is, the field of force was assumed to fall off sufficiently rapidly with distance that at large separations the particles could be considered as free. In the case of collisions between neutrons and protons this assumption is valid because of the short-range character of nuclear forces. However, the collisions between protons are complicated by the Coulomb interaction as well as the specifically nuclear interaction. The Coulomb field is not a short range force; the asymptotic form (2.1) is not valid. Gordon⁽¹²⁾ has shown that (2.1) must be replaced by:

$$\psi \sim e^{i[kz + \eta \ln(kr - kz)]} + \frac{f(\theta)}{r} e^{i[kr - \eta \ln(2kr) + \pi + 2\sigma_0]} \quad (2.10)$$

where $\eta = \frac{e^2}{k\hbar v}$, $\sigma_0 = \arg \Gamma(1 + i\eta)$

(2.10) shows that the Coulomb field distorts the plane wave even at infinity. For purely Coulomb scattering the solution corresponding to (2.4) is:

$$\psi = \sum_{l=0}^{\infty} i^l (2l+1) e^{i\sigma_l} P_l(\cos \theta) \frac{F_l(r)}{kr} \quad (2.11)$$

where $\sigma_l = \arg \Gamma(l+1+i\eta)$ are the Coulombian phase shifts for the partial waves of angular momentum lh ; and asymptotically,

$$F_l(r) \sim \sin\left(kr - \frac{l\pi}{2} - \eta \ln(2kr) + \sigma_l\right) \quad (2.12)$$

The scattering amplitude corresponding to (2.5) can be summed directly to yield:

$$f(\theta) = \frac{\eta^2}{2m v^2} \operatorname{cosec}^2 \frac{\theta}{2} e^{-i\eta \ln \sin^2 \frac{\theta}{2}} \quad (2.13)$$

which gives the classical cross section of Rutherford:

$$\sigma_{cl}(\theta) = \left(\frac{\eta^2}{2m v^2}\right)^2 \operatorname{cosec}^4 \frac{\theta}{2} \quad (2.14)$$

Mott⁽¹³⁾ has generalized the result (2.14) to the collision of two identical charged particles obeying Fermi-Dirac statistics:

$$\sigma_M(\theta) = \left(\frac{\eta^2}{2m v^2}\right)^2 \left[\operatorname{cosec}^4 \frac{\theta}{2} + \sec^4 \frac{\theta}{2} - \operatorname{cosec}^2 \frac{\theta}{2} \sec^2 \frac{\theta}{2} \cos(\eta \ln \tan^2 \frac{\theta}{2}) \right] \quad (2.15)$$

This result follows directly from (2.13) in conjunction with (2.8).

The presence of the short-range nuclear interaction between the two protons in addition to the Coulomb field will cause the scattering to deviate from the Mott formula (2.15). Because the range of the nuclear force will be small compared to the deBroglie wavelength of the protons for energies

less than 10 Mev, only the $l = 0$ (S-wave) part of the incident plane wave will be changed by the nuclear force. The waves of higher angular momenta will be unaffected to a good approximation for energies below this limit. Thus the asymptotic form of such waves will be given by (2.12), while the $l = 0$ term will behave as:

$$u \sim e^{i\delta_0} \sin(kr - \eta \ln(2kr) + \sigma_0 + \delta_0) \quad (2.16)$$

where δ_0 is the phase shift caused by the specifically nuclear force. The scattering amplitude turns out to be a linear superposition of Coulomb and nuclear contributions:

$$f(\theta) = \left(\frac{e^2}{2mV^2} \right) \operatorname{cosec}^2 \frac{\theta}{2} e^{-i\eta \ln \sin^2 \frac{\theta}{2}} + \frac{i}{2k} (e^{2i\delta_0} - 1) \quad (2.17)$$

The S-wave nuclear scattering is spherically symmetric. From (2.6) and (2.7) it is seen that the nuclear term in $f(\theta)$ contributes only to the singlet part of the cross section (2.8). Consequently, as was mentioned in Section 1, proton-proton scattering gives information about the nuclear proton-proton force only in the singlet state, as long as the nuclear scattering is predominantly S-wave. It is necessary to use relatively high energies where waves of higher angular momentum contribute to the scattering to get any information about the triplet interaction. As yet no experimental data are available which shed any real light on the triplet interaction (see Section 4).

The differential cross section for proton-proton scattering taking into account the effect of the nuclear field on the S wave only can be written, in view of (2.8) and (2.17),

as:

$$\sigma(\theta) = \left(\frac{e^2}{2m\alpha^2}\right)^2 \left[\operatorname{cosec}^4 \frac{\theta}{2} + \sec^4 \frac{\theta}{2} - \frac{\cos(\eta \ln \tan^2 \frac{\theta}{2})}{\sin^2 \frac{\theta}{2} \cos^2 \frac{\theta}{2}} - \frac{2 \sin \delta_0}{\eta} \left(\frac{\cos(\delta_0 + \eta \ln \sin^2 \frac{\theta}{2})}{\sin^2 \frac{\theta}{2}} + \frac{\cos(\delta_0 + \eta \ln \cos^2 \frac{\theta}{2})}{\cos^2 \frac{\theta}{2}} \right) + \frac{4}{\eta^2} \sin^2 \delta_0 \right] \quad (2.18)$$

The first term is just the Mott result (2.15), the second term is an interference term between the Coulomb and nuclear effects, while the last term is the purely nuclear contribution. The only unknown quantity in (2.18) is the S-wave nuclear phase shift δ_0 . This analysis then predicts that the magnitude and the angular distribution of the observed proton-proton scattering can be fitted by the choice of only one constant (δ_0) at each energy. That this is indeed the case was first demonstrated by Breit and his collaborators⁽¹⁾ for the experimental data below 2.5 Mev.

Formulae generalizing (2.18) to include the effects of P and D-wave nuclear scattering in addition to the S-wave contribution have been given by Breit, Condon, and Present⁽¹⁾, and are given in Appendix 1 for reference purposes.

(3) Qualitative considerations of proton-proton scattering

The qualitative behavior of the scattering of protons by protons will be discussed briefly in this section. While somewhat irrelevant to the main thread of analysis, such a discussion was felt worthwhile because it will give a background and perspective upon which to base the examination of the actual experimental results. In Section 2 the effects of the identity of the protons were examined. It was found that the cross section was symmetrical about $\theta = 90$ degrees in the center of mass reference system, and that the cross section contained specifically Coulombian and nuclear terms plus interference terms between the two. A qualitative examination of the cross section given by (2.18), both as to magnitude and angular dependence, as a function of energy will follow.

The fact that the nuclear scattering term in $f(\theta)$ contributes to the cross section only in the singlet state for low energies can be seen in another way. The Pauli principle effectively prevents two protons with parallel spins from approaching one another closer than $\lambda = \hbar/mv$. Since λ is large compared to the range of nuclear forces for energies below 10 Mev, the protons never get close enough together to have any nuclear interaction, and the triplet contribution to the scattering is purely Coulombian.

The Coulomb repulsion also keeps the protons apart even in the singlet state. However, this is effective only at quite low energies. Classically the closest distance of approach is given by $d = e^2/E$, where E is the energy in the

center of mass system. Due to the wave nature of the particles, the Coulomb field cannot prevent the particles from coming close together if their deBroglie wavelength λ is bigger than d . This happens for energies greater than

$E_c \sim \frac{2me^4}{\hbar^2}$ (about 50 Kev, i.e. 100 Kev in the laboratory system). For energies less than this value the nuclear scattering is completely negligible, and the Mott formula (2.15) describes the scattering as to both magnitude and angular dependence.

There is another energy of interest here, namely, the energy at which the probability of finding two protons together is of the same order of magnitude as in the absence of the Coulomb field. For energies above this value, the nuclear scattering will predominate greatly over the Coulomb scattering, except at small scattering angles (i.e. distant collisions). Note that, because of the symmetry of the scattering around 90 degrees, references to small scattering angles imply angles close to 180 degrees as well as 0 degrees. In between these two energies strong destructive interference effects will appear if the nuclear potential is attractive (as is actually the case), the Coulomb interaction being repulsive. The relative probability of finding two protons together as compared to the probability of finding two uncharged particles together in the S-state is given by the Coulomb penetration factor $C^2 = \frac{2\pi\eta}{e^{2\pi\eta} - 1}$ (see Appendix 4), where $\eta = \frac{e^2}{\hbar v}$. For C^2 to be of order 1/2 or greater, $E \gtrsim 800$ Kev (in the laboratory

system). In consequence, it is expected that the scattering will be roughly Coulombian for energies below 100 Kev, will exhibit marked interference effects in the energy range 100 Kev to 800 Kev, and will be predominantly nuclear in character for energies above 800 Kev (except at small angles). These effects will now be considered in more detail.

The angular dependence of the cross-section (2.18) is seen to involve the nuclear phase shift δ_0 , and so depends upon the properties of the nuclear proton-proton force. It is convenient to describe the angular variation in terms of the ratio \mathcal{R} of the nuclear plus Coulomb scattering given by (2.18) to the purely Coulomb scattering given by the Mott formula (2.15). If the nuclear interaction is repulsive, it will always enhance the Coulomb effect, so that \mathcal{R} will always be larger than unity and will have a maximum at $\theta = 90$ degrees (where the Coulomb term has its minimum). The behavior is more complicated if the nuclear interaction is attractive (the actual situation). At very low energies, the nuclear scattering is negligible, and $\mathcal{R} = 1$. At energies above $E_c \sim 2me^4/h^2$, the nuclear interaction will give rise to destructive interference effects that will make $\mathcal{R} < 1$ at all angles, with a minimum at $\theta = 90$ degrees. As the energy is increased, \mathcal{R} will still remain less than unity, but the minimum at 90 degrees will change into a maximum. With further increase in energy, \mathcal{R} will stay less than one for small angles, but will become greater than unity for angles near $\theta = 90$ degrees as the Coulomb field becomes

ineffective in keeping the protons apart. In the limit of high energies the nuclear scattering will predominate at almost all angles, and \mathcal{R} will be much greater than one for all angles (except extremely small ones) with a maximum at $\theta = 90$ degrees (for example, $\mathcal{R} \sim 100$ at $\theta = 90$ degrees when $E \sim 4$ Mev). There will, of course, be some small angle where the Coulomb scattering and the nuclear scattering are of equal magnitude, and destructive interference effects will appear. Near that angle, \mathcal{R} will be less than unity. However, this effect is not very pronounced (see Figure (3.2a)).

Typical cases for moderately low and high energies are sketched in Figures (3.1) and (3.2) respectively. The ratios \mathcal{R} are shown in part (a), and the actual cross sections in the center of mass system in part (b) of the figures. The values of the cross section are in barns (10^{-24} cm.). At low energies (Figure (3.1)) the cross section has only one extreme, the minimum at $\theta = 90$ degrees. The interference effects are pronounced even at 250 Kev; the scattering at 90 degrees is reduced to one third of the value predicted by the Mott formula (2.15). At higher energies, shown in Figure 3.2, the cross section shows a very different character. It has three extreme values, a maximum at $\theta = 90$ degrees, and two minima at $\theta = \theta_m$ and $\pi - \theta_m$; but these are not very pronounced and the region in the middle is relatively flat (as would be expected from S-wave scattering alone). As the energy increases the nuclear scattering is predominant; the minima in the cross section move away from 90 degrees more and more; and the cross section becomes more and

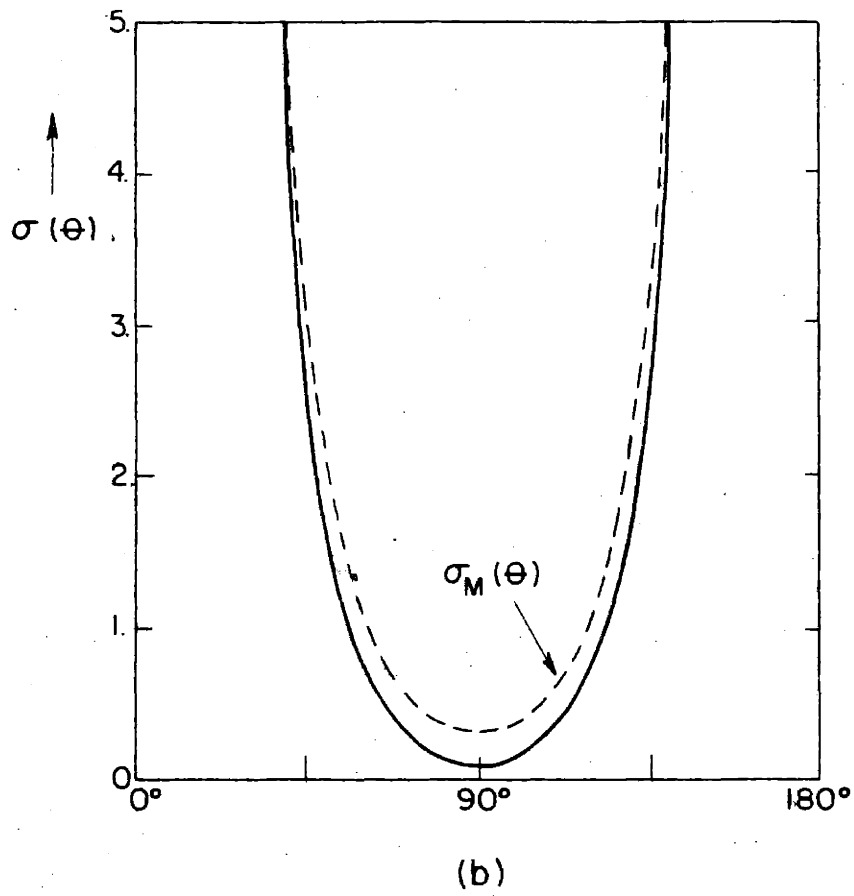
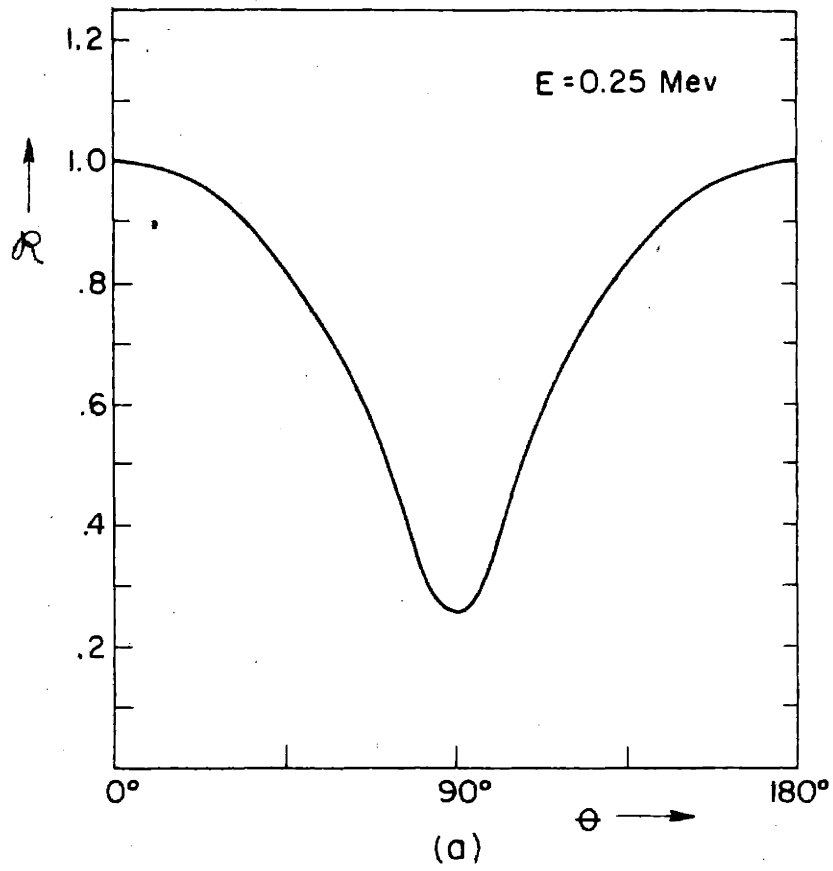


Figure 3.1: Differential scattering cross section in the center of mass system, and the ratio to Mott scattering at an energy of 250 Kev in the laboratory. The destructive interference effects are apparent.

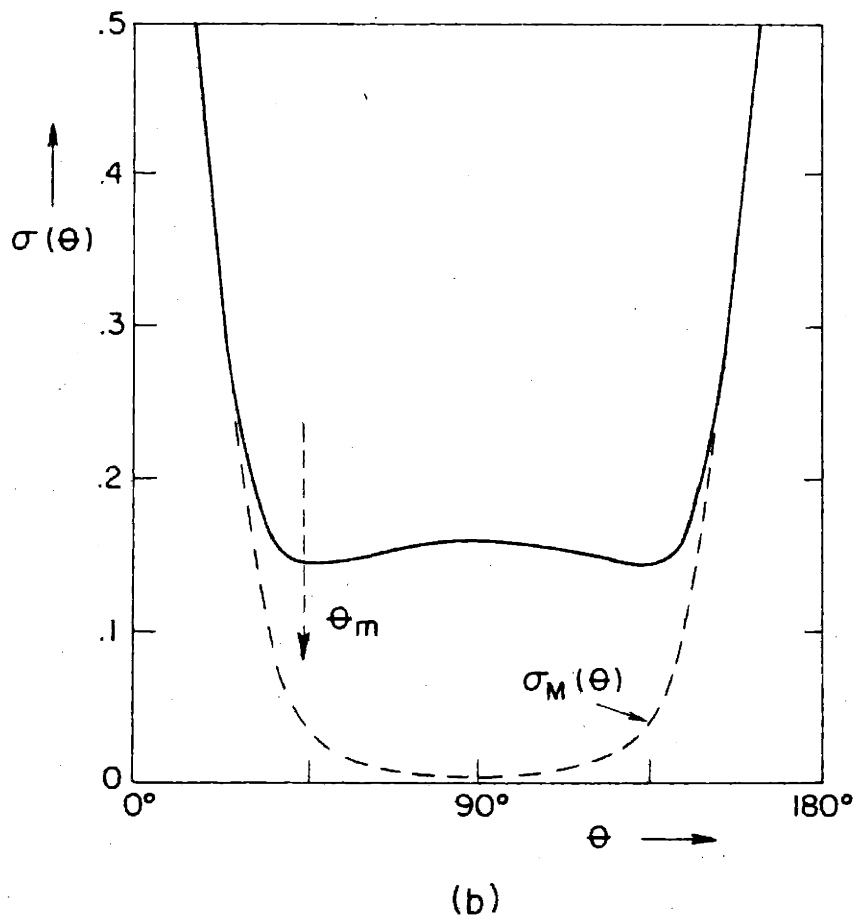
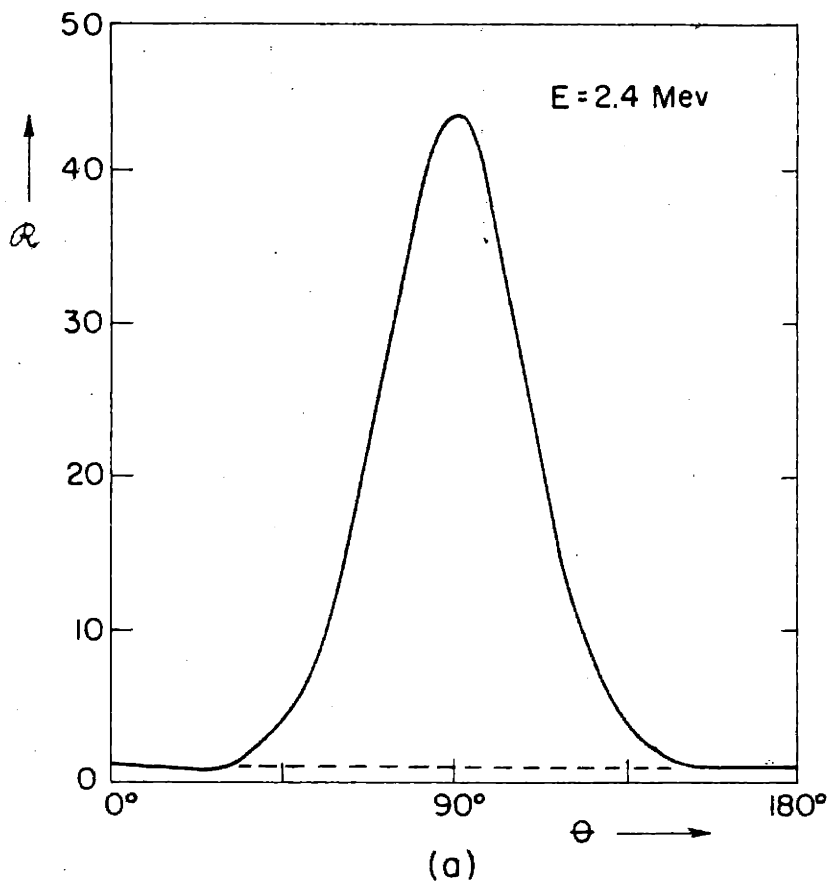


Figure 3.2: Differential scattering cross section in the center of mass system, and the ratio to Mott scattering at an energy of 2.4 Mev. The scattering is predominantly nuclear except at small (and large) angles.

more isotropic except at angles less than θ_m and greater than $\pi - \theta_m$ where the Coulomb contribution enters significantly. The positions of the minima can be found from the expression (2.18). For energies above 1 Mev the result is:

$$\operatorname{cosec}^2 \theta_m \approx \frac{1}{8} \left[3 + \frac{2 \sin \delta_0}{\eta} (\cos \delta_0 + \eta \sin \delta_0) \right] \quad (3.1)$$

This formula can be used to determine an approximate value for the phase shift δ_0 from the angular distribution of the scattering alone without knowledge of the absolute magnitude of the cross section. For this purpose it is convenient to rewrite (3.1) so as to be able to solve for δ_0 directly:

$$\sin(2\delta_0 - \tan^{-1} \eta) \approx \frac{4\eta}{\sqrt{1+\eta^2}} (2 \operatorname{cosec}^2 \theta_m - 1) \quad (3.2)$$

It should be pointed out that this relation can give only approximate values for δ_0 since (1) the minima involved are rather broad and flat, and it is correspondingly hard to determine the value of θ_m , (2) the value of δ_0 is quite sensitive to the choice of θ_m ($\frac{\partial \delta_0}{\partial \theta_m} \sim 5$ in the energy range 3 to 10 Mev).

In view of formula (3.2) and considerations concerning the minima in the angular distribution at $\theta = \theta_m$, and $\pi - \theta_m$, the question arises as to whether or not a more detailed analysis of the angular distribution alone might allow an accurate determination of the phase shift. In principle, the interference between the known Coulomb scattering and the unknown nuclear scattering allows such a deter-

mination. In practice, the accuracy attainable is relatively poor even with a careful analysis. The reason is that over most of the angular range the interference phenomena are not very pronounced. The nuclear part of the cross section is practically independent of angle in the center of mass system, while the Coulomb part varies rapidly with angle. As a result there is, in general, only a very small angular region where the two are of the same order of magnitude and interference effects become pronounced. In fact this region is just the region in the neighborhood of θ_m (and $\pi - \theta_m$); a more detailed analysis of the angular distribution yields little more about the phase shift than does equation (3.2). As a consequence, it is clear that absolute measurements are necessary in order to determine the phase shifts with any degree of precision, and to obtain really useful information about the proton-proton nuclear force.

At any fixed angle, the ratio \mathcal{R} of observed scattering to Mott scattering is approximately unity at low energies. As the energy increases, and the protons interact more closely, the destructive interference between the repulsive Coulomb field and the attractive nuclear interaction causes \mathcal{R} to decrease. With further increase in energy (above $E \sim 800$ Kev, as was seen earlier), the nuclear scattering is relatively great, and the value of \mathcal{R} becomes large compared to unity. The destructive interference effects can be most easily pictured in terms of an Argand diagram on which a vector representing the Coulomb part of scattering amplitude (which depends

on both ϕ and E) and a vector representing the nuclear part of the scattering amplitude (which depends only on E) are plotted. The vector representing the total scattering amplitude will be the vector sum of the two component vectors. The destructive interference will be most pronounced when the two vectors are approximately equal in magnitude, but opposite in phase so that their vector sum is a minimum. At any given scattering angle there will be an energy at which this situation is more or less approximated. At that energy, the greatest amount of interference will occur for that particular angle. The ratio \mathcal{R} will be less than unity at that point. However, as can be seen from Figure (3.2), the effect is not pronounced at small scattering angles. The destructive interference is most nearly complete at 90 degrees. The value of $\mathcal{R}(90 \text{ degrees})$ is plotted in Figure (3.3) as a function of energy in the laboratory for the energy region where the destructive interference effects appear. The value of $\mathcal{R}(90 \text{ degrees})$ from (2.18) is:

$$\mathcal{R}(90^\circ) = \left(1 - \frac{\sin \delta_0}{\eta}\right)^2 + \frac{4 \sin \delta_0}{\eta} \sin^2 \left(\frac{\delta_0 - \eta \ln 2}{2}\right) \quad (3.3)$$

The minimum in $\mathcal{R}(90 \text{ degrees})$ occurs when $\sin \delta \sim \eta$ (actually $\delta \approx \eta - .046 \eta^3 + \dots$). The value of $\sin \delta / \eta$ will increase with energy, both because δ will increase as the nuclear force comes into play more and more, and

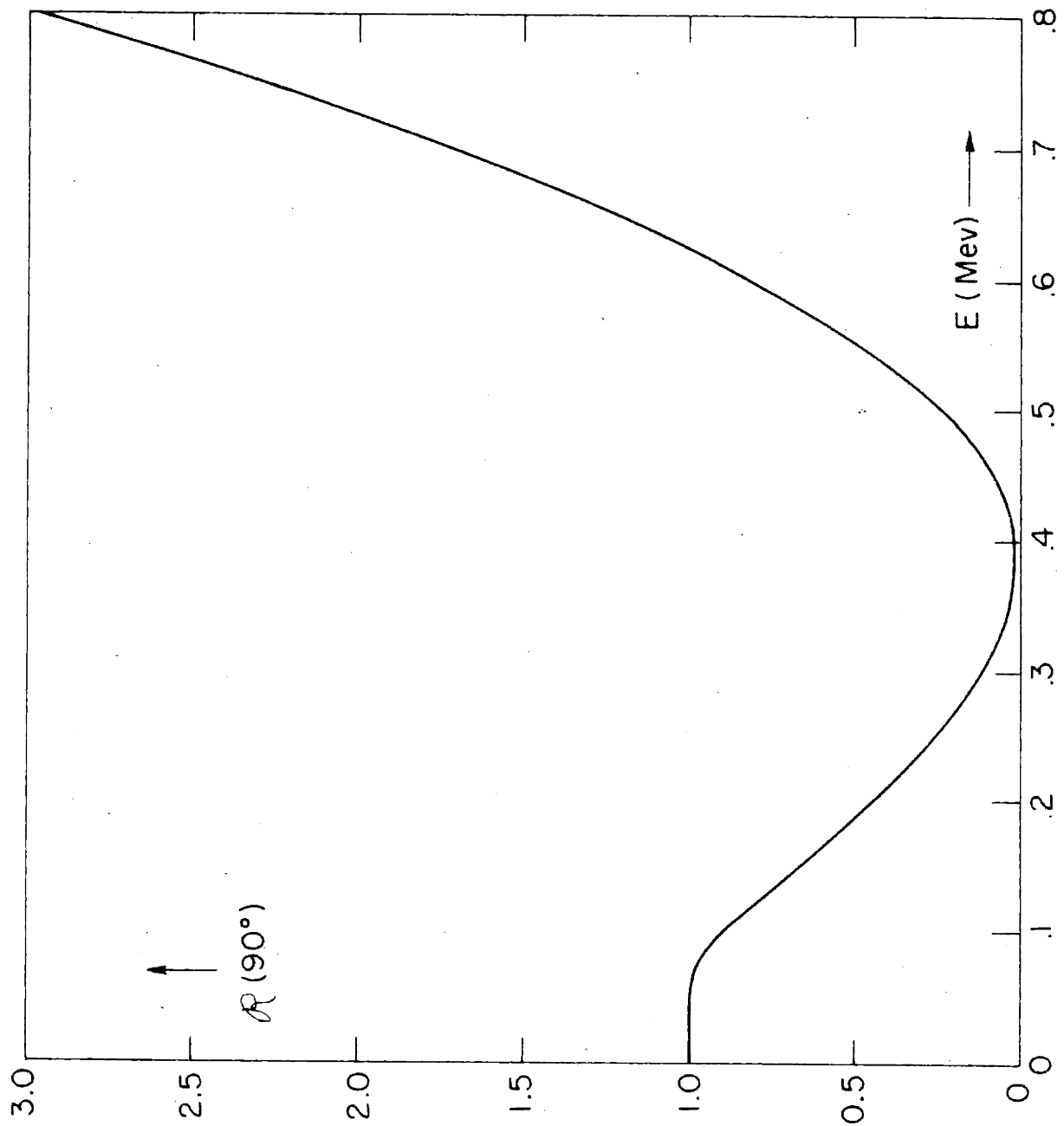


Figure 3.3: Ratio of observed to Mott scattering at a scattering angle of 90 degrees in the center of mass system. The destructive interference is most pronounced near 400 KeV.

because η^{-1} increases as $E^{\frac{1}{2}}$; \mathcal{R} (90 degrees) will rapidly become large compared to unity.

It should be pointed out that, while it has been assumed here from the beginning that the nuclear proton-proton interaction was attractive, the historical development was quite the opposite. Experimentally, it was observed that the cross section had the behavior shown in Figures (3.1), (3.2), and (3.3). From this, it was found that δ_0 must be positive, and hence that the nuclear proton-proton force must be an attractive one, at least in the singlet S state. The detailed behavior of δ_0 with energy led Breit and coworkers⁽¹⁾ to conclude that the proton-proton force was of the same order of magnitude as the singlet neutron-proton interaction.

The discussion so far has been mainly concerned with the qualitative aspects of the angular distribution of the scattering. It is of interest to examine in passing the total cross section, as would be observed in a transmission-attenuation experiment such as those normally done in neutron-proton scattering. Such an experiment would be useful if the nuclear contribution to the total cross section was appreciable compared to the Coulomb effect. The first point to be made is that the differential cross sections given by (2.15) or (2.18) actually give an infinite result for the total cross section due to $\text{cosec}^4 \frac{\theta}{2}$ divergence at small angles of scattering. This is because the Coulomb field was treated as "unscreened"; that is, it was assumed to be exactly of

the form $1/r$ even at large distances. Such an unscreened field produces a slight scattering of protons making even the most distant collisions, and leads to an infinite total cross section. Actually, the incident protons are scattered in hydrogen gas, or a hydrogenous foil. The bound electron around the target proton shields those protons making distant collisions from the Coulomb field of the target. This leads to a cut-off of the $\text{cosec}^4 \frac{\theta}{2}$ dependence at small angles and makes the total cross section finite. The effect of the electronic screening can be accounted for approximately by writing the screened Coulomb field as:

$$V(r) = (e^2/r) e^{-(r/a_0)}$$

where a_0 is taken as the first Bohr orbit of the electron i.e. $a_0 = \hbar^2/m_e e^2$, m_e being the electron mass. It can be easily shown that the classical Rutherford cross section (2.14) is modified by the screening to be:

$$\sigma_{sc}(\theta) = \left(\frac{e^2}{Mv^2} \right)^2 \left[\frac{1}{\left(\frac{m_e}{M} \eta \right)^2 + \sin^2 \frac{\theta}{2}} \right]^2 \quad (3.4)$$

where, to avoid confusion, the nuclear reduced mass has been replaced by $M/2$ ($M =$ proton mass). (3.4) implies that for large angles the scattering is the same as in the unscreened case, while for angles smaller than the critical angle $\theta_c \approx (2 m_e/M) \eta$ the differential cross section is essentially constant at a value:

$$(M/m_e)^2 (\hbar^2/m_e e^2)^2 = (M/m_e)^2 a_0^2$$

Note that this value is independent of energy. The fact that there is a nuclear interaction present does not change things appreciably at small angles since the Coulombian effect predominates greatly there. Figure (3.4) shows the differential cross section for proton-proton scattering taking into account the screening due to the electron in the hydrogen atom. The figure is greatly exaggerated in scale. The angle θ_c is actually extremely small, and the corresponding value of $\sigma(\theta_c)$ extremely large.

With Figure(3.4) in mind, it is possible to discuss the usefulness of a transmission experiment in which the total cross section is observed, rather than the angular distribution. The critical quantity by which the usefulness of such an experiment can be judged as far as nuclear forces are concerned is the ratio of the contributions to the total cross section made by the predominantly nuclear scattering as compared to that made by the predominantly Coulomb scattering. The scattering from θ_m to 90 degrees is almost isotropic (see Figure (3.4)), and is due to the nuclear interaction. The scattering from zero to θ_m varies rapidly with angle, and is mainly Coulomb scattering. The significant ratio is then the ratio of $\sigma(\theta)$ integrated from θ_m to 90 degrees and $\sigma(\theta)$ integrated from zero to θ_m . It will be sufficient to consider only a part of the latter integral,

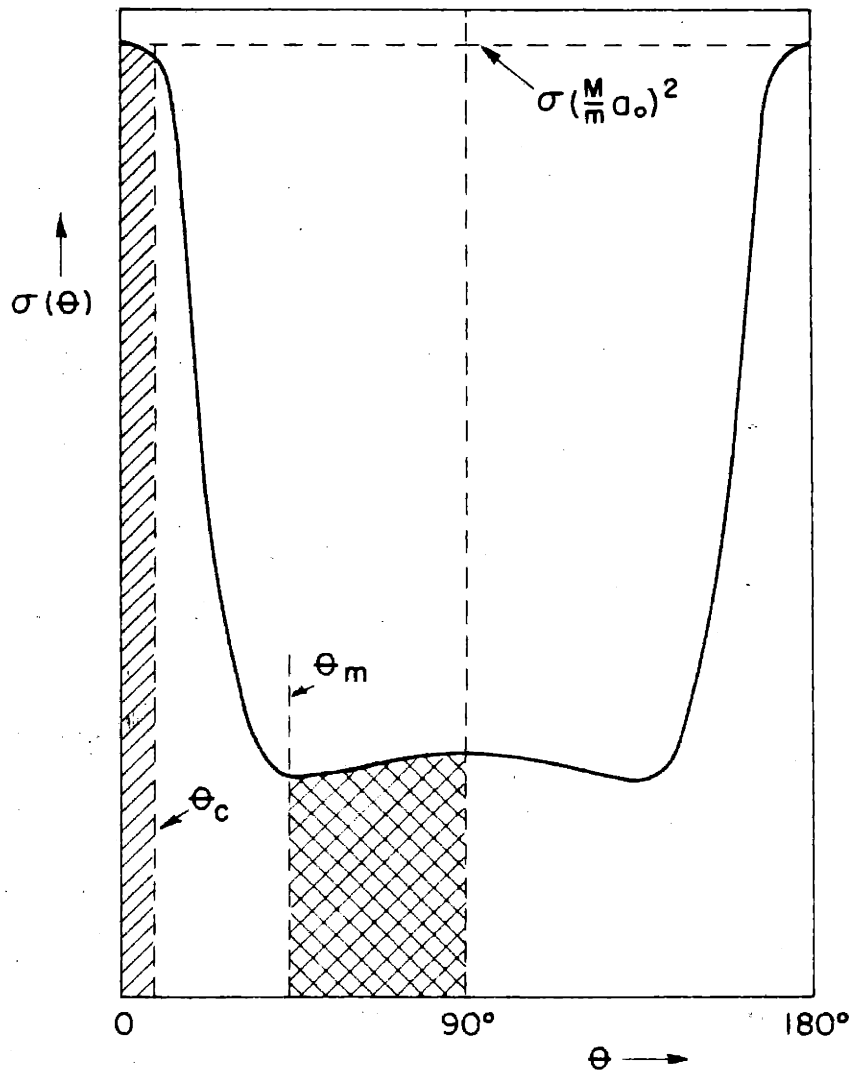


Figure 3.4: Differential cross section in the center of mass system, showing schematically the effects of the screening by the orbital electron.

namely the integral of $\sigma(\theta)$ from zero to θ_c . This integral is approximately given by:

$$C \approx 2\pi \int_0^{\theta_c} \left(\frac{M}{m_e}\right)^2 a_0^2 \theta d\theta = 4\pi \left(\frac{\hbar}{m_e v}\right)^2$$

For energies where the scattering is still mainly S-wave, the nuclear contribution will be less than the integral of $\chi^2 = (2\hbar/Mv)^2$ from zero to 90 degrees (i.e. put $\sin\delta = 1$ and replace θ_m by zero).

$$N < 2\pi \int_0^{\frac{\pi}{2}} \left(\frac{2\hbar}{Mv}\right)^2 \sin\theta d\theta = 8\pi \left(\frac{\hbar}{Mv}\right)^2$$

The ratio of the nuclear contribution to the Coulomb contribution is:

$$N/C < 2(m/M)^2 \ll 1$$

This ratio is so very small that, even at energies of the order of 100 Mev where higher angular momenta (up to $l \sim 5$, or so) contribute appreciably to the scattering, the nuclear part of the total cross section will still be small compared to the Coulomb part. Thus transmission-attenuation experiments below 100 Mev will certainly yield no information about the proton-proton nuclear force. Of course, for cosmic ray energies the deBroglie wavelength of the protons will be small compared to the range of the nuclear force, and the nuclear scattering will become constant at the geometric cross section. Then the effect will be mainly nuclear,

and transmission experiments would give information on the specifically nuclear interaction. The problem would then not be one of elastic scattering alone, but would involve meson production and so on.

(4) Determination of the phase shifts from the experimental cross sections

The techniques of determining phase shifts from the experimental data have been described in detail by Breit, Thaxton and Eisenbud⁽¹⁾, and in other papers by Breit and collaborators. The essential formulae are tabulated in Appendix 1, including the formulae for the analysis including $l = 1$ and $l = 2$ nuclear phase shifts. It will suffice to describe a somewhat simpler formula for the phase shift than has been given previously, and to tabulate the few auxiliary formulae necessary for its use. Also to be described is a rapid method for analyzing the effects of waves of higher angular momenta which is valid if the corresponding phase shifts are small.

If waves of higher angular momenta do not contribute appreciably to the nuclear scattering, the differential cross section is given by (2.18). The form (2.18) is inconvenient for evaluating δ_0 because the interference term involves δ_0 in a complicated way. Breit writes (2.18) in the alternative form given by (A1.10). A still simpler form is:

$$\sigma(\theta) = \sigma_M(\theta) \left[1 + \frac{1}{q} (\sin w - \sin(2\delta_0 + w)) \right] \quad (4.1)$$

where σ_M is given by (2.15), ω and q are known functions of θ and E defined by formulae (A1.11) and (A1.12). Rapidly convergent expansions for q and $\sin\omega$ in powers of E^{-1} (E = energy in laboratory system) can be found from their analytic definitions. Such expansions are tabulated in Table (A1.1) for scattering angles from 40 to 90 degrees (center of mass angles). The expansions for $\sigma_M(\theta)$ are also given in Table (A1.1). The corresponding equation for δ_0 is readily seen to be:

$$2\delta_0 = \sin^{-1}(\sin\omega - q(R-1)) - \omega \quad (4.2)$$

where $R = \sigma(\theta)/\sigma_M(\theta)$ is the ratio of observed scattering to that predicted by the Mott formula (2.15) (see section 3). The use of (4.2) in conjunction with the expansions for q and $\sin\omega$ given in Table (A1.1) gives a rapid and simple means of determining the S-wave phase shift from the experimental cross section. A formula for $2\delta_0$ closely related to (4.2) has been given recently by Critchfield.⁽¹⁴⁾

It is found that for angles less than 40 degrees the expansions for q and $\sin\omega$ do not converge sufficiently rapidly to be convenient. For these angles Q , defined by (A1.15), and $\tan\omega$ yield useful expansions. The relation between Q and q is:

$$q = Q \cos \omega$$

Thus (4.2) is replaced by:

$$2\delta_0 = \sin^{-1} \left(\sin \omega - Q \cos \omega (R-1) \right) - \omega \quad (4.3)$$

In table (A1.2) the expansions for Q , $\tan \omega$, and $\sigma_M(\theta)$ are given for angles from 16 to 40 degrees.

It should be noted that (4.2) or (4.3) leads to certain ambiguities as to the sign and magnitude of $2\delta_0 + \omega$ (due to the fact that an angle is not uniquely determined by the value of its sine). The correct value of δ_0 cannot be determined from the value of the cross section at one angle and energy. As was pointed out in Section 3, it is necessary to know the magnitude and angular distribution of the scattering as a function of energy in order to determine the correct sign and magnitude of the phase shift. For example, suppose the correct value of δ_0 is α . For S-wave scattering alone, α would be independent of scattering angle. Now (4.2) or (4.3) allows another solution, $\delta'_0 = \pi/2 - \omega - \alpha$. However, $\omega = \omega(\theta)$ so that δ'_0 would have the dependence on scattering angle characteristic of ω ; hence this solution could be excluded provided the scattering were known at more than one angle. Physically, the phase shift can be seen to approach zero very rapidly at zero energy (actually, $\delta \sim e^{-2\pi\eta}$ for small k (large η), from (1.2) and (1.3)) because the Coulomb repulsion keeps the protons apart, far outside the

range of the nuclear force. These facts plus the assumption of a smooth functional dependence on energy allows one to determine the correct value of δ_0 .

All the necessary machinery for the determination of S-wave phase shifts from the experimental cross sections is given in Appendix 1.

The analysis of experimental cross sections for P-wave and D-wave phase shifts by means of the formulae (A1.4) and (A1.5) is cumbersome and involved. A quick and relatively easy method for such analysis can be found under the assumption that the higher phase shifts δ_1 (P-wave), and δ_2 (D-wave) are very small. Such an assumption is expected to be valid for energies below 10 Mev, where the data can almost be fitted by a S-wave phase shift δ_0 alone. It is reasonable therefore to introduce the concept of an "apparent S-wave phase shift" δ_a defined as follows: The experimental cross section at a given energy E and angle θ is a function of the phase shifts $\delta_0, \delta_1, \delta_2, \dots$

$$\sigma = \sigma(E, \theta, \delta_0, \delta_1, \delta_2, \dots) \quad (4.4)$$

The apparent S-wave phase shift δ_a is defined by setting all the higher phase shifts equal to zero and solving for the resulting "apparent" δ_0 .

$$\sigma = \sigma(E, \theta, \delta_a, 0, 0, \dots) \quad (4.5)$$

If the higher phase shifts are actually zero, the apparent S-wave phase shift will be equal to the true S-wave phase shift, and will therefore be independent of the scattering angle θ at any one energy E . If the higher phase shifts are not zero but still small, δ_a will be a slowly varying function of θ at constant energy E . Under the assumption that $\delta_1, \delta_2, \dots$ are small, (4.4) can be expanded in a Taylor series in the higher phase shifts.

$$\sigma = \sigma(E, \theta, \delta_0, 0, 0, \dots) + \left(\frac{\partial \sigma}{\partial \delta_1}\right) \delta_1 + \left(\frac{\partial \sigma}{\partial \delta_2}\right) \delta_2 + \dots$$

Similarly (4.5) can be expanded in a Taylor series in the difference between the true and apparent S-wave phase shifts.

$$\sigma = \sigma(E, \theta, \delta_0, 0, 0, \dots) + \left(\frac{\partial \sigma}{\partial \delta_0}\right) (\delta_a - \delta_0) + \dots$$

Equating the two expansions, and keeping only the linear terms yields:

$$\delta_a = \delta_0 + p_1 \delta_1 + p_2 \delta_2 + \dots \quad (4.6)$$

where

$$p_n(E, \theta, \delta_0) = \frac{\left(\frac{\partial \sigma}{\partial \delta_n}\right)}{\left(\frac{\partial \sigma}{\partial \delta_0}\right)} \quad (4.7)$$

The partial derivatives are to be taken at the correct value of δ_0 but at $\delta_1 = \delta_2 = \dots = 0$.

At this point the method does not appear to be at all advantageous since the unknown phase shift δ_0 enters into the functions p_n . However, these functions do not depend very critically upon δ_0 . The Schwinger expansion (1.3) allows a rapid interpolation or extrapolation for the phase shift δ_0 at an energy E from the measured phase shifts δ_0 at other energies. Hence $\delta_0 = \delta_0(E)$ can be found approximately and used to compute the functions $p_n(E, \theta, \delta_0) = p_n(E, \theta)$ once and for all. The results of these computations for p_1 and p_2 are given in Tables (A2.1) and (A2.2) and Figures (A2.1), (A2.2), (A2.3), (A2.4) of Appendix 2. The explicit forms of the functions p_1 and p_2 are stated there, as well as the values of the coefficients in the Schwinger expansion used to obtain $\delta_0(E)$.

If only the S-wave and P-wave phase shifts have to be taken into account, formula (4.6) shows that for any one energy E a plot of the apparent phase shift δ_a vs. $p_1(\theta)$ should be a straight line with intercept δ_0 and slope δ_1 . If the plot turns out to have some curvature, this can be the

result of two causes (aside from experimental inaccuracies): the phase shift δ_1 may be too large to allow the linear approximation to be valid, or higher phase shifts (eg. δ_2) may enter significantly. As to the first possibility, estimates show that with the best experimental accuracies attainable the linear approximation is valid as long as the P-wave phase shift is less than π radians (less than 2 or 3 degrees at 10 Mev). If the D-wave phase shift is responsible for the curvature, one can assume a trial value of δ_1 and plot $\delta_a - \delta_1 p_1(\theta)$ vs. $p_2(\theta)$. The resulting plot should be a straight line with intercept δ_0 and slope δ_2 . The trial value of δ_1 is then adjusted until the best linear fit is obtained.

This analysis is not only quite rapid, but it also shows quickly whether the data are consistent with a small P-wave anomaly, or whether D-wave effects have to be included also. In view of the conjecture of Serber⁽¹⁵⁾ that the exchange character of the nuclear forces is such as to give no nuclear force at all in states of odd angular momentum, this feature of the method may be quite useful.

Another advantage of the method is that one does not have to worry about those systematic experimental errors which affect all angles of scattering equally (eg. error in pressure measurement, or current calibration) as far as the values of δ_1 or δ_2 are concerned. Except for the points at very small angles of scattering (which are likely to be less ac-

curate anyhow because of the very rapid variation of the Coulomb part of the cross section with angle), a small error of that type will shift all values of the apparent phase shift by about the same amount, without changing the slope of the δ_a vs. p_1 (\ominus) (or $\delta_a - p_1 \delta_1$ vs. p_2 (\ominus)) plot appreciably (see discussion later on, and Figure (4.1)).

Breit, Kittel and Thaxton⁽¹⁶⁾ have pointed out that the presence of a tensor force in the 3P state complicates the analysis of the scattering data, since three P-wave phase shifts are then required to fit the data, namely $\delta(^3P_0)$, $\delta(^3P_1)$ and $\delta(^3P_2)$. However, their formulae show that to the extent that one can restrict oneself to the terms linear in the P-wave phase shifts, they enter only in the combination

$$\delta_1 = \frac{1}{9} \delta(^3P_0) + \frac{3}{9} \delta(^3P_1) + \frac{5}{9} \delta(^3P_2) \quad (4.8)$$

This is to be expected since the 3P_0 , 3P_1 , 3P_2 states have the statistical weights 1/9, 3/9, 5/9 respectively. The combination δ_1 (4.8) enters the scattering cross section in exactly the same way as if no tensor force existed.]

Hence the tensor force matters only if the P-wave phase shifts are large enough that their squares cannot be neglected. In this connection it should be pointed out that the combination δ_1 (4.8) could be very small due to cancella-

tions even though the component δ 's are appreciable in magnitude, so appreciable, in fact, that the simplified scheme of analysis given here will not be valid. Thus, in addition to the two causes of curvature in the δ_a vs. p_1 plot given above, the possibility of an appreciable tensor force contribution in the P state must also be included. There is, of course, no tensor force effect in the D-wave scattering.

Before examining the experimental data in detail, some discussion will be made of the effects of systematic errors in cross section and energy measurement and their relation to the effects of P-wave and D-wave anomalies. This will allow a better understanding of the detailed analysis of the experimental measurements which follows. In addition, such considerations are of use to the experimentalists directly. Information telling at what angles the scattering cross section is sensitive, or insensitive, to the presence of P or D-wave effects, and at what angles errors in measurement of σ and E affect the phase shifts most, etc. is of value in the planning of experiments so that a maximum of useful information can be obtained with a minimum of effort.

It is necessary to have a means of estimating the effects of errors in σ and E on the phase shifts so that reasonable account can be taken of experimental uncertainties when plots of δ_a vs. $p_1(\theta)$ or $p_2(\theta)$ are made. For this purpose, tables of $\sigma(\partial\delta_a/\partial\sigma)_E$ and $E(\partial\delta_a/\partial E)_\sigma$ are given in Appendix 3. These tables extend the earlier tables

of Breit, Thaxton and Eisenbud⁽¹⁾ to smaller angles and higher energies (scattering angles from 16 to 90 degrees, energies from .175 Mev to 10 Mev).

To facilitate an understanding of the angular dependence of these various effects, the first-order changes in the apparent S-wave phase shift due to errors in cross section, beam energy, presence of P-wave anomaly and presence of D-wave anomaly are shown in Figure (4.1) for $E=5$ Mev.

Δ_E ($= .01 E (\partial \delta_a / \partial E) \sigma$) is the change in the apparent S-wave phase shift due to a one percent change in beam energy; Δ_σ ($= .01 \sigma (\partial \delta_a / \partial \sigma)_E$) is the effect produced by a one percent change in scattering cross section;

Δ_P ($= p_1(\theta)$) is the change in the apparent S-wave phase shift due to the presence of a P-wave phase shift of one degree; Δ_D ($= p_2(\theta)$) is the change due to a D-wave phase shift of one degree. The curves are drawn for $E = 5$ Mev, but the general behavior is typical of energies in the range 2 Mev to 15 Mev (the upper limit being set at that energy where the P- and D-wave phase shifts cease to be small).

The first point to be noted is the flat central part of the Δ_E and Δ_σ curves with the sharp rise at either end. The flat region in the center is due to the fact that the nuclear scattering is predominant at these angles, and being mostly S-wave scattering is isotropic in the center of mass system (see Figure (3.2)). Thus errors in energy and cross section affect all angles equally as is shown. The sharp

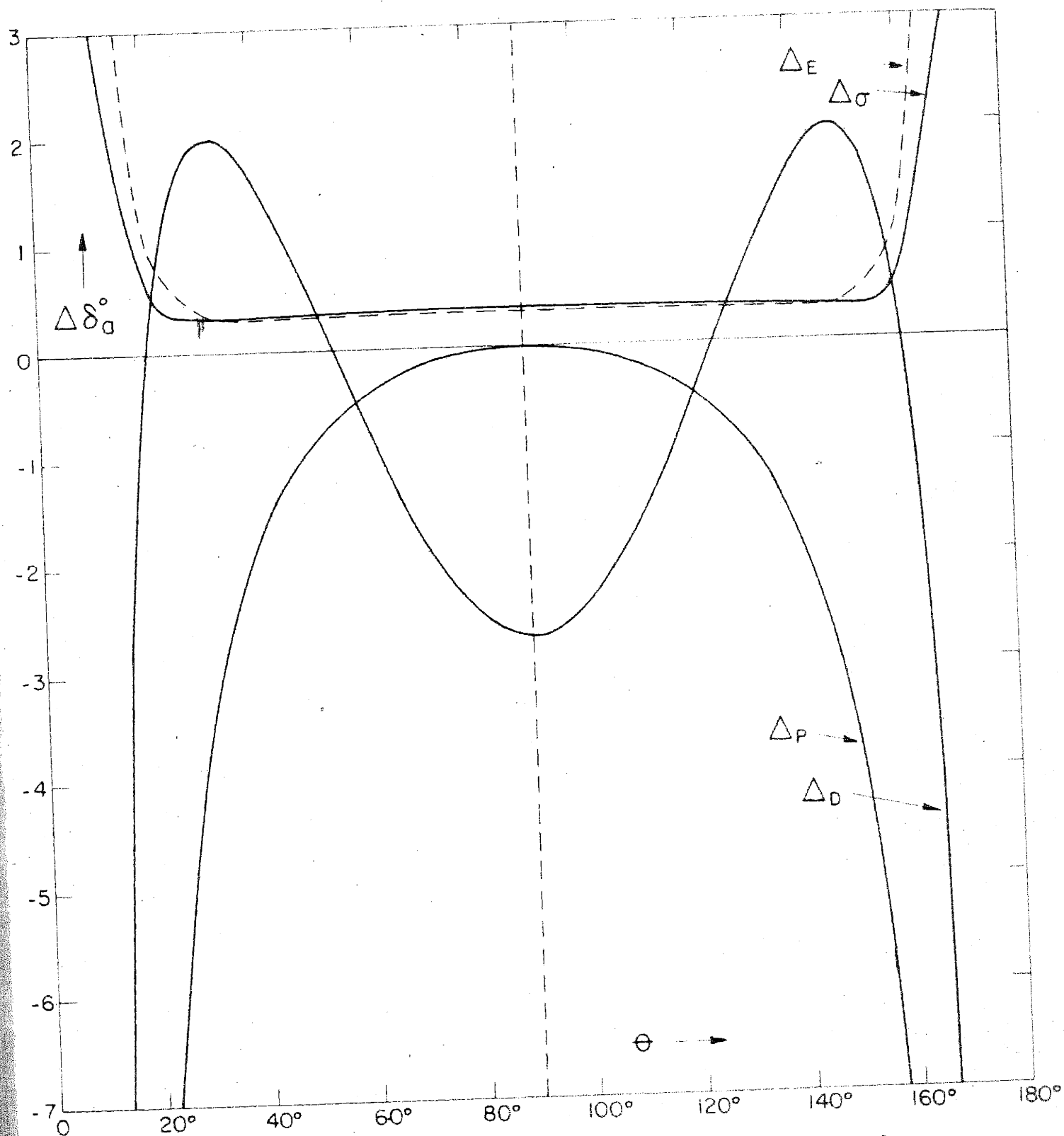


Figure 4.1: Effects of small changes in energy, cross section, and the presence of P and D-wave anomalies on the apparent S-wave phase shift as a function of scattering angle at an energy of 5 Mev.

rise at either end is due to the presence of the Coulomb contribution to the scattering, and its predominance at small angles. The nuclear scattering becomes a small part of the total at these angles, and as a result, the sensitivity of the nuclear phase shift to errors in E and σ increases rapidly. In the example shown, useful measurements much below 20 degrees (center of mass) would be practically impossible since they would involve prohibitive accuracy in the cross section and energy determinations. Systematic errors in energy and cross section (those that do not depend on angle) are seen to be unimportant as far as P- or D-wave effects are concerned for scattering angles greater than 30 degrees (and less than 150 degrees, although measurements at such large angles are experimentally unfeasible) since they add a constant amount to the apparent S-wave phase shift independent of angle. However, at angles smaller than 30 degrees, such systematic errors would introduce angular dependent changes in δ_a .

The qualitative effects of a P-wave anomaly and a D-wave anomaly are seen to be quite different in their overall angular dependence. The presence of a P-wave phase shift changes the apparent S-wave phase shift more and more as the scattering angle moves away from $\theta = 90$ degrees.

The angular dependence of Δ_P is essentially $\cot^2 \theta$ (see equation (A2.4)). On the other hand, Δ_D is, for angles from 40 to 90 degrees, very closely given by the second

Legendre polynomial $P_2(\cos \theta)$. At scattering angles less than 40 degrees, Δ_D deviates from $P_2(\cos \theta)$ markedly, going through another zero near 20 degrees, and increasing rapidly (negatively) for still smaller angles.

The angular dependences of Δ_P and Δ_D in the region from 40 to 90 degrees explain why the data of Ralph, Worthington and Herb⁽¹⁷⁾ could be fitted reasonably by either a P- or a D-wave phase shift (see later on, especially Figures (4.4) and (4.5)). If one ignores the intercepts of Δ_P and Δ_D at $\theta = 90$ degrees, one sees that from $\theta = 40$ degrees to $\theta = 90$ degrees (where their measurements were made) Δ_P and Δ_D have roughly the same kind of (parabolic) shape, although of different sign. Consequently, the plots of δ_a vs. $p_1(\theta)$ and $p_2(\theta)$ would leave little to choose from as to which gave a better fit to the data. Examination of Figures (4.4) and (4.5) shows that this is indeed the case. It should be noted that measurements between 20 and 40 degrees where Δ_P and Δ_D differ radically in shape should discriminate between these two possibilities. The lower limit of 20 degrees is set by the increase in uncertainty of δ_a due to errors in E and σ as was mentioned earlier.

In brief, measurements at scattering angles much less than 20 degrees become rapidly unproductive because of the high accuracy in cross section and energy necessary to give usable values of phase shifts. The presence of a P-wave anomaly makes itself felt most strongly at small scattering

angles; the D-wave effects are most pronounced at 90 degrees, near 30 degrees and at angles less than 20 degrees, with null points near 55 and 20 degrees. Measurements at angles between 20 and 40 degrees together with measurements at larger angles can discriminate between P- and D-wave anomalies most effectively.

A discussion of the experimental data and the phase shifts implied by these data will now be given. The data at higher energies will be examined for P-wave (or D-wave) effects wherever the accuracy warrants it. The following data are available at this time:

(1) Data obtained with Van de Graaff generators (in order of increasing energy)

RKT: Ragan, Kanne, and Taschek⁽¹⁸⁾ have made measurements in the 200 - 300 Kev region. Their high voltage apparatus was actually a transformer-rectifier device, not a Van de Graaf generator. However, for simplicity their measurements have been grouped with the those made with electrostatic generators as distinct from data obtained with cyclotrons. These measurements were mostly exploratory in character and do not claim very high accuracy. The points at $\theta = 90$ degrees (center of mass angle) were corrected most carefully for various sources of experimental error; therefore these points were used to determine the phase shifts.

HHT: The data of Heydenburg, Hafstad and Tuve⁽¹⁹⁾ in the 670 - 870 Kev region were analyzed by Breit, Thaxton and Eisen-

bud⁽¹⁾. Later, Creutz⁽²⁰⁾ re-analyzed these data obtaining slightly different results for the phase shifts. Creutz looked for P-wave effects and found some; however, he interpreted them as being spurious. The S-wave phase shifts given by Creutz will be used here.

HKPP: The data of Herb, Kerst, Parkinson and Plain⁽²¹⁾ were taken with extreme care, and are still the most accurate data available to-day. Breit, Thaxton and Eisenbud showed that these data, covering the energy region from 860 Kev to 2.4 Mev, could be interpreted in terms of S-wave phase shifts only (i.e. in terms of formula (2.18)). To show how such a conclusion might be reached on the basis of the simplified method of analysis for P-wave and D-wave effects presented here the experimental values of δ_a for $E = 2.39$ Mev are plotted against $p_1(\ominus)$ and $p_2(\ominus)$ in Figure (4.2). The number in degrees beside each point is the scattering angle in the center of mass system corresponding to the particular point. It is seen that, within the experimental uncertainties, the P-wave and D-wave phase shifts are zero (the slopes of the lines drawn through the points are zero), confirming the interpretation of BTE. The phase shifts found by Breit, Thaxton and Eisenbud for these data will be used in what follows.

BFLSW: More recently, Blair, Freier, Lampi, Sleator, and Williams⁽²²⁾ have extended the measurements to higher energies (from 2.4 Mev to 3.5 Mev). An analysis of these data

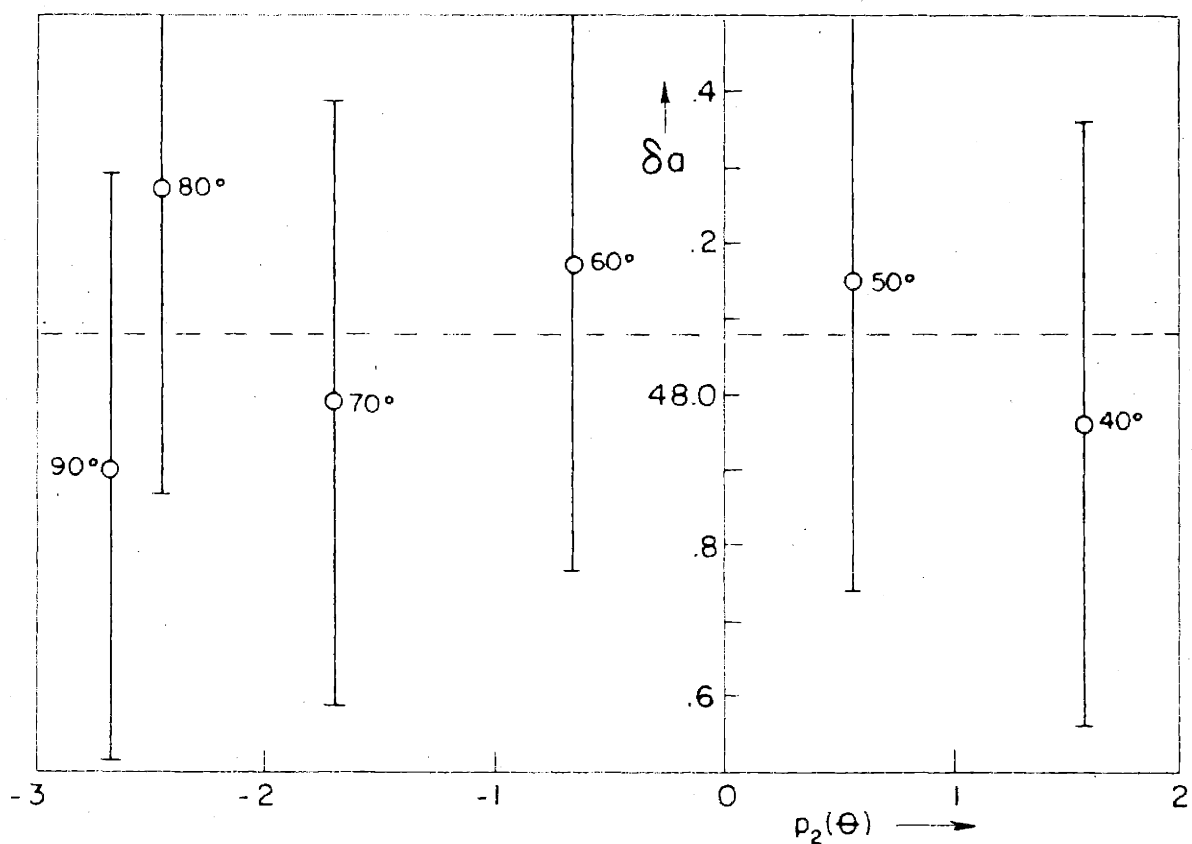
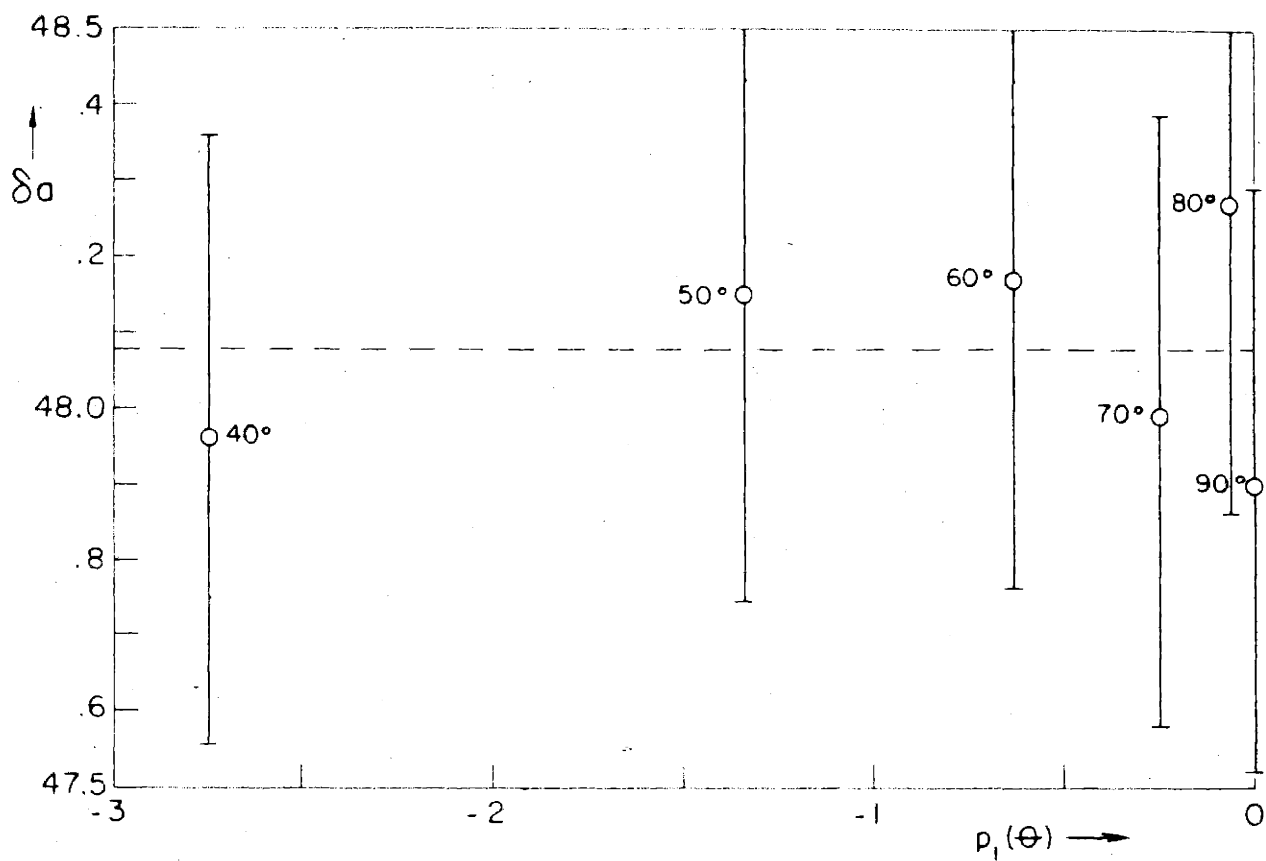


Figure 4.2: Apparent S-wave phase shifts from the HKPP data at 2.39 Mev plotted against $p_1(\theta)$ and $p_2(\theta)$.

by Critchfield⁽¹⁴⁾ showed that they could not be fitted by S-wave phase shifts only. Furthermore, Critchfield states that a combination of S-wave and P-wave phase shifts still does not give good agreement with the experimental data. For comparison, a plot of the apparent S-wave phase shift δ_a vs. $p_1(\ominus)$ for the data at 3.53 Mev is shown in Figure (4.3). A slight downward trend of δ_a with increasing p_1 seems to exist, indicating a small P-wave phase shift of the order of 0.13 degrees, with a negative sign (repulsive potential in the 3P state). Critchfield, by a rather different method of analysis, arrived at a value of -2.3 degrees for the P-wave phase shift at this energy. In view of Figure (4.3) such a large negative value of δ_1 is rather difficult to reconcile with the analysis given here.

It should be noted that the data represented in Figure (4.3) do not appear to be incompatible with a zero or slightly positive value for the P-wave phase shift. The experimental errors are large, and it is felt that definite conclusions about P-wave effects cannot be drawn from these data. As far as determining δ_1 is concerned, the experimental errors shown in Figure (4.3) could be considered as over-estimates since they include all experimental errors, whether they affect all angles equally or not (see earlier discussion). However, the scatter of the points themselves indicates that the errors shown are not gross over-estimates, and are probably quite reasonable. In consequence, the

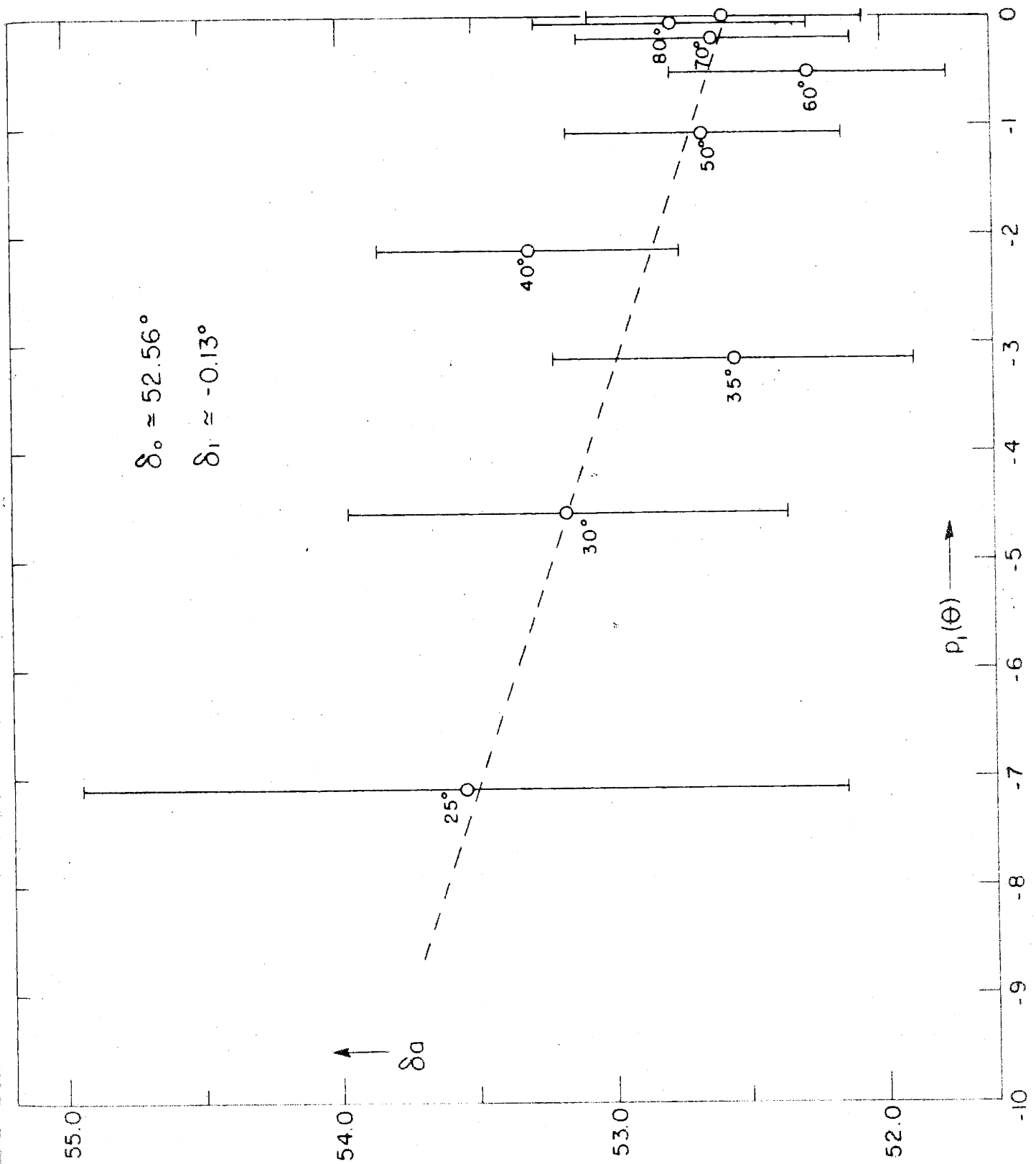


Figure 4.3: Apparent S-wave phase shifts from BFLSW data at 3.53 Mev plotted against $p_1(\theta)$. A slight repulsive interaction in the $3P$ state is indicated.

possible P-wave effects indicated will be ignored; only the S-wave phase shifts will be utilized. These S-wave phase shifts were computed independently of Critchfield; the values found are in close agreement with those found by him. He does not quote any error for the phase shifts. The errors given in Table (4.1) appear to be reasonable from an examination of the experimental data.

RWH: The most recent Van de Graaff data are that of Ralph, Worthington and Herb⁽¹⁷⁾, taken at the same energies as that of the Minnesota group. They state that the data cannot be fitted by a S-wave anomaly only. A plot of δ_a vs. $p_1(\ominus)$ for their data at 3.53 Mev is given in Figure (4.4). The experimental errors shown exclude errors in pressure and current measurement (which affect all angles nearly equally), and are assumed to be reasonable errors as far as the slope determination is concerned. The two limiting straight lines drawn on the figure indicate that the P-wave phase shift lies between $-.15$ and $-.45$ degrees (Ralph, Worthington and Herb put it at $-.30$ degrees) i.e. a repulsive potential in the 3P states. However, two additional views can be taken. If one suspects that the experimental errors have been underestimated, only a slight stretching of the errors would make the points in Figure (4.4) not inconsistent with a horizontal line i.e. pure S-wave scattering, with no P-wave effects at all. On the other hand, from the discussion based on Figure (4.1), it is clear that the data could probably be fitted

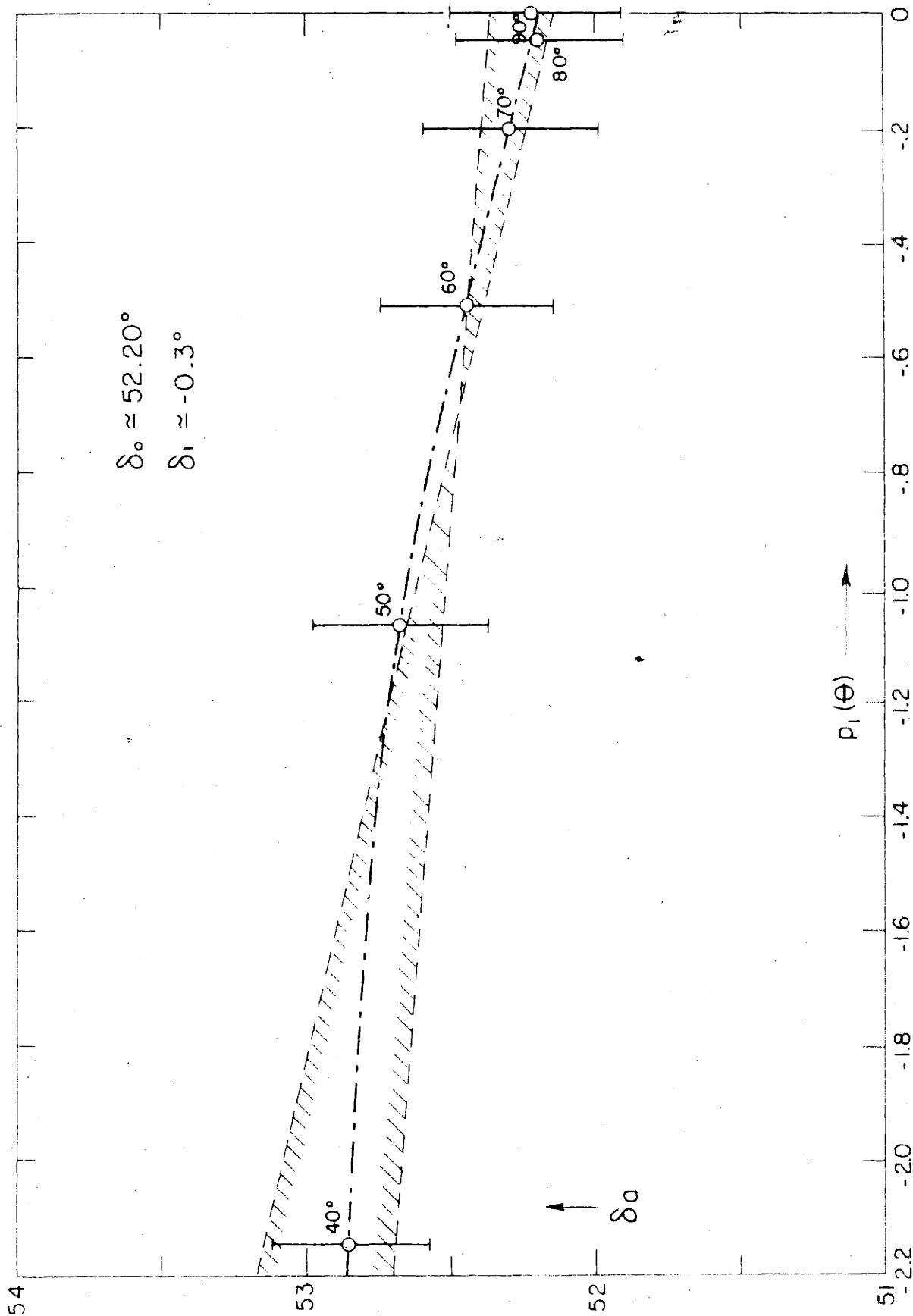


Figure 4.4: Apparent S-wave phase shifts from RWH data at 3.53 Mev plotted against $p_1(\theta)$. Repulsion in the 3P state is implied.

by a D-wave anomaly just as well as by a P-wave anomaly. The fact that the points in Figure (4.4) lie on a smooth curve, more closely than on any straight line might imply such a thing, disregarding for a moment the relatively large experimental uncertainties. The possibility a D-wave effect instead of a P-wave effect is illustrated in Figure (4.5) where δ_a is plotted vs. $p_2(\theta)$. The D-wave phase shift (assuming the P-wave phase shift is zero) is seen to lie between $+.07$ and $+.24$ degrees, and the points fall along a straight line more closely than in the P-wave case. The data at 2.42, 3.04, and 3.28 Mev all give slightly better fits to the D-wave anomaly than to the P-wave. However, the D-wave phase shifts so determined are abnormally large. If one assumes that the potentials in the 1S and 1D are the same, the theoretical estimates (see Section 10) for δ_2 are from 5 to 50 times smaller than the values implied by these data, depending upon the well shape assumed. In addition, the energy dependence for δ_2 (and also for δ_1) implied by the data is not at all reasonable. It is unlikely that the slightly better fit to the D-wave anomaly is significant in view of the relatively large experimental uncertainties and the possibility of unknown systematic errors. As was indicated earlier, measurements between 20 and 40 degrees would almost certainly settle this point.

There is even reason to question the existence of a P-wave effect. If one compares the pre-war values of apparent S-wave

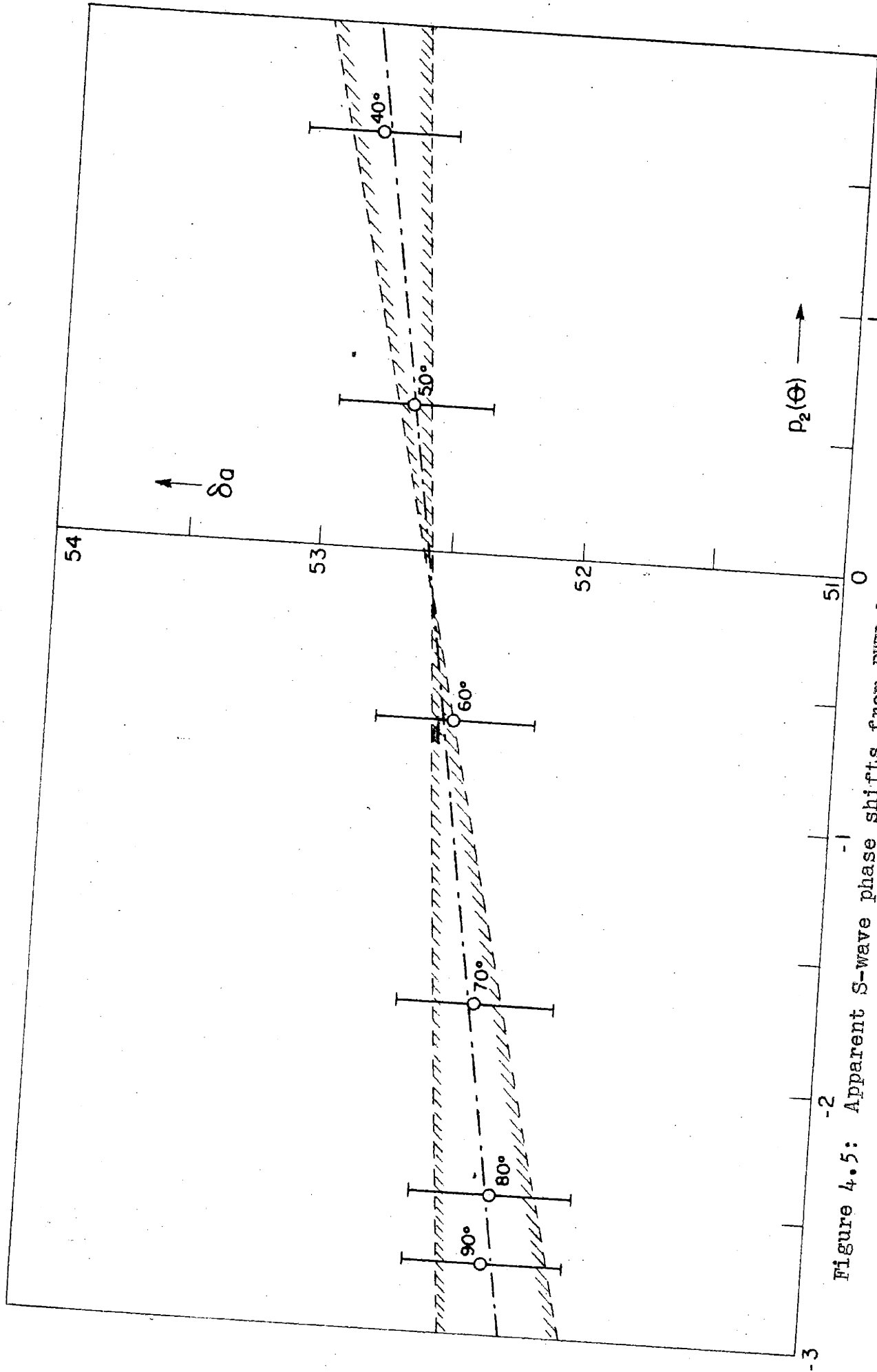


Figure 4.5: Apparent S-wave phase shifts from RWH data at 3.53 Mev plotted against $p_2(\theta)$ in the 3P state. The points imply an unreasonably strong attraction in the 1D state, assuming no interaction

P-P S scattering

J. D. Jackson

Change bottom of p. 49 to read
as follows:

----- incorrectly by Lubanski and
de Jager (24). These authors misstate
the most probable value of the S-wave
phase shift implied by these data (it is
52.7 degrees rather than 54.0). Since
their analysis depends very critically -----

phase shift found by the Wisconsin group at 2.39 Mev (which were interpreted in terms of S-wave effects only - see Figure (4.2)) with the recent values at 2.42 Mev, one sees a marked difference in trend and a considerable difference in numerical values at the smaller angles. The overall accuracy of the present measurements is not significantly greater than that of the earlier measurements. Because of this discrepancy at the one point of overlap of the two sets of data and all the other uncertainties involved, it seems unwise to draw any definite conclusions about P- or D-wave effects at this time. Only the values of the S-wave phase shift from these data will be used in what follows.

(2) Data obtained with cyclotrons

MP: May and Powell⁽²³⁾ determined the ratio of observed scattering to Mott scattering at $\Theta = 90$ degrees (center of mass) with 4.2 Mev protons using photographic techniques. The ratio has an uncertainty of about 6 percent, and is therefore of negligible value to this analysis. The only reason for mentioning this experimental point is the fact that it was used incorrectly by Lubanski and deJager⁽²⁴⁾. Not only did these authors misstate the most probable value of the S-wave phase shift implied by these data (it is 52.7 degrees rather than 54.0) but they also neglected to take into account the very large probable error (± 2 degrees). Since their analysis depends very critically on this particular point, their result cannot be considered as valid (al-

though, by a combination of errors, it is rather close to the truth).

M: Very recently, Meagher⁽²⁵⁾ has made measurements at 5 Mev using photographic plate detection. A plot of the apparent S-wave phase shift δ_a vs. $p_1(\theta)$ is given in Figure (4.6). The horizontal line is the best fit to the points near $\theta = 90$ degrees (center of mass), assuming $\delta_1 = 0$. It is seen that the data allow such a fit, but that a line of positive slope would provide somewhat better agreement. In view of the fact that the (more accurate) Van de Graaff data at 3.5 Mev indicate a zero or negative P-wave phase shift, the slight positive P-wave phase shift indicated here should be taken very cautiously. Only the S-wave phase shift, determined from the data near $\theta = 90$ degrees, will be used in what follows.

DOP: Dearnley, Oxley and Perry⁽²⁶⁾ have used the same technique at 7 Mev. They state that their data are in agreement with a slightly negative P-wave phase shift. Figure (4.7) shows a plot of δ_a vs. $p_1(\theta)$ which bears out this analysis. The dotted line represents their values of the P-wave phase shift (-.22 degrees) and S-wave phase shift. It is seen to give a reasonable fit to the experimental points although the large experimental uncertainties allow considerable leeway. The accuracy of the data is too low to draw definite conclusions about the P-wave phase shift. It will turn out later that the S-wave phase shift implied by these data is

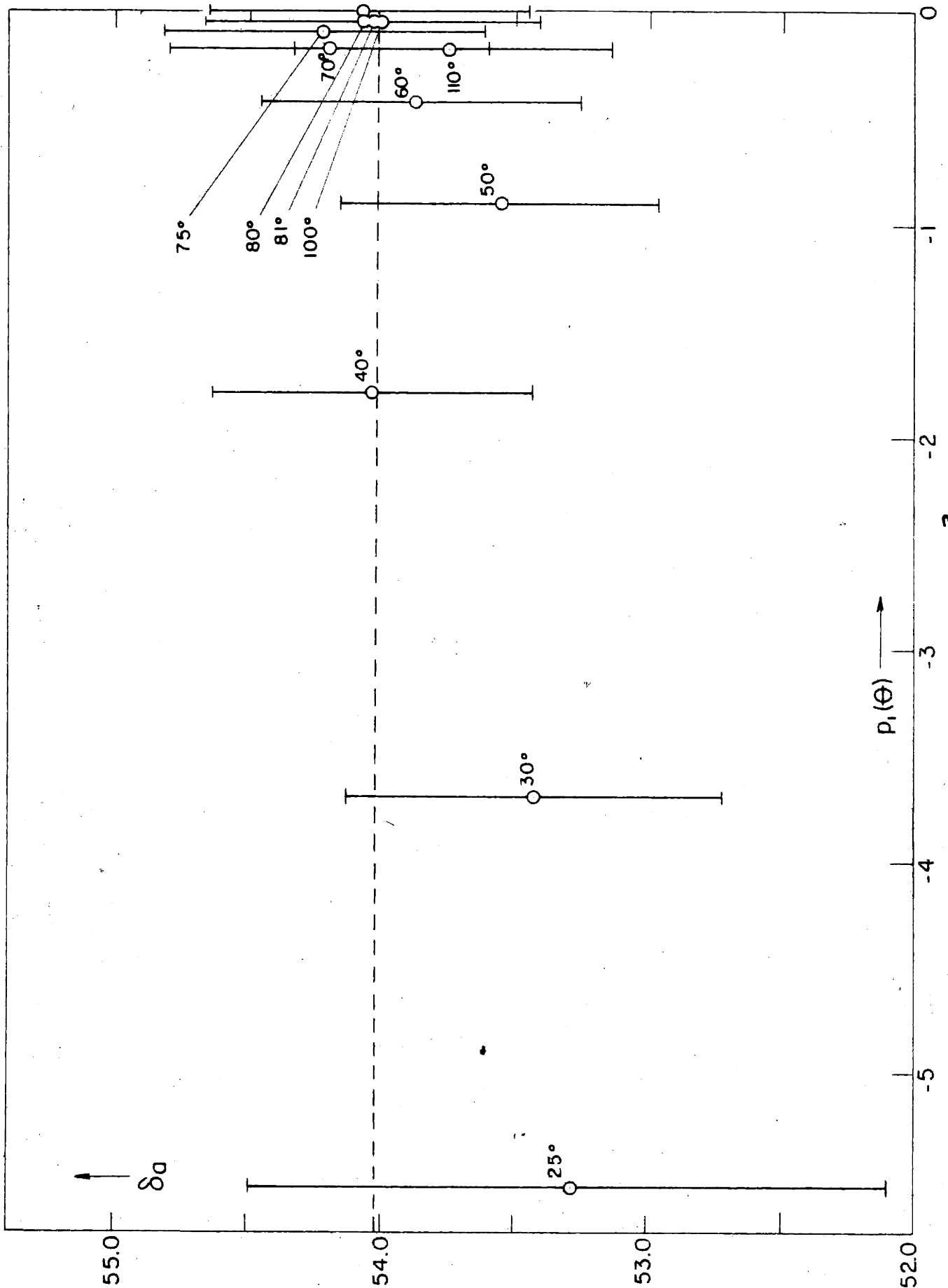


Figure 4.6: Apparent S-wave phase shifts from the data of Meagher at 4.9 Mev plotted against $p_1(\theta)$.

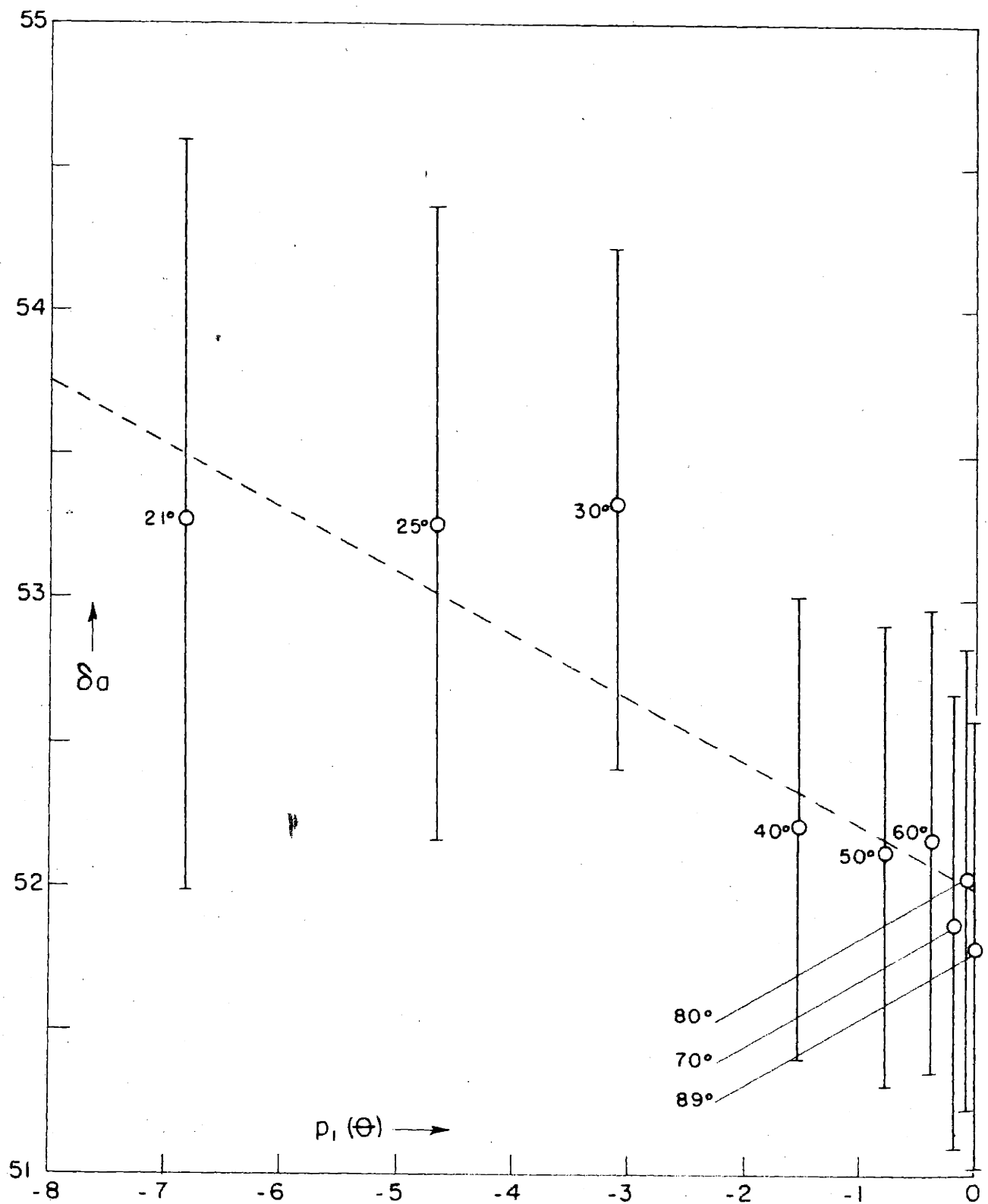


Figure 4.7: Apparent S-wave phase shifts from the DQP data at 7. Mev plotted against $p_1(\theta)$. A slight repulsive interaction in the 3P state is indicated.

very hard to reconcile with the lower energy measurements quoted above. A redetermination of the scattering at this energy would be very desirable.

WC: Wilson and Creutz⁽²⁷⁾ have made measurements at 8 Mev in which they determined the absolute value of the cross section at 90 degrees (center of mass), and made relative measurements at other angles. The accuracy of their absolute measurement was about ± 5 percent. The data at other angles based on the point at 90 degrees are consistent with S-wave scattering only, but the accuracy is comparatively poor, and a detailed analysis is not warranted. The value of the S-wave phase shift determined from these data is given in Table (4.1).

W: Wilson⁽²⁸⁾ has made relative measurements of the angular distribution of scattering at 10 Mev. A theoretical analysis of his data has been given by Peierls and Preston⁽²⁹⁾ and by Foldy⁽³⁰⁾ with different results. Preston and Peierls find that the P-wave phase shift is approximately -0.8 degrees, and state that a repulsive square well potential of range 2.5×10^{-13} cm. and depth 10 Mev will give this value of δ_1 at an energy of 10 Mev. Foldy claims that the data imply a P-wave phase shift of about -0.4 degrees, in disagreement with Preston and Peierls. For comparison purposes, Figure (4.8) shows a plot of δ_a vs. $p_1(\theta)$ under various reasonable assumptions as to the absolute value of the cross section. The actual magnitude of δ_a has no meaning, only the change with scattering angle is important. Accordingly,

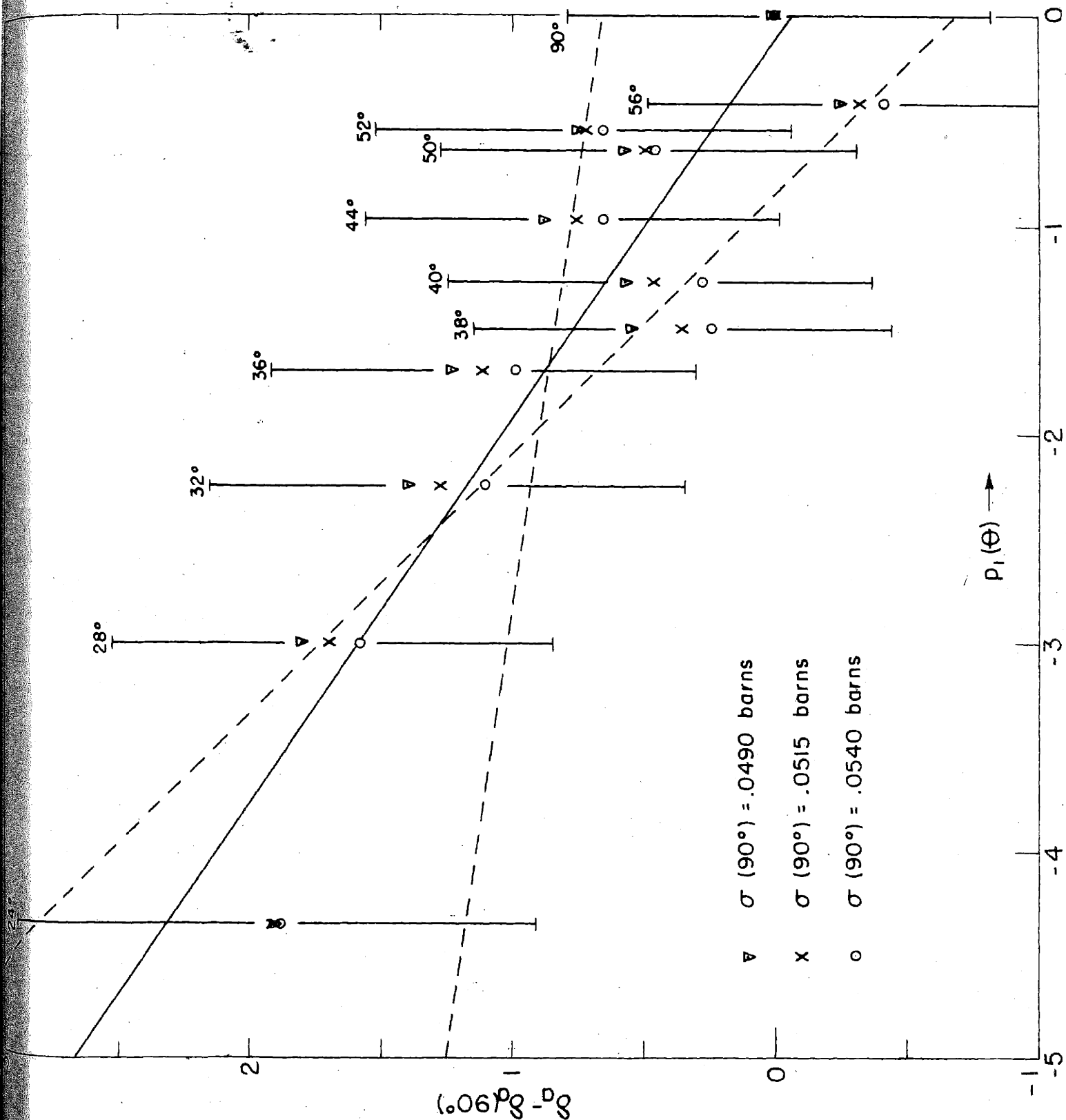


Figure 4.8: Relative values of apparent S-wave phase shifts from the data of Wilson at 10. Mev vs. $p_1(\theta)$ for various reasonable assumptions as to the absolute values of cross section at 90 degrees.

the differences $\delta_a - \delta_a(90^\circ)$ are plotted. The errors indicated are due to statistics only (about 2 percent). It is seen that the overall variation of 10 percent in the normalizing values for the cross section at $\theta = 90$ degrees produces a change in the relative position of the points that is small compared to their statistical uncertainties. The two dotted lines indicate possible extremes (-0.80 and -0.12 degrees) in the value of δ_1 , while the solid line, giving some sort of average fit, implies $\delta_1 \approx -0.5$ degrees. The analysis given here shows that (1) the data are sufficiently uncertain to make any detailed interpretation doubtful; (2) the data, assuming no unknown systematic errors, imply a small repulsive potential in the 3P state or else a small attractive 1D potential, since, for the angular region in question, a D-wave fit would give just as good agreement as a P-wave (see earlier discussion); (3) the value of the P-wave phase shift found here is more in accord with Foldy's value than that of Preston and Peierls; however, the difference is within the experimental errors.

WLRWS: Wilson, Lofgren, Richardson, Wright, and Shankland (31) have made measurements at 14.5 Mev. Their measurements were absolute in nature, but relatively inaccurate. The point at $\theta = 90$ degrees was determined with more precision; accordingly it was used to evaluate the S-wave phase shift. It is seen from Table (4.1) that the uncertainty in the phase shift is quite large (as is true for most of the

cyclotron data).

The values of the S-wave phase shift for all the experimental data are gathered in Table (4.1). For the data of RKT⁽¹⁸⁾ and BFLSW⁽²²⁾ the agreement with the phase shifts given by Bethe⁽⁷⁾ is satisfactory. The quantity K defined by equation (1.2) with its probable error is also given in the table for each set of experimental data. The analysis of the experiments in terms of the function K will be taken up in the next section. Appendix 3 gives the values of the apparent S-wave phase shift which were used in the figures of this section, as well as stating how each of the S-wave phase shifts in Table (4.1) was determined.

Table 4.1a: Data obtained with Van de Graaff generators

$$k^2 = 1.205 \cdot 10^{24} E(\text{MEV}) \text{ cm}^{-2}$$

Energy (MEV)	S-wave phase shift(degrees)	η	$h(\eta)$	K	k^2 10^{24} cm^{-2}	Source
.1765	5.78 \pm .35	.376	.552	3.79 \pm .16	.213	RKT
.2002	6.80 \pm .32	.353	.600	3.82 \pm .14	.241	RKT
.2259	7.82 \pm .30	.333	.644	3.87 \pm .12	.272	RKT
.2495	9.03 \pm .30	.316	.686	3.83 \pm .11	.301	RKT
.2753	10.06 \pm .28	.303	.719	3.82 \pm .09	.332	RKT
.2983	10.96 \pm .26	.289	.758	3.91 \pm .09	.359	RKT
.3214	11.82 \pm .30	.279	.787	3.93 \pm .15	.387	RKT
.670	24.68 \pm .40	.1931	1.111	4.00 \pm .10	.807	HHT
.776	27.12 \pm .40	.1795	1.178	4.12 \pm .08	.935	HHT
.867	29.32 \pm .40	.1697	1.230	4.17 \pm .07	1.045	HHT
.860	29.28 \pm .40	.1704	1.226	4.15 \pm .03	1.036	HKPP
1.200	35.94 \pm .40	.1444	1.383	4.32 \pm .03	1.446	HKPP
1.390	38.76 \pm .40	.1341	1.453	4.41 \pm .03	1.675	HKPP
1.830	44.02 \pm .40	.1169	1.586	4.59 \pm .02	2.206	HKPP
2.105	46.18 \pm .40	.1090	1.653	4.72 \pm .03	2.537	HKPP
2.392	48.08 \pm .40	.1022	1.716	4.85 \pm .03	2.883	HKPP
2.42	48.24 \pm .50	.1016	1.725	4.86 \pm .05	2.917	BFLSW
3.04	50.95 \pm .50	.0906 ₅	1.834	5.15 \pm .06	3.664	BFLSW
3.27	51.89 \pm .50	.0874	1.870	5.24 \pm .06	3.941	BFLSW
3.53	52.58 \pm .50	.0841	1.907	5.36 \pm .07	4.254	BFLSW
2.42	47.91 \pm .40	.1016	1.725	4.90 \pm .05	2.917	RWH
3.04	50.80 \pm .30	.0906 ₅	1.834	5.17 \pm .05	3.664	RWH
3.28	51.77 \pm .40	.0873	1.870	5.26 \pm .06	3.953	RWH
3.53	52.20 \pm .30	.0841	1.907	5.41 \pm .06	4.254	RWH

Table 4.1b: Data obtained with cyclotrons

Energy (MEV)	S-wave phase shift(degrees)	η	$h(\eta)$	K	k^2 10^{24} cm^{-2}	Source
4.2	52.7 ± 2.0	.0771	1.995	$5.83 \pm .30$	5.06	MP
$4.9 \pm .07$	$54.02 \pm .60$.0714	2.070	$6.10 \pm .10$	$5.91 \pm .08$	M
$7.03 \pm .06$	$52.0 \pm .60$.0598	2.243	$7.63 \pm .11$	$8.48 \pm .07$	DOP
$8.0 \pm .1$	52.7 ± 2.0	.0559	2.31	$8.00 \pm .40$	$9.64 \pm .12$	WC
$14.5 \pm .7$	52.2 ± 3.5	.0415	2.61	$10.78 \pm .80$	$17.5 \pm .8$	WLRWS

(5) The determination of the variational parameters from the experimental data

In the definition of K (1.2) the function $h(\eta)$ was not defined. The definition of $h(\eta)$ is:

$$h(\eta) = \operatorname{Re} \frac{\Gamma'(-i\eta)}{\Gamma(-i\eta)} - \ln \eta \quad (5.1)$$

Here Re stands for the real part of the logarithmic derivative of the Γ -function. The function $h(\eta)$ is shown plotted against energy in the laboratory system in Figure (5.1). For more accurate work $h(\eta)$ can be written in the form:

$$h(\eta) = -\ln \eta - 0.5772\dots + \eta^2 \sum_{n=1}^{\infty} \frac{1}{n(n^2 + \eta^2)} \quad (5.2)$$

where 0.5772... is Euler's constant, and the sum in (5.2) is plotted as a function of η in Figure (5.2). This sum is a slowly varying function of energy, and for energies over 200 Kev enters only as a small correction term. This formula (5.2) in conjunction with Figure (5.2) gives considerably more accuracy than is necessary considering the uncertainties in the experimental data.

The values of K (1.2) determined from the experimental data were given in Table (4.1). These values are plotted against k^2 (i.e. against energy) in Figures (5.3) (Van de Graaff

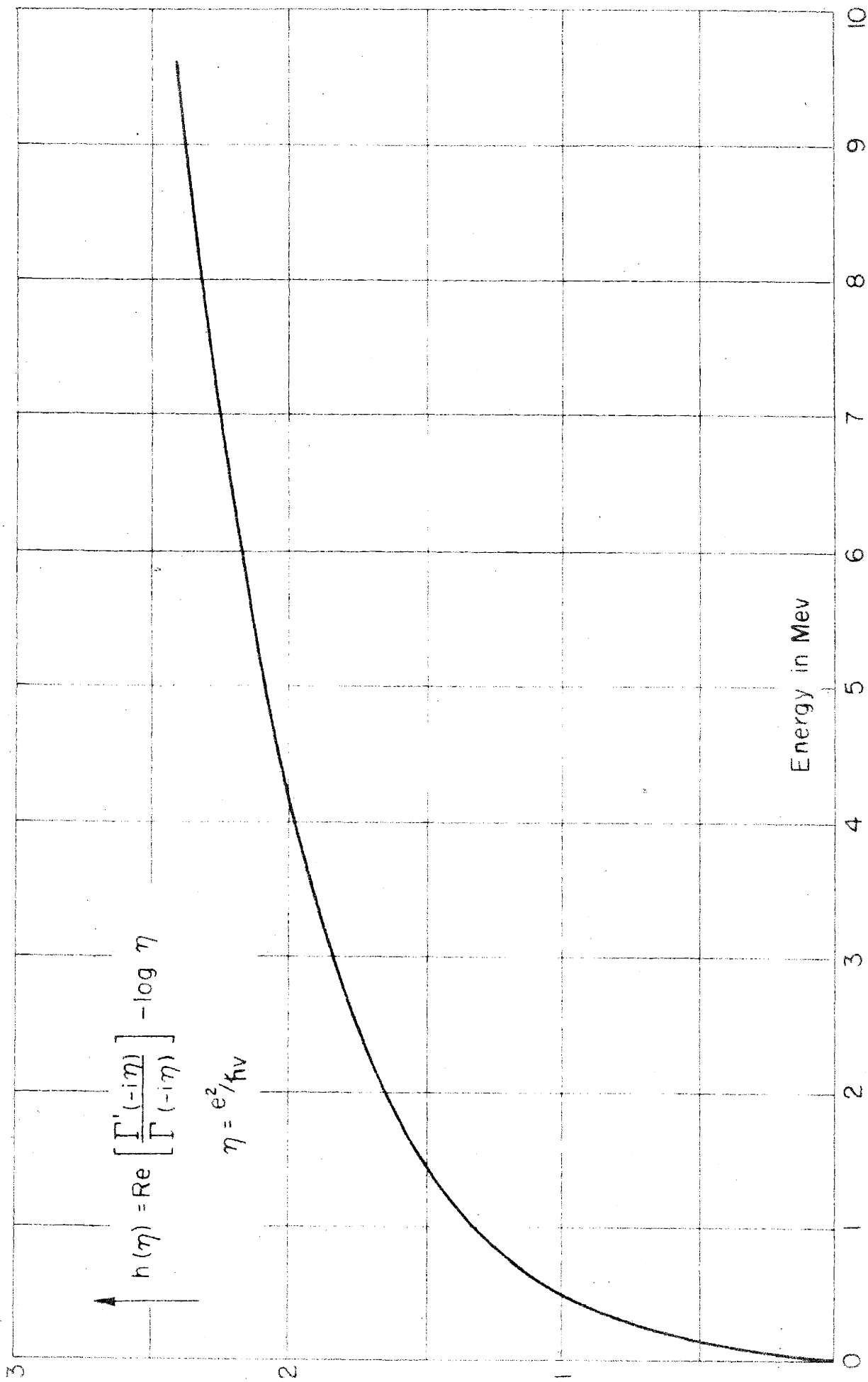


Figure 5.1: $h(\eta)$ as a function of the energy in the laboratory.

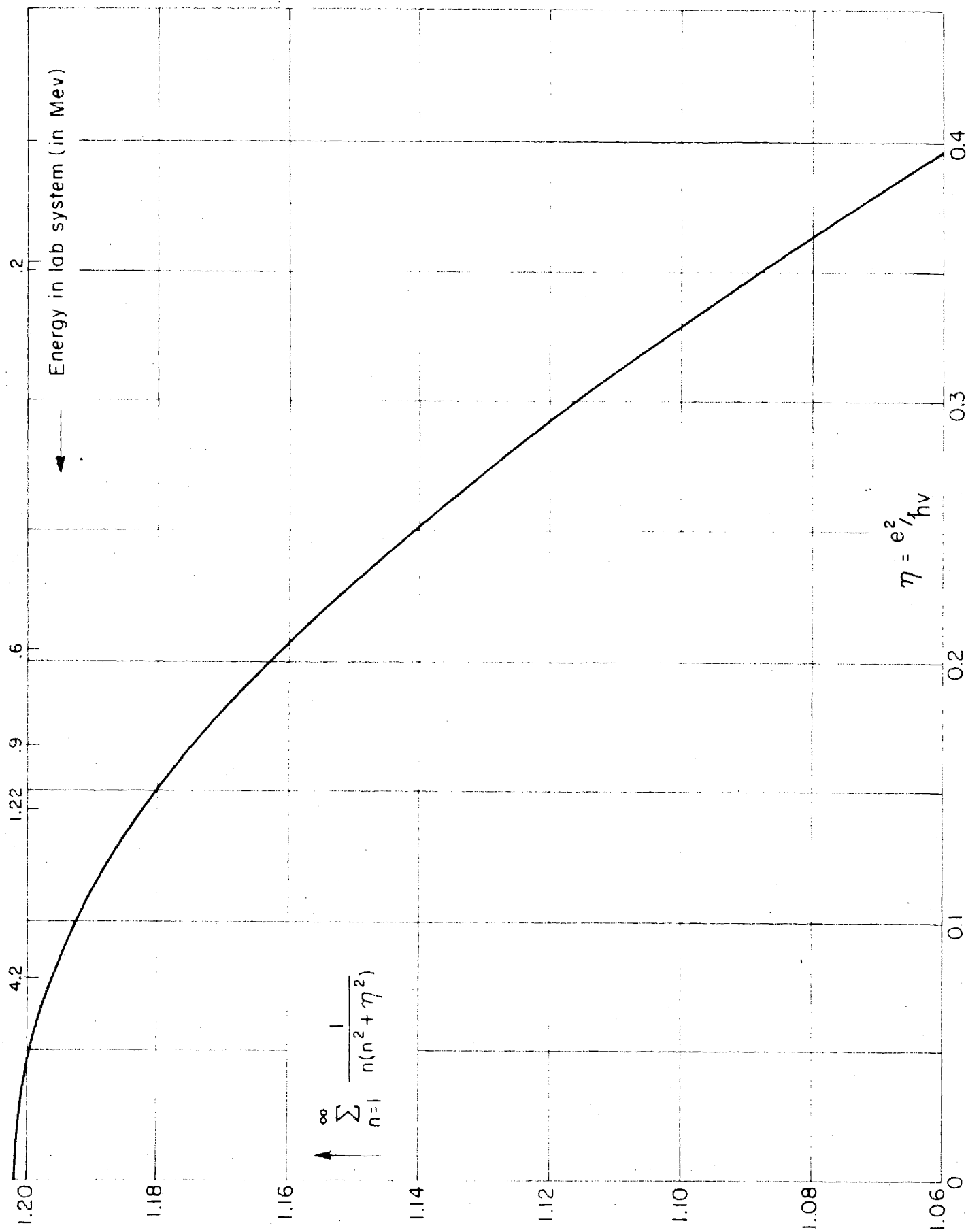


Figure 5.2: Auxiliary summation occurring in $h(\eta)$ plotted against η .

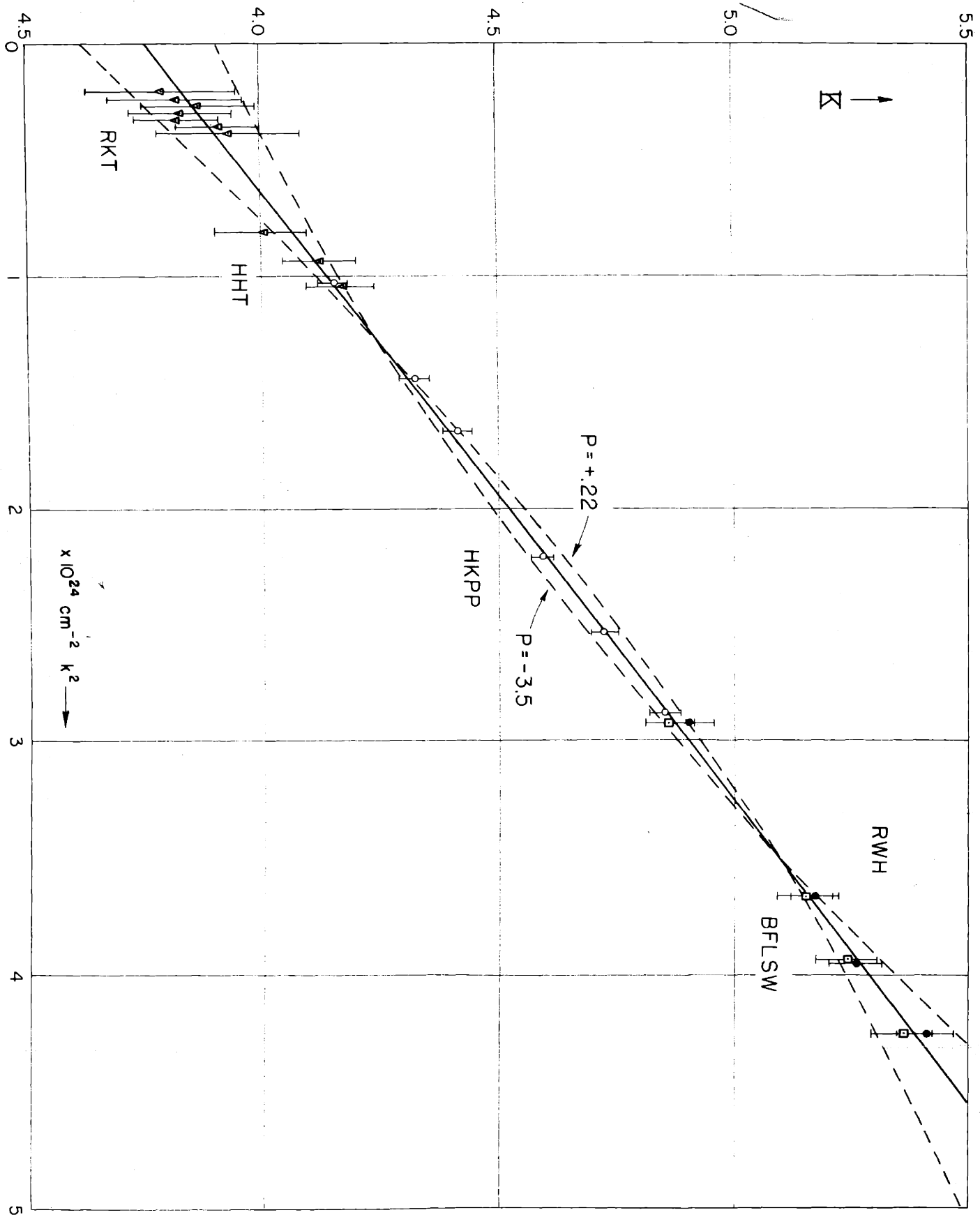


Figure 5.3: The experimental values of K as a function of k^2 for the Van de Graaff data. The best shape-independent approximation is shown, along with two parabolic fits to the data. $k^2 = 1.205 \times 10^{24} \text{ E (MeV)} \text{ cm}^{-2}$.

data) and (5.4) (cyclotron data). It is obvious from Figure (5.3) that the Van de Graaff data allow an extremely good straight line fit. The best straight line is drawn in on the figure. Its parameters, as determined by a least squares analysis with proper weighting of the data according to the probable errors given in Table (4.1a), are:

$$\begin{aligned}
 -R/a &= 3.755 \pm .024 \\
 a &= -7.67 \pm .05 \times 10^{-13} \text{ cm.} \\
 \frac{1}{2}Rr_0 &= 0.382 \pm .010 \times 10^{-24} \text{ cm}^2 \\
 r_0 &= 2.65 \pm .07 \times 10^{-13} \text{ cm.}
 \end{aligned}
 \tag{5.3}$$

Since the data of Heydenburg, Hafstad and Tuve⁽¹⁸⁾ are considered unreliable because of possible systematic errors, it is of interest to determine the best linear fit to the data omitting the HHT points. When such a fit is made, the resulting values for the coefficients are:

$$\begin{aligned}
 -R/a &= 3.757 \\
 \frac{1}{2}Rr_0 &= 0.381 \times 10^{-24} \text{ cm}^2
 \end{aligned}$$

These values are seen to be almost exactly the same as those given in (5.3).

Having determined the best values of the coefficients in the expansion (1.3) for the shape-independent approximation, it is pertinent to ask just how much the data delimit the shape of the nuclear potential. The seemingly obvious method to answer this question is to make a least squares

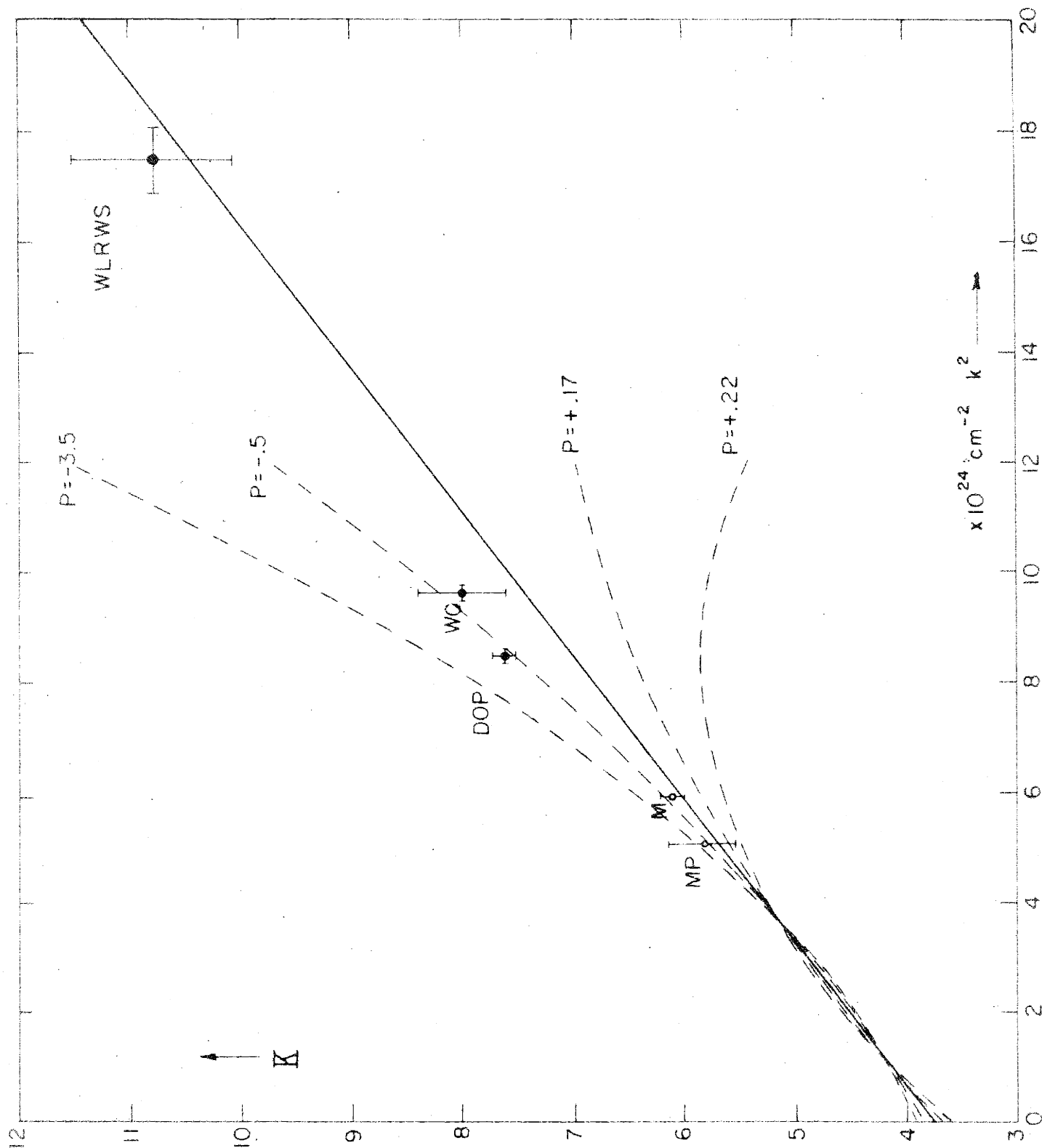


Figure 5.4: Experimental values of K for the cyclotron data plotted against k^2 , with the best shape-independent fit and several parabolic fits to the Van de Graaff data extrapolated.

fit to the data with a polynomial of higher order in k^2 than the linear approximation; and thus determine higher coefficients in the expansion which are sensitive to potential shape. However, the probable errors of the data are so large that such a determination becomes meaningless. One must therefore resort to a somewhat less direct method of approach. For that purpose it was assumed that the terms in k^6 and higher powers of k in (1.3) do not contribute appreciably to the value of K . The one remaining shape-dependent parameter, P , was then assigned various values and least squares fits were made to the data. Two typical "best fit" parabolas are shown in Figure (5.3). These two parabolas, with $P = +.22$ and -3.5 , appear to be excluded by the experimental data. The large asymmetry in the values of P for curves which appear essentially as mirror images of each other in the $P = 0$ (shape independent) curve is due to the fact that the quantity in the expansion (1.3) which determines the curvature is $Pr_0^3 R$, not P . For P negative, the "best" value of r_0 is smaller than for $P = 0$; for P positive, it is larger than for $P = 0$. Hence, to give the same value of $|Pr_0^3 R|$, P will be much larger for negative P (r_0 is smaller) than for positive P (r_0 larger).

The cyclotron data are plotted in Figure (5.4). The point of Meagher at 4.9 Mev is reasonably accurate and is seen to lie fairly close to the extrapolated best linear fit to the Van de Graaff data; it might have been used in the least squares analysis above. However, the other points (except

the DOP point at 7 Mev) are rather inaccurate, and it was felt that until the accuracy of the data obtained with cyclotrons is improved, all cyclotron data should be consistently excluded from any least squares analysis. The peculiarities of the DOP point will be examined below.

In spite of its relatively poor accuracy, the cyclotron data can be used in a qualitative way to narrow the limits on P somewhat. In Figure (5.4), in addition to the best linear fit to the Van de Graaff data extrapolated to higher energies, several "best fit" (to the Van de Graaff data) parabolas are shown for comparison. The data are seen to exclude any large positive value of P, and perhaps any positive value of P. They are also seen to exclude negative values of P as large (negatively) as 3.5. In fact, except for the DOP point at 7 Mev, these data seem to exclude negative P's appreciably greater than 0.5. The DOP point, on the contrary, implies that negative values of P less (in absolute value) than 0.5 should be excluded. Such a conclusion is difficult to reconcile with the other cyclotron data, in particular the WLRWS point at 14.5 Mev, and presents a puzzling situation especially with the accuracy claimed for this measurement. It seems reasonable to ignore the DOP point in this connection, and to say that the cyclotron data indicate that appreciable positive values of P are improbable, and that P lies most likely in the range + 0.15 to -0.8.

For each assumed value of P within a reasonable range

($+ .2$ to -1.0 , as far as the Van de Graaff data alone are concerned), one gets a "best" value for the scattering length a and the effective range r_0 by the least squares fit. The values of a and r_0 can deviate around their "best" values somewhat without destroying the fit to the data entirely. For example, for $P=0$ (shape-independent approximation) the possible deviations are given in (5.3) by the probable errors attached to a and r_0 . One therefore gets an allowed region on a plot of a vs. P and also on a plot of r_0 vs. P . These are shown in Figures (5.5) and (5.6) respectively. The arrows indicate that the deviations from the most probable value are correlated i.e. if one picks a scattering length somewhat smaller (more negative) than the best fit, the corresponding effective range is somewhat larger than the best fit.

It will be seen from Figures (5.5) and (5.6) that the best values of a and r_0 depend considerably on the value assumed for P . In that sense the two term approximation to the series (1.3) is not really shape independent (since $P=0$ in itself implies a certain shape of potential). The reason for this behavior is the fact that there are no data at all at zero energy (unlike neutron-proton scattering where the best data are at zero energy and at the negative energy corresponding to the binding energy of the deuteron), and there are only very inadequate data at energies lower than 800 Kev. From that point of view it might have been advantageous to expand K in a power series in the energy centered

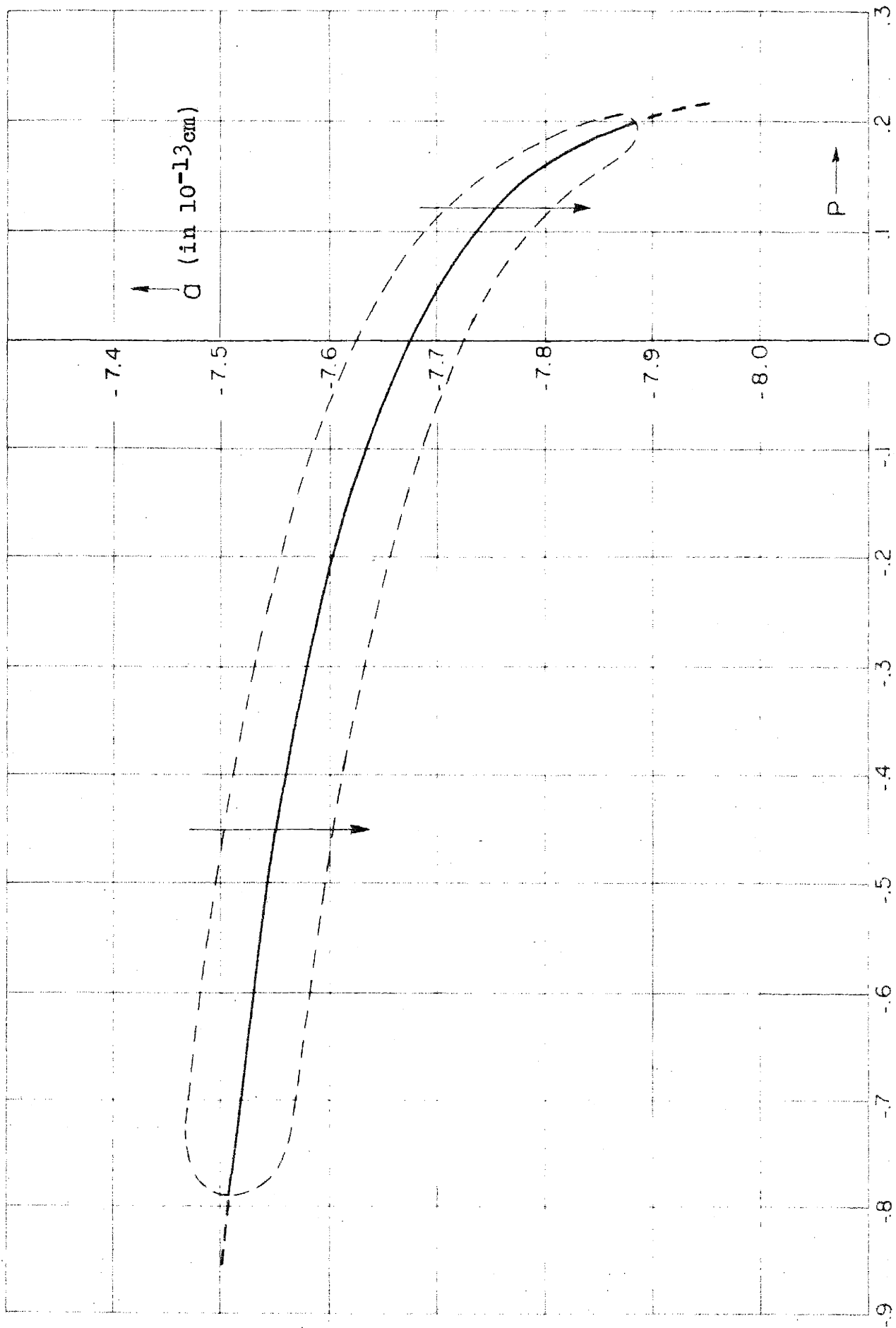


Figure 5.5: Values of the scattering length a implied by experiment (Van de Graaff data) as a function of the well-shape parameter P .

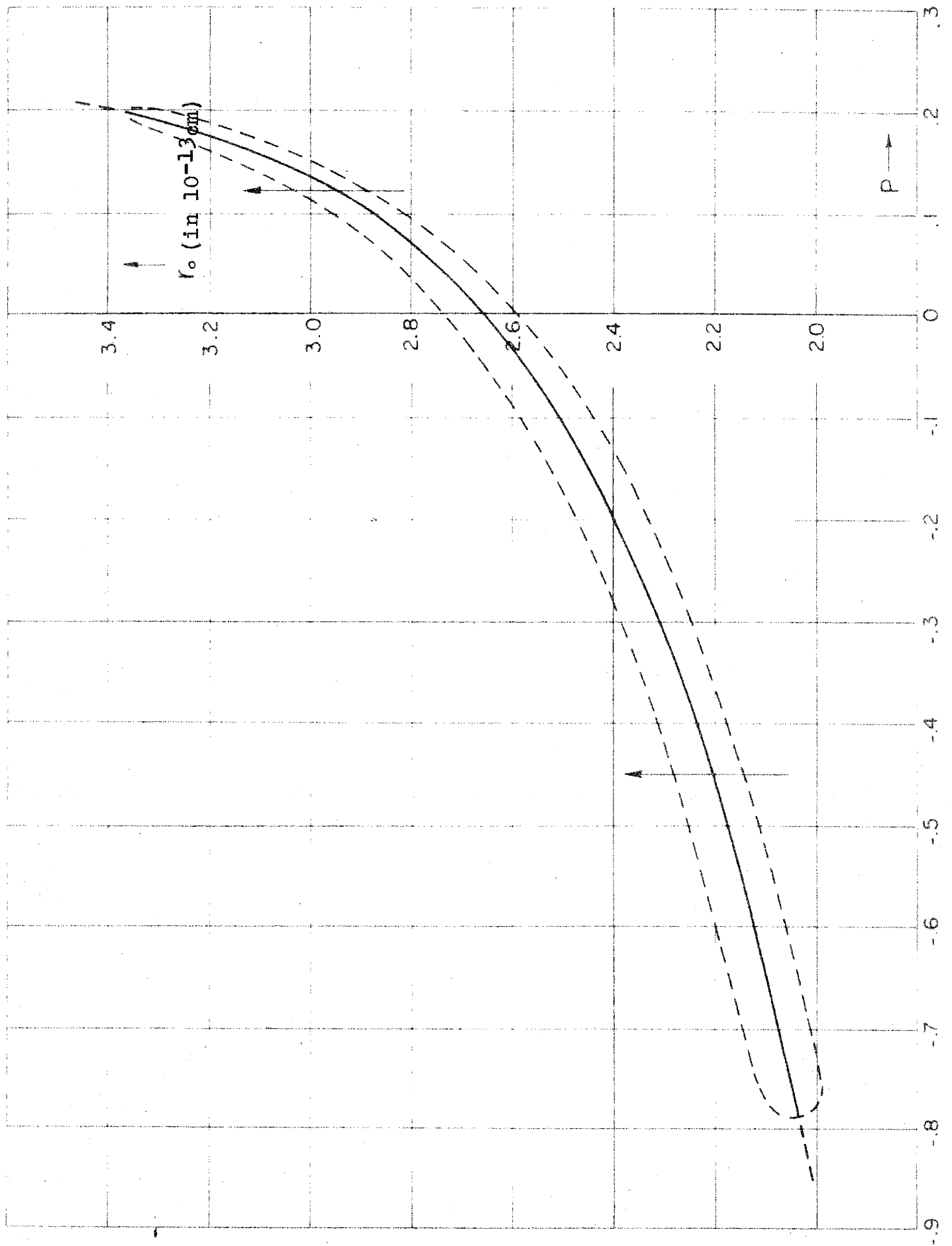


Figure 5.6: Values of r_0 implied by experiment as a function of the well-shape parameter P .

around 2 Mev, say, rather than about zero energy. The two term approximation to a series centered around 2 Mev would really be shape-independent i.e. the coefficients of these two terms would then not depend upon the shape of the well (the value of P). However, even though at present the best data are in the region between one and three Mev, there is no reason why very good data cannot be taken at lower and higher energies. If and when this is done, the choice of 2 Mev. as the center point in an expansion of K will be just as arbitrary (and more tedious from a computing point of view) than the zero energy center chosen here.

As an aid to planning future experiments it is of interest to know how sensitive the function K is to errors in cross section and energy measurements at various scattering angles and energies. For that purpose the quantities $E \left(\frac{\partial K}{\partial E} \right)_{\sigma}$ and $\sigma \left(\frac{\partial K}{\partial \sigma} \right)_E$ have been computed for the energy range up to 10 Mev. These derivatives, when multiplied by the relative error in E and σ respectively, give directly the resulting error in K. The phase shift δ_0 enters these derivatives. As was done for $p_1(\theta)$ etc., the linear approximation to K given in Appendix 2 was used to determine $\delta_0(E)$ over the energy range in question. This will not lead to appreciable error in the results. The quantities $E \left(\frac{\partial K}{\partial E} \right)_{\sigma}$ and $\sigma \left(\frac{\partial K}{\partial \sigma} \right)_E$ are shown in Figures (5.7) and (5.8) for various scattering angles (center of mass) as functions of the energy in the laboratory.

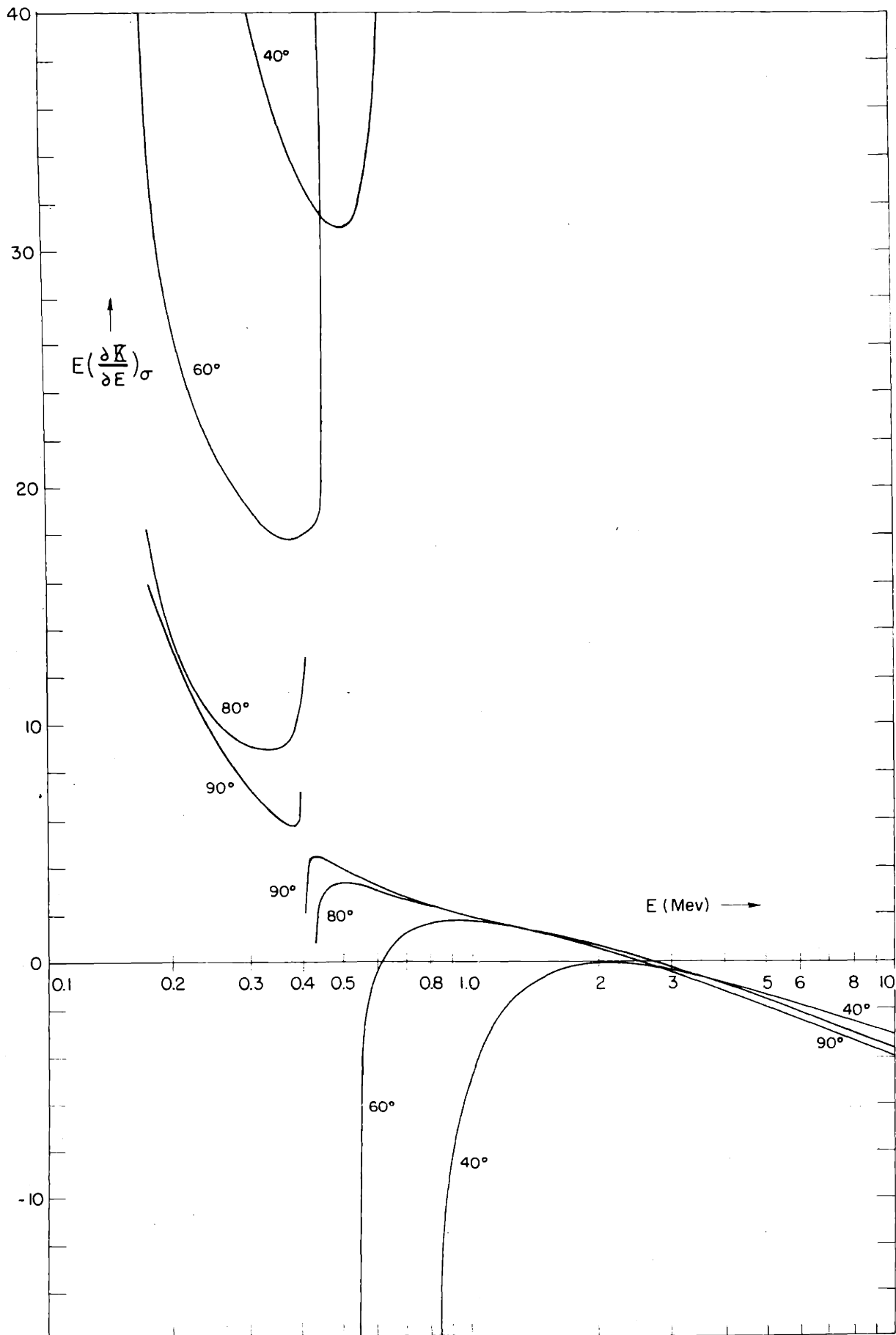


Figure 5.7: The function $E \left(\frac{\partial K}{\partial E} \right)_\sigma$ as a function of energy in the laboratory for various scattering angles. Multiplication by the relative uncertainty in energy gives directly the uncertainty implied in K , assuming the cross section is known exactly.

The curves in both Figures all show a characteristic behavior with energy. The curves of $E \left(\frac{\partial K}{\partial E} \right)_\sigma$ are very similar to those of $\sigma \left(\frac{\partial K}{\partial \sigma} \right)_E$, but with a constant displacement upwards. At a given angle, the curve of $\sigma \left(\frac{\partial K}{\partial \sigma} \right)_E$ decreases with energy to a minimum, then increases rapidly to infinity at a certain energy. Above that energy the function decreases in absolute value from minus infinity, has another minimum, and then increases (negatively) in a regular fashion.

The infinite value of $\sigma \left(\frac{\partial K}{\partial \sigma} \right)_E$ ($E \left(\frac{\partial K}{\partial E} \right)_\sigma$) at a certain energy does not mean that the value of K is infinitely sensitive to errors in cross section (energy) at that energy. Rather, it means that the error in K will be of the order of the square root of the relative error in cross section (energy). This can be seen readily when one considers the cross section as a function of energy and phase shift. At the singularities in $\sigma \left(\frac{\partial K}{\partial \sigma} \right)_E$ the cross section can be shown to be insensitive to first order changes in the phase shift, depending only upon second order variations i.e. $\Delta\sigma \sim (\Delta\delta)^2$. This means that σ is insensitive to first order variations in K (since K is a function of δ and E), and hence $\Delta\sigma \sim (\Delta K)^2$. In consequence, the curves cease to have more than qualitative meaning in the immediate neighborhood of their singularities. Investigation shows that for the $\theta = 90$ degrees curve the region of non-validity is confined to an energy range of ± 15 Kev about the singularity if the relative error in cross section

is less than 10 percent, or ± 10 Kev if the relative error is less than 5 percent. Measurements are not likely to be made at exactly the energies and angles corresponding to these singularities because of the very high accuracy necessary to get useful data. Hence the fact that the curves are not valid in the immediate neighborhood of these points is no serious drawback.

One interesting point is the behavior of $\sigma \left(\frac{\partial K}{\partial \sigma} \right)_E$ at scattering angles near 90 degrees at energies around 400 Kev. This energy range is where the interference between Coulomb and nuclear scattering produces the pronounced minimum in the scattering (see Figure (3.3)). Exactly at the minimum (400 Kev) the value of $\sigma \left(\frac{\partial K}{\partial \sigma} \right)_E$ at $\theta = 90$ degrees becomes infinite. But on either side of the minimum it has a very small absolute value. This means that on either side of the scattering minimum a very precise value of K could be determined with reasonable experimental uncertainties. Long ago, Breit, Thaxton and Eisenbud⁽¹⁾ arrived at what amounts to the same conclusion from a different point of view. Measurements exactly at the minimum (or within five or ten Kev of it) are not useful because of the fact that (1) the errors in K will be proportional to the square root of the relative error in σ (2) the differential cross section itself is extremely small (a few millibarns per steradian) so that accuracy of any sort is very difficult to attain.

Since a very accurate determination of K in the low energy

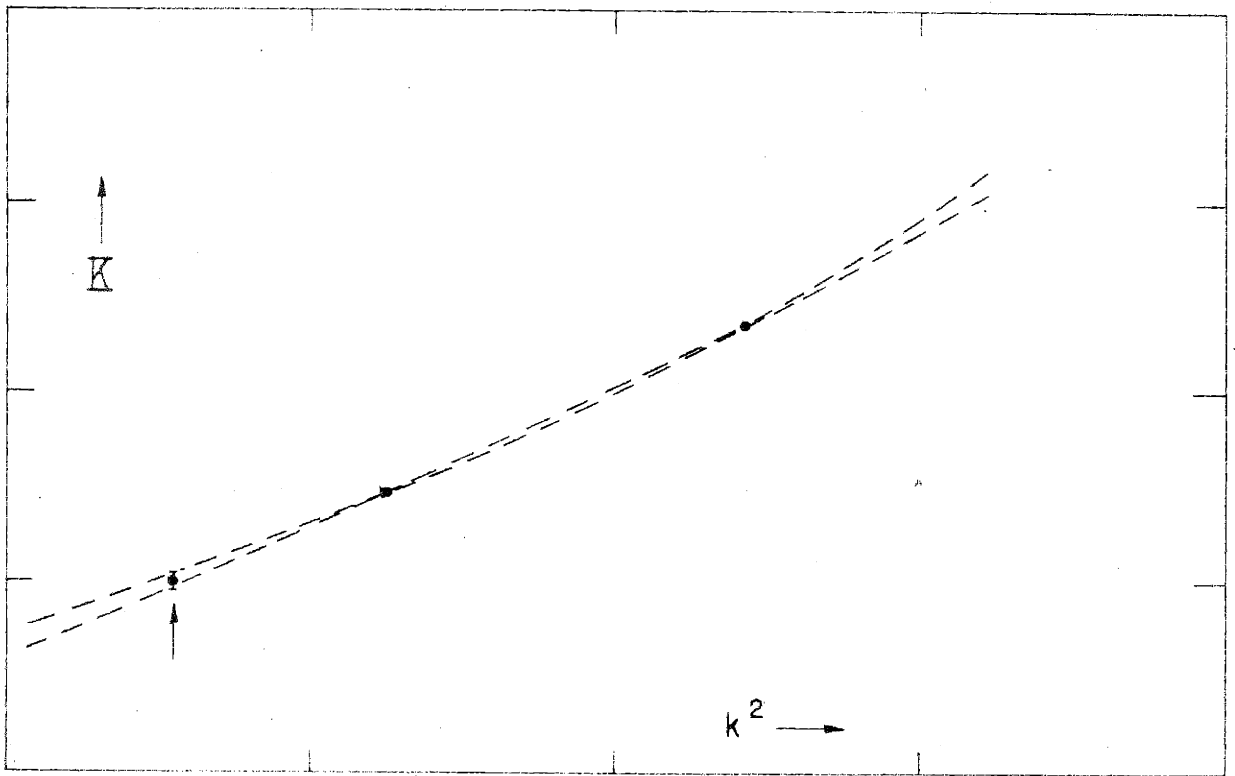
region seems both possible and desirable, it is worthwhile to discuss some of the considerations which enter into the planning of such an experiment. First of all, with present day machines with very good voltage control, it is not too difficult to keep the error in the voltage of the beam low enough so that it does not influence the value of K appreciably. A voltage controlled to $\pm 0.1\%$ is adequate for that purpose (Figure (5.7) shows that the resultant uncertainty in K is about $\pm .005$ which is quite small compared to the errors on the points in Table (4.1)). Second, it is not possible to eliminate certain systematic errors in the calibration of the yield of the apparatus; in particular, the calibration of the current to much better than $\pm 1\%$ seems to present great experimental difficulties. This implies that one should take measurements at energies E not too far removed from the energy E_{\min} of the interference minimum, in order to take full advantage of the small values of $\sigma(\partial K/\partial \sigma)_E$ in that region. Third, the scattering cross section at the minimum energy is very small so that one encounters difficulties due to the low counting rate and due to in-scattering from angles scattering different from 90 degrees (since the scattering cross section is much larger at these other angles). This implies that one should stay away from E_{\min} as much as possible. Clearly, the points 2 and 3 narrow down the useful energy region to two strips at somewhat lower and somewhat higher energy than the interference minimum. There remains

the choice of going either higher or lower in energy than E_{\min} . It appears that the behavior of the cross section as a function of angle implies that one should go to energies somewhat above E_{\min} , since there the cross section is rather flat around $\theta = 90$ degrees, whereas it rises rapidly on both sides of 90 degrees at energies below E_{\min} . Hence in-scattering ought to be a much less serious effect at the higher energies, allowing one to use wider slits and correspondingly greater counting rates. In view of all these considerations, the author would like to recommend measurements of 90 degree scattering in the energy region 420 - 450 Kev with an energy definition of $\pm 0.1\%$ and an overall error in cross section around $\pm 1\%$. In view of the fact that no effects due to waves of higher angular momentum have been found at considerably larger energies, an angular distribution measurement seems to be an unnecessary luxury here.

Figure (5.3) shows that a very accurate point around 400 Kev would narrow down the possible values of the shape-parameter P considerably. Furthermore, it would make the variation of a and r_0 with the choice of P much less pronounced, i.e. the two-term approximation to the series (1.3) would become much more shape-independent.

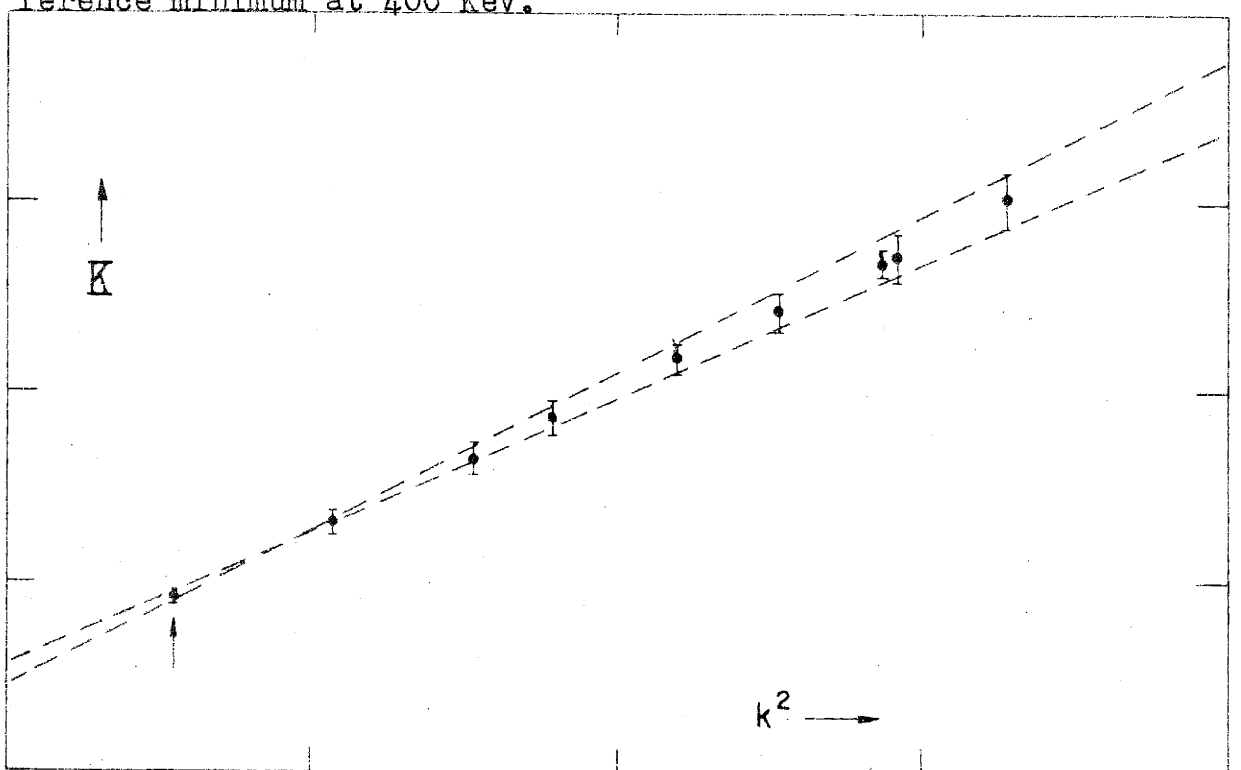
Breit, Broyles and Hull⁽³²⁾ have given arguments for accurate measurements in that same energy region. They claim that such a measurement, in conjunction with the data at higher energies, will allow one to say something quite definite

about the shape of the well. Their argument depends upon adjusting the well constants to fit measurements at 1 and 2 Mev (or 1 and 4 Mev) precisely. In terms of a K vs. k^2 plot, the situation envisaged by these authors is illustrated schematically in Figure (5.9a). The two hypothetical perfect points at one and two Mev, together with a very good actual point around 400 Kev, determine the three parameters of a parabola quite well. However, the author feels that this is not a realistic approach to the actual situation. In reality, the value of K at 400 Kev will soon be known to much higher accuracy than at one or two Mev. The situation will then be as depicted schematically in Figure (5.9b). The measurement at 400 Kev will provide a fulcrum, so to speak, around which a K vs. k^2 plot will turn, but this measurement will not determine the shape of the well to anything like the accuracy envisaged by Breit et. al. Rather one will need to take measurements over a wider range of energies, at least up to 7 or 8 Mev, before the curvature of the K vs. k^2 plot (i.e. the value of P) can be determined with sufficient accuracy to say something about the shape of the potential well. Breit et. al. point out that in order to determine four parameters from the data it is necessary to have two regions of sensitivity, and recommend measurements near 400 Kev plus measurements above 10 Mev for this purpose. However, the analysis presented here shows that to determine even three parameters with any accuracy



(a)

Schematic representation of the situation envisioned by Breit, Broyles, and Hull in recommending measurements near the interference minimum at 400 KeV.



(b)

Schematic representation of the actual situation when measurements at 400 KeV are obtained.

measurements must be taken over an energy range wide enough to bring out the curvature (or lack of it) in the K vs. k^2 plot. In any event, the recommendation made here is in agreement with that made by Breit, Broyles and Hull, even though the opinions as to detailed interpretation differ somewhat.

(6) Landau-Smorodinsky result and an approximate relation
between the neutron-proton and the
proton-proton scattering lengths.

Before describing the variational derivation of the expansion of K (1.3) it is worthwhile because of the qualitative understanding gained to examine the Landau-Smorodinsky result for the energy independent approximation to (1.3), and to make a simple extension of their result in order to relate the neutron-proton singlet scattering length to the proton-proton scattering length for the same nuclear potential.

Outside the range of nuclear forces, the wavefunction of the system of two protons satisfies the Schrodinger equation for a pure Coulomb potential. The partial wave of zero angular momentum satisfies:

$$\left[-\left(\frac{d^2}{dr^2}\right) + \left(\frac{1}{Rr}\right) \right] \varphi(r) = k^2 \varphi(r) \quad (6.1)$$

where $\varphi(r) = r \psi_0(r)$; R was defined in connection with the expansion (1.3); and $k^2 = 2mE/\hbar^2$ is the square of the relative wavenumber. The wave function $\varphi(r)$ for the region outside the range of the nuclear force can be written as:

$$\varphi(r) = G(r) + \cot \delta F(r) \quad (6.2)$$

where $G(r)$ and $F(r)$ are the irregular and regular solutions of the equation (6.1) describing two charged particles in an

S-state under electrostatic interaction only. They go over into sines and cosines in the absence of the Coulomb field (i.e. as $R \rightarrow \infty$).

These solutions have been treated by Yost, Wheeler and Breit⁽³³⁾ and others, and are considered in some detail in Appendix 4 where an expansion in powers of the energy is obtained for $G(r)$ analogous to that deduced by Beckerley⁽³⁴⁾ for $F(r)$. $F(r)$ and $G(r)$ are defined in such a way that they behave for large r ($k^2 R r \gg 1$) like:

$$\begin{aligned} F(r) &\sim \sin (kr - \eta \ln 2 kr + \sigma_0) \\ G(r) &\sim \cos (kr - \eta \ln 2 kr + \sigma_0) \end{aligned} \quad (6.3)$$

where η and σ_0 were defined in Section 2. Note that $F(r)$ is just the function $F_0(r)$ defined by equation (2.12), and that $\Phi(r)$ (6.2) is proportional to the wavefunction (2.16).

δ is interpreted as the phase shift in $\Phi(r)$ caused by the specifically nuclear force i.e. the S-wave phase shift used in the preceding sections.

For small values of r and low energies ($kr \ll 1$ and $r \ll R$) $F(r)$ and $G(r)$ become:

$$\begin{aligned} F(r) &= C kr (1 + r/2R + \dots) \\ G(r) &= 1/C [1 + (r/R) (\ln(r/R) + 2\delta - 1 + h(\eta)) \dots] \end{aligned} \quad (6.4)$$

where

$$c^2 = \frac{2\pi\eta}{e^{2\pi\eta} - 1} \quad (6.5)$$

is the Coulomb penetration factor, and can be interpreted as the relative probability of finding two protons together compared to the probability of finding two uncharged particles together, other things being equal. $h(\eta)$ is given by (5.1), and $\gamma = 0.5772\dots$ is Euler's constant. In the absence of the Coulomb field $c^2 = 1$, $R = \infty$; and $F(r)$ and $G(r)$ in (6.4) go over into the first terms in the expansions of $\sin(kr)$ and $\cos(kr)$, namely kr and 1 respectively.

Landau and Smorodinsky proceed to match the logarithmic derivative of the wave function inside the nuclear potential with the logarithmic derivative of $\Phi(r)$ (6.2) at the boundary of the nuclear potential. r times the logarithmic derivative of $\Phi(r)$ at $r=b$ (the range of the nuclear force) is:

$$r(b) \equiv b \frac{\Phi'(b)}{\Phi(b)} \approx (kb) c^2 \cot \delta + (b/R) (\ln(b/R) + 2\gamma + h(\eta)) \quad (6.6)$$

where terms of order $(kb)^2$ and $(b/R)^2$ etc. have been neglected. The logarithmic derivative of the wavefunction inside $r = b$ is nearly independent of energy for low energies at least,

since the strength of the nuclear potential is much greater than the kinetic energy outside the range of nuclear forces. Therefore $f(b)$ inside is approximated by its value f_0 at $E=0$. Putting (6.6) equal to f_0 , and dividing by b leads to:

$$kC^2 \cot \delta + 1/R [\ln(b/R) + 2\delta + h(\eta)] \approx f_0/b \quad (6.7)$$

Use is made of the relation $2k\eta R = 1$, and the singlet proton-proton scattering length a_p is defined by:

$$a_p^{-1} \equiv -f_0/b + 1/R [\ln(b/R) + 2\delta] \quad (6.8)$$

The result (6.7) can then be written as:

$$K \equiv (\pi \cot \delta) / (e^{2\pi\eta} - 1) + h(\eta) \approx -R/a_p \quad (6.9)$$

(6.9) is the result obtained by Landau and Smorodinsky, and served as the basis of their analysis of the experimental data. The form (6.9) is seen to be the same as the expansion (1.3) in the limit of zero energy.

As was mentioned in Section 1, Landau and Smorodinsky found that the "constant" a_p^{-1} was experimentally very nearly a

linear function of the energy (see Figure (5.3)), and interpreted this correctly as meaning that a range correction was necessary. They also showed that there will be a stable diproton if and only if the proton-proton scattering length is positive. The fact that a is actually negative implies that there cannot be any stable He^2 in nature. The beauty of this argument lies in the fact that nothing need be assumed about the nuclear forces except the experimentally known parameter a .

The neutron-proton formula equivalent to (6.7) is:

$$f/b = k \cot \delta \simeq - a_N^{-1} + \frac{1}{2} r k^2 + \dots$$

so that the neutron-proton scattering length a_N is defined by:

$$a_N^{-1} \equiv -f_N/b \tag{6.10}$$

where f_N/b is the logarithmic derivative of the zero energy neutron-proton wave function at $r=b$ (formally (6.10) can be obtained from (6.8) by letting $R \rightarrow \infty$). As a very crude approximation one would expect that the Coulomb field would have a negligible effect on the wave function so that one could substitute f_N for f_0 in (6.8) to get an approximate relation between the two scattering lengths. However, the terms in R^{-1} in (6.8) are first-order effects due to the Coulomb field so that it is necessary to include the first order change in the logarithmic derivative as well.

The first order change in the logarithmic derivative at $r=b$ due to a change in potential is (see Section 8, in

particular equation (8.3)):

$$u^2(b) \frac{\partial}{\partial \epsilon} \left[\frac{f(b)}{b} \right] = - \int_0^b W'(r) u^2(r) dr \quad (6.11)$$

where $u(r)$ is the wave function inside the range of nuclear forces in the absence of the Coulomb field, and the (attractive) potential is changed from $W(r) \rightarrow W(r) + \epsilon W'(r)$. $W(r) = -\frac{2m}{\hbar^2} V(r)$. If the Coulomb potential is switched on in addition to the nuclear potential, then $W(r) \rightarrow W(r) - 1/Rr$, that is, $\epsilon = 1/R$ and $W'(r) = -1/r$. It is assumed that the nuclear potential stays the same, i.e. the comparison is between scattering lengths for a given nuclear potential in the absence and presence of the Coulomb potential. Consequently, the logarithmic derivative in the proton-proton case is approximately:

$$\frac{f_0(b)}{b} \approx \frac{f_N(b)}{b} + \frac{1}{R} \frac{\partial}{\partial \epsilon} \left[\frac{f(b)}{b} \right] + \dots \quad (6.12)$$

where the quantities on the right hand side involve the neutron-proton wavefunction. To evaluate $\frac{\partial}{\partial \epsilon} \left[\frac{f(b)}{b} \right]$ exactly one must know the wave function for the neutron-proton system inside the range of nuclear forces. However, one can obtain a reasonable approximation by using $u \approx \sin\left(\frac{\pi r}{2b}\right)/b$ in (6.11) (this expression is exact for a square well potential with a depth such that $a_N^{-1} = 0$ i.e. resonance). The result is:

$$\frac{\partial}{\partial \epsilon} \left[\frac{f(b)}{b} \right] \approx \frac{1}{2} \left[\ln \pi + \gamma - \text{Ci}(\pi) \right] = 0.8241$$

where $\text{Ci}(x)$ is the cosine integral. Thus the logarithmic derivative (6.12) is given by:

$$\frac{f_0(b)}{b} \approx -a_N^{-1} + \frac{1}{R} (0.824) \quad (6.13)$$

The proton-proton scattering length a_p (6.8) is:

$$\begin{aligned} a_p^{-1} &\approx a_N^{-1} + \frac{1}{R} \left[\ln \left(\frac{b}{R} \right) + 2\gamma - 0.824 \right] \\ &\approx a_N^{-1} + \frac{1}{R} \left[\ln \left(\frac{b}{R} \right) + 0.330 \right] \end{aligned} \quad (6.14)$$

where a_N is the corresponding neutron-proton scattering length for the same nuclear potential, and b is the "range" of the nuclear force. Estimates show that this relation (6.14) is valid to within about 2.5 percent for the commonly assumed potentials which fit the proton-proton scattering data (see Section 9). The values obtained for a_p are low in absolute value by about 2.5 percent for the square well, and high in absolute value by the same amount for the Yukawa well. For these numerical estimates the value of b was taken to be equal to the intrinsic range of the potential as defined in reference (2).

Bethe ⁽⁷⁾ has obtained a relation quite similar to (6.14) from somewhat different considerations, based on the fact that at some distance of the order $\frac{1}{2}b$ the logarithmic derivatives of the proton-proton wave function and the neutron-proton wave function are equal.

Chew and Goldberger ⁽⁸⁾ have given a more exact relation than (6.14), taking into account higher order changes due to the Coulomb field. When more accurate estimates of the scattering lengths are needed, one must resort to their formula, or to the results of Section 9. However, (6.14) allows a rapid comparison of scattering lengths and is useful as a first approximation.

The fact that an approximation for a_p accurate to only a few percent is at all useful is connected with the closeness of the scattering to a "resonance at zero energy" ($a_p^{-1} = 0$). The value of a_p is large compared to the range of the forces. In consequence, a small change in the force strength implies a large change in the scattering length. Conversely, an error of a few percent in the comparison of scattering lengths for proton-proton and neutron-proton (singlet) scattering implies an error of only a few tenths of a percent in the comparison of the force-strengths..

(7) The variational principle for scattering and the expansion (1.3)

Since a detailed derivation of the Schwinger variational method for scattering problems has been given in an earlier paper on neutron-proton scattering⁽²⁾, it will suffice to restrict the presentation to the special features which show up when the method is applied to proton-proton scattering. It will be assumed that there is only S-wave nuclear scattering in addition to the Coulomb interaction. The quantity of interest is the nuclear scattering. Accordingly, the asymptotic wave function (outside the range of the nuclear force) will be made up of the Coulomb wave functions (6.3) in the linear combination (6.2) with the nuclear phase shift δ describing the effect of the nuclear potential.

The differential equation satisfied by the radial wave function $u(r) = r \Psi_0(r)$ is:

$$\left[-\frac{d^2}{dr^2} - k^2 + \frac{1}{Rr} \right] u(r) = W(r)u(r) \quad (7.1)$$

where $W(r)$ is related to the nuclear potential $V(r)$ through

$$W(r) = -\frac{2m}{\hbar^2} V(r) = -\frac{M}{\hbar^2} V(r) \quad (7.2)$$

M being the mass of the proton. $W(r)$ is assumed to approach zero rapidly outside the range b of the nuclear force.

In analogy with the derivation in reference (2) one introduces a Green's function $K(r, r')$ for the left hand side of (7.1). $K(r, r')$ satisfies the equation:

$$\left[-\frac{d^2}{dr^2} - k^2 + \frac{1}{Rr} \right] K(r, r') = \delta(r - r') \quad (7.3)$$

and is given by:

$$K(r, r') = \frac{1}{k} F(r_{<}) G(r_{>}) \quad (7.4)$$

where $F(r)$ and $G(r)$ are the Coulomb functions (6.3), and $r_{<}$ means the smaller of r and r' , $r_{>}$ means the greater of r and r' . The derivation then proceeds just as before with sines and cosines replaced by $F(r)$ and $G(r)$, respectively. The result for the variational principle is:

$$k \alpha \delta = \frac{\int_0^{\infty} W(r) u^2(r) dr - \int_0^{\infty} dr \int_0^{\infty} dr' W(r) u(r) K(r, r') W(r') u(r')}{\left[\frac{1}{k} \int_0^{\infty} W(r) u(r) F(r) dr \right]^2} \quad (7.5)$$

(7.5) is stationary with respect to first-order changes in $u(r)$, as can be shown by direct substitution.

To obtain an expansion of the form (1.3) from (7.5) it will be necessary to have expansions of the Coulomb wave functions in powers of k^2 . As was mentioned in Section 6, considerable work has been done on these functions. The main results of interest are given in Appendix 4. Several combinations of Bessel functions arise in these expansions. To be consistent, the following convention will be adopted: all the auxiliary functions defined below approach unity at $r = 0$. Furthermore, in the limit $R \rightarrow \infty$ and $\eta \rightarrow 0$ (i.e. in the limit of neutron-proton scattering) all these functions can be replaced by unity. Since the expansions for $F(r)$ and $G(r)$ must reduce in that limit to the well-known power series expansions of $\sin(kr)$ and $\cos(kr)$, respectively, this gives a simple way of checking these more complicated expansions. The following auxiliary functions will be needed (see Appendix 4):

$$L_n(r) = n! (r/R)^{-\frac{1}{2}n} I_n(2\sqrt{r/R}) \quad (7.6)$$

$$H_n(r) = \frac{2}{(n-1)!} (r/R)^{\frac{1}{2}n} K_n(2\sqrt{r/R}) \quad (7.7)$$

$$M(r) = \frac{2}{3} \frac{R}{r} [L_1(r) - H_2(r)] = 1 - 4r/9R - \dots + \\ + (r/3R) (\log(r/R) + 2\gamma) + \dots \quad (7.8)$$

Here $I_n(z)$ and $K_n(z)$ are modified Bessel functions defined in Watson. (35)

In terms of the auxiliary functions (7.6) - (7.8) and the penetration factor defined in (6.5), the Coulomb wave-functions $F(r)$ and $G(r)$ can be expanded as follows:

$$F(r) = C k r \left[L_1(r) - (1/6)(kr)^2 L_2(r) + \dots \right] \quad (7.9)$$

$$G(r) = C^{-1} \left[H_1(r) - \frac{1}{2} (kr)^2 M(r) + \dots \right] + \\ + C^{-1} h(\eta) (r/R) \left[L_1(r) - (1/6) (kr)^2 L_2(r) + \dots \right] \quad (7.10)$$

(7.9) obviously reduces to the expansion of $\sin(kr)$ in the limit of neutron-proton scattering. The first line of equation (7.10) reduces to the expansion of $\cos(kr)$ in the same limit, while the coefficient of the series in the second line of (7.10) approaches zero (the function $h(\eta)$ was defined earlier, equation (5.1)).

The shielding effect of the Coulomb field enters mostly through the penetration factor C . There is an additional differential shielding effect which depends upon the distance r ; it appears through the auxiliary functions (7.6) - (7.8). However, the expansions given in Appendix 4 show that these auxiliary functions are quite closely equal to unity for values of r much less than R . This is due to the fact that the Coulomb

potential at these distances varies very rapidly compared to the deBroglie wavelength of the protons; hence the potential does not exert anywhere near as large an effect on the wavefunction in that region as one would estimate by just looking at its absolute value. This behaviour of the Coulomb wavefunctions implies that there is very little differential shielding of the nuclear potential as long as its range is small compared to R ; i.e. either all of the nuclear potential is shielded or none of it, (rather than, say, the tail being accessible while the main inside part of the potential is shielded.)

The variational principle (7.5) can be used to obtain a simple expression such as (1.3) for the energy dependence of the phase shift δ . To do this, the wave function $u(r)$ in (7.5) is replaced by a trial wave function $u_0(r)$ which is the correct expression for $u(r)$ at some particular energy, say k_0^2 . Then the error in $k \cot \delta$ will be in the terms proportional to the square of the difference in the energies (i.e. in the coefficient of $(k^2 - k_0^2)^2$) because of the stationary property of (7.5). It is most convenient to choose $u_0(r)$ appropriate to zero energy, and to expand (7.5) in powers of k^2 , retaining the first two terms (since the terms in k^4 and higher are in error). This will be the "shape-independent" approximation discussed above.

The two independent solutions of the equation for a free particle at zero energy are l and r . The corresponding solu-

tions for a particle of zero energy in a pure Coulomb field (i.e. solutions of equation (7.1) with $k^2 = 0$ and $W(r) = 0$) are $H_1(r)$ and $rL_1(r)$. Hence the correct wavefunction (including the effect of the nuclear potential) at zero energy will behave in the "outside" region (beyond the range of the nuclear forces) like

$$u_0(r) \sim H_1(r) - (r/a) L_1(r) \equiv \varphi_0(r) \text{ for } r \gg b \quad (7.11)$$

The quantity a defined by this equation is the proton-proton scattering length which enters into the expansion (1.3).

(7.11) can be obtained from (6.2) in the limit $k^2 \rightarrow 0$. The zero energy wave function $u_0(r)$ is conveniently written in the form:

$$\begin{aligned} u_0(r) &= H_1(r) - (r/a)L_1(r) - g(r) \\ &\equiv \varphi_0(r) - g(r) \end{aligned} \quad (7.12)$$

The function $g(r)$ defined in this way is unity at the origin and approaches zero rapidly outside the range of the nuclear force. $u_0(r)$ is then substituted for the correct $u(r)$ into (7.5). The manipulation of the integrals is completely analogous to that given in reference (2). To terms of order k^2 inclusive, the numerator N of (7.5) becomes:

$$N \approx -\frac{h(\eta)}{R} - a^{-1} + k^2 \int_0^{\infty} \left[2H_1(\kappa) + 2\frac{h(\eta)}{R} \kappa L_1(\kappa) - g(\kappa) \right] g(\kappa) d\kappa \quad (7.13)$$

while the denominator D reduces to:

$$D \approx c^2 \left[1 - 2k^2 \int_0^{\infty} \kappa L_1(\kappa) g(\kappa) d\kappa \right] \quad (7.14)$$

The combination of (7.13) and (7.14) gives the shape-independent approximation:

$$c^2 k \cot \delta = -\frac{h(\eta)}{R} - \frac{1}{a} + \frac{1}{2} r_0 k^2 + O(k^4) \quad (7.15)$$

where the effective range r_0 for proton-proton scattering is:

$$r_0 = 2 \int_0^{\infty} \left[\varphi_0^2(\kappa) - u_0^2(\kappa) \right] d\kappa \quad (7.16)$$

(7.15) clearly reduces to the first two terms of the expansion (1.3). This result was first derived by Schwinger⁽⁴⁾.

The next step is to derive the expressions for the k^4 and the k^6 terms in the expansion of K (1.3). Since (7.5) is a variational expression for $k \cot \delta$, an error of order k^4 in the trial wave function implies an error of order k^8 in the result for $k \cot \delta$. Hence one can obtain the terms to order k^6 inclusive in the expansion of $k \cot \delta$ by the use of a trial wave function correct to order k^2 only. The non-vari-

tional derivation (7,8) of the expansion (1.3) would lead one to suspect that a knowledge of the wavefunction to order k^{2n} gives the coefficients in (1.3) only up to the order k^{2n+2} whereas actually it gives the coefficients up to order k^{4n+2} . This statement does not imply that these coefficients cannot be derived directly from the differential equation without variation principles. However, the derivation then involves integrations by parts which are not always obvious. The variational approach makes it perfectly evident that the corresponding expressions must exist, even though the detailed derivation is slightly more lengthy.

Unlike the work of reference (2), the integral equation will not be used to iterate on the wavefunction. Rather, use will be made of the differential equation directly. The wavefunction $u(r)$ is written as an expansion in k^2 :

$$u(r) = u_0(r) + k^2 v_1(r) + k^4 v_2(r) + \dots \quad (7.17)$$

where only the first two terms need be considered in order to obtain terms up to k^6 in the expansion (1.3). Substitution of (7.17) into the differential equation (7.1) and the equating of coefficients in k^2 leads to the differential equation for $v_1(r)$:

$$\left[-\frac{d^2}{dk^2} + \frac{1}{Rk} - W(k) \right] v_1(k) = u_0(k) \quad (7.18)$$

This equation must be solved (usually numerically) subject to the initial condition $v_1(0) = 0$. The solution is then defined up to the addition of an arbitrary constant multiple of $u(r)$ which can be easily shown⁽²⁾ to be equivalent to a change of normalization of the trial wave function and hence without influence on the final result. It is convenient to normalize $u(r)$ (i.e. $v_1(r)$ in this case) and its asymptotic form $\varphi(r)$ so that:

$$\varphi(r) = C G(r) + C \cot \delta F(r) \quad (7.19)$$

If one writes:

$$\varphi(r) = \varphi_0(r) + k^2 \chi_1(r) + k^4 \chi_2(r) \dots \quad (7.20)$$

then $\varphi_0(r)$ is given by (7.11) as before, while the asymptotic form of $v_1(r)$ is:

$$v_1(r) \sim \chi_1(r) \equiv \frac{1}{2} r_0 r L_1(r) - \frac{1}{2} r^2 M(r) + \frac{r^3}{6a} L_2(r) \quad (7.21)$$

In numerical integration of (7.18) the solution obtained will, in general, be of the form, asymptotically:

$$\chi_1(r) + A \varphi_0(r) = D H_1(r) + E r L_1(r) - \frac{1}{2} r^2 M(r) + r^3 / 6a L_2(r)$$

From (7.11) and (7.21) it is apparent that the following relations hold:

$$A = D, \quad \frac{r_0}{2} = E + \frac{D}{a} \quad (7.22)$$

Since r_0 has previously been determined by use of $u_0(r)$ in (7.16) and a is known if $u_0(r)$ is known, the relations (7.22) provide a valuable check on the results of the numerical integration for $v_1(r)$. The convenient normalization for $v_1(r)$ given by (7.19) and (7.21) is readily obtained by subtracting $A \varphi_0(r)$ from the result of the numerical integration.

In analogy to the derivation of the shape-independent approximation, the first two terms of (7.17) are substituted into (7.5) as an approximation to $u(r)$. In the reduction of (7.5) to the form (1.3) it is convenient to define the function $z(r)$ in analogy to $g(r)$ by the equation:

$$z(r) \equiv \chi_1(r) - v_1(r) \quad (7.23)$$

$z(0) = 0$, and $z(r)$ rapidly goes to zero outside the range of nuclear forces. From (7.18) it is easy to show that $z(r)$ satisfies:

$$\left(\frac{d^2}{dr^2} - \frac{1}{Rr} \right) z(r) + g(r) = W(r) v_1(r) \quad (7.24)$$

The numerator N of (7.5), after some integrations by parts, can be written as:

$$N = \int_0^{\infty} W(r)u(r) [u(r) - J(r)] dr \quad (7.25)$$

where $J(r) = CG(r) - g(r) - k^2 z(r)$

$$- k^4 \int_0^{\infty} K(r,r')z(r')dr' \quad (7.26)$$

Use of the differential equations satisfied by $g(r)$ and $z(r)$, together with further integrations by parts, yields:

$$\begin{aligned} N \approx & -\frac{h(\eta)}{R} - a^{-1} + \frac{1}{2} \mu_0 k^2 + \\ & + k^4 \int_0^{\infty} \left[\chi_1(\mu)g(\mu) + z(\mu) \left\{ H_1(\mu) - g(\mu) + 2 \left(\frac{h(\eta)}{R} + \frac{a^{-1}}{2} \right) \mu L_1(\mu) \right\} \right] d\mu \\ & - k^6 \int_0^{\infty} z(\mu) \left[z(\mu) + \frac{2\mu^2}{2} M(\mu) + \frac{2h(\eta)}{R} \frac{\mu^3}{6} L_2(\mu) \right] d\mu \end{aligned} \quad (7.27)$$

up to order k^6 inclusive.

The denominator D is the square of the integral:

$$D^{\frac{1}{2}} = \frac{1}{k} \int_0^{\infty} F(r)W(r)u(r)dr$$

Integration by parts leads to:

$$D^{\frac{1}{2}} = C \left[1 - k^3 \int_0^{\infty} \frac{F(r)}{C} z(r)dr \right]$$

Inserting the expansion (7.9) for $F(r)$, it is found that to order k^6 inclusive the reciprocal of the denominator is:

$$D^{-1} \approx \frac{1}{c^2} \left[1 + 2k^4 \int_0^{\infty} z(\lambda) \lambda L_1(\lambda) d\lambda - \right. \\ \left. - 2k^6 \int_0^{\infty} z(\lambda) \frac{\lambda^3}{6} L_2(\lambda) d\lambda \right] \quad (7.28)$$

Combination of (7.27) and (7.28) leads to the result:

$$c^2 k \cot \delta + \frac{h(\eta)}{R} = -\frac{1}{a} + \frac{1}{2} r_0 k^2 - \\ - Pr_0^3 k^4 + Qr_0^5 k^6 + \dots \quad (7.29)$$

where a is defined by (7.11), r_0 is given by (7.16), and

$$Pr_0^3 = \int_0^{\infty} [z(\lambda) \{z(\lambda) - \chi_1(\lambda)\} - \varphi_0(\lambda) z(\lambda)] d\lambda \\ = - \int_0^{\infty} [\varphi_0(\lambda) \chi_1(\lambda) - u_0(\lambda) \nu_1(\lambda)] d\lambda \quad (7.30)$$

and

$$Qr_0^5 = \int_0^{\infty} [2\chi_1(\lambda) - z(\lambda)] z(\lambda) d\lambda \\ = \int_0^{\infty} [\chi_1^2(\lambda) - \nu_1^2(\lambda)] d\lambda \quad (7.31)$$

(7.29) is seen to be just the expansion (1.3) for $K(1.2)$, correct to terms in k^6 inclusive.

In reference (2) the expansion for $k \cot \delta$ and the variational parameters a and r_0 were used to define an "intrinsic range" and a "well-depth parameter" for the nuclear potential. A similar specification could be made here for the proton-proton system. However, the need for two sets of parameters to describe the same nuclear potential, depending upon whether the Coulomb field is switched on or off, is seen to be unnecessary and superfluous. In addition, a range defined in analogy with the neutron-proton intrinsic range would not be an intrinsic property of the nuclear potential since another length would enter in, namely the characteristic length R of the Coulomb field. Accordingly, use will be made of the conventions of reference (2) as to the specification of the nuclear potentials. It should be remembered that a well with well-depth parameter $s=1$ does not lead to a zero energy resonance in proton-proton scattering (i.e. the proton-proton scattering length is not infinite). Rather, a well with $s=1$ would lead to a resonance at zero energy in the absence of the Coulomb field.

(8) The effect of small changes in the potential on the variational parameters

Unlike neutron-proton scattering, the data in proton-proton scattering are sufficiently accurate and sufficiently easy to interpret (only one phase shift at low energies) so that the effective range and scattering length are known with reasonable accuracy (see Section 5). Hence it is advantageous to make calculations with each potential shape for only one choice of the intrinsic range b and well-depth parameter s , and to find a and r_0 for slightly different choices of b and s by a perturbation calculation.

The variational principle (7.5) provides an easy means of getting the answer. Assume that one knows the wavefunction $u(r)$ appropriate to a potential $W(r)$. Now consider scattering due to the modified potential $W(r) + \epsilon W'(r)$ where ϵ is a small number. The correct wavefunction for this modified potential will differ from $u(r)$ by terms of order ϵ . Since (7.5) is a variational expression for $k \cot \delta$, one will obtain $k \cot \delta$ correct to terms of order ϵ inclusive by substituting the unperturbed wavefunction $u(r)$ instead of the correct wavefunction. Hence one can get the first order change of $k \cot \delta$ with a small change in the potential directly from the unperturbed wavefunction, by a process of quadratures only.

There is one caution to be observed here. The trial wavefunction which is going to be substituted into (7.5)

differs from the true wavefunction for two reasons: (1) it is not correct for the energy in question i.e. it will differ from the true $u(r)$ in the unperturbed potential by terms of order k^{2n+2} (2) it is a wavefunction appropriate to the unperturbed potential rather than the perturbed potential, i.e. it differs from the true $u(r)$ by terms of order ϵ . The error in $k \cot \delta$ will be of the order of the square of the error in the trial wavefunction, i.e. it will be of order

$$(k^{2n+2} + \epsilon)^2 = k^{4n+4} + 2\epsilon k^{2n+2} + \epsilon^2$$

The occurrence of errors of order k^{2n+2} shows that a wavefunction correct to order k^{2n} will give the change of the variational parameters with small changes in the potential only up to the coefficients of k^{2n} , whereas it will give the parameters in the unperturbed potential ($\epsilon = 0$) up to the coefficients of k^{4n+2} .

In particular, the numerical wave functions have been calculated up to order k^2 inclusive (i.e. $u_0(r)$ and $v_1(r)$ are known in each case). Hence one can get a , r_0 , P , Q for the unperturbed potential, and $\partial a / \partial \epsilon$, $\partial r_0 / \partial \epsilon$ for small changes in the potential. Since the terms with P and Q already are quite small corrections to the value of K , this is not a serious shortcoming. The calculations of reference (2) have shown that P , at any rate, is a slowly varying function of the well-parameters s and b . Accordingly it seems to be perfectly reasonable to use the unperturbed values of P and

Q for the perturbed potentials. This procedure will give much better accuracy than necessary for the interpretation of the experimental data.

The result for the changes in a and r_0 due to a small change in the potential can be obtained in another way. This method has been employed by Breit⁽¹⁾ in another connection, and is closely related to the derivation of the expansion (1.3) by Bethe⁽⁷⁾. It is of use in the extension of the Landau-Smorodinsky result made in Section 6 (see equation (6.11)). The quantity of interest is the logarithmic derivative of the radial wave function $u(r)$ at some position r_1 , and its variation with a change in the potential, $W(r) \rightarrow W(r) + \epsilon W'(r)$. The differential equation satisfied by $u_1(r)$ (where $u_1(r)$ refers to the original potential) is:

$$\left[-\frac{d^2}{d\mu^2} + \frac{1}{R\mu} - W(\mu) \right] u_1(\mu) = k^2 u_1(\mu) \quad (8.1)$$

while $u_2(r)$, the wave function for the altered potential, satisfies:

$$\left[-\frac{d^2}{d\mu^2} + \frac{1}{R\mu} - W(\mu) - \epsilon W'(\mu) \right] u_2(\mu) = k^2 u_2(\mu) \quad (8.2)$$

Multiplication of (8.1) by $u_2(r)$, (8.2) by $u_1(r)$, integration from 0 to r_1 , and subtraction in the usual way leads to:

$$\int_0^{r_1} \left[u_1 \frac{d^2 u_2}{dr^2} - u_2 \frac{d^2 u_1}{dr^2} \right] dr = -\epsilon \int_0^{r_1} W'(r) u_1(r) u_2(r) dr$$

Integration by parts on the left hand side yields:

$$u_1 u_2 \left[\frac{1}{u_2} \frac{du_2}{dr} - \frac{1}{u_1} \frac{du_1}{dr} \right] = -\epsilon \int_0^{r_1} W'(r) u_1(r) u_2(r) dr$$

Or, in the limit as $\epsilon \rightarrow 0$,

$$u^2 \frac{d}{d\epsilon} \left(\frac{1}{u} \frac{du}{dr} \right) = - \int_0^{r_1} W'(r) u^2(r) dr \quad (8.3)$$

where the left hand side is evaluated at $r=r_1$.

If $r_1 \gg b$, then $u(r_1) \rightarrow \varphi(r_1)$, given by (7.19). It should be noted, however, that in evaluating the derivative with respect to ϵ on the left side of (8.3) it is necessary to write:

$$C^2 k \cot \delta = (C^2 k \cot \delta)_{\epsilon=0} + \epsilon \frac{d}{d\epsilon} (C^2 k \cot \delta) + \dots$$

to account for the change in phase shift produced by $\epsilon W'(r)$.

When (7.19) is substituted into (8.3) on the left side, the result, correct to zero order in ϵ , is:

$$u^2 \frac{\partial}{\partial \epsilon} \left(\frac{1}{u} \frac{du}{d\kappa} \right) = \frac{1}{R} \left[G \frac{dF}{d\kappa} - \frac{dG}{d\kappa} F \right] \frac{\partial}{\partial \epsilon} (c^2 k \cot \delta)$$

The Wronskian condition on F and G is $[GF' - FG'] = k$, so that:

$$u^2 \frac{\partial}{\partial \epsilon} \left(\frac{1}{u} \frac{du}{d\kappa} \right) = \frac{\partial}{\partial \epsilon} (c^2 k \cot \delta) = \frac{1}{R} \frac{\partial K}{\partial \epsilon}$$

since $RC^2 k \cot \delta + h(\eta) = K$. The upper integration limit in (8.3) can be taken as infinity, since $W'(r)$ is assumed to vanish rapidly for $r_1 \gg b$. Therefore the first-order variation of K (1.2) due to a change $W(r) \rightarrow W(r) + \epsilon W'(r)$ in the potential is:

$$\frac{\partial K}{\partial \epsilon} = -R \int_0^{\infty} W'(r) u^2(r) dr \quad (8.4)$$

If the expansion (7.17) of $u(r)$ in powers of k^2 is inserted in (8.4), the result for the first order change in the coefficients a and r_0 is:

$$\begin{aligned} \frac{\partial}{\partial \epsilon} \left(\frac{1}{a} \right) &= \int_0^{\infty} W'(r) u_0^2(r) dr \\ \frac{\partial r_0}{\partial \epsilon} &= -4 \int_0^{\infty} W'(r) u_0(r) v_1(r) dr \end{aligned} \quad (8.5)$$

Accordingly, the changed coefficients a' and r'_0 have the form:

$$\begin{aligned} a' &= a - \epsilon a^2 \int_0^{\infty} W'(r) u_0^2(r) dr \\ r'_0 &= r_0 - 4 \epsilon \int_0^{\infty} W'(r) u_0(r) v_1(r) dr \end{aligned} \quad (8.6)$$

Of particular interest are the variations in a and r_0 due to changes in the well depth parameter s and in the intrinsic range b of the nuclear potential. $W(r)$ can be written for each well shape in the standard form:

$$W(r) = s b^{-2} f(r/b) \quad (8.7)$$

where $f(x)$ specifies the well shape. A change in the well-depth parameter s by an amount Δs leads to a perturbed potential of the form:

$$W(r) + \epsilon W'(r) = W(r) + \frac{\Delta s}{s} W(r) \quad (8.8)$$

If the small change consists of a change in the intrinsic range b by an amount Δb , the perturbed potential is:

$$W(r) + \epsilon W'(r) = W(r) - \frac{\Delta b}{b} \left[2W(r) + s b^{-2} \left(\frac{r}{b} \right) f' \left(\frac{r}{b} \right) \right] \quad (8.9)$$

where $f'(x)$ is the derivative of $f(x)$. With equations (8.5)-(8.9) the quantities $\left(\frac{\partial a}{\partial s} \right)$, $\left(\frac{\partial r_0}{\partial s} \right)$, $\left(\frac{\partial a}{\partial b} \right)$, $\left(\frac{\partial r_0}{\partial b} \right)$ can be readily calculated.

(9) Numerical results for various potential shapes and comparison with experiment.

The variational parameters and their derivatives with respect to small changes in the potential have been calculated for the four usual choices of potential (square, Gaussian, exponential and Yukawa wells). It should be remarked that, although the calculations have been performed only for static potentials, the expansion (1.3) is valid for more general interactions described by Wheeler's velocity-dependent forces⁽³⁶⁾. This is apparent in view of the fact that the expressions (7.16), (7.30), (7.31) for the coefficients involve integrals over the wave functions only; the potential $W(r)$ does not appear explicitly⁽²⁾.

For the sake of convenience, the specification of $W(r)$ and $V(r)$ given in reference (2) will be repeated here:

$$\begin{aligned}
 \text{Square well} \quad W(r) &= s \left(\frac{\pi}{2}\right)^2 b^{-2} \quad (r < b); \quad W(r) = 0 \quad (r > b) \\
 \text{Gaussian well} \quad W(r) &= s b^{-2} (5.5296) \exp \left[-2.0604 \left(\frac{r}{b}\right)^2 \right] \\
 \text{Exponential well} \quad W(r) &= s b^{-2} (18.1308) \exp(-3.5412 r/b) \\
 \text{Yukawa well} \quad W(r) &= s b^{-2} (3.5605) (b/r) \exp(-2.1196 r/b)
 \end{aligned} \tag{9.1}$$

Here $W(r)$ is in cm^{-2} if b is given in cm. The conversion to energy units is slightly different from the neutron-proton case because the reduced mass in the neutron-proton case differs slightly from the reduced mass in the proton-proton case (i.e. from $\frac{1}{2} M_p$). Since the neutron-proton mass-difference is very small, this change in the conversion to energy units has no practical significance in the interpretation of

scattering experiments. Below are the expressions for the potential $V(r)$ in Mev under the assumption that b is measured in units of 10^{-13} cm, correct for proton-proton scattering:

$$\begin{aligned}
 \text{Square well } V(r) &= -s b^{-2} (102.35) \quad (r < b); \quad V(r) = 0 \quad (r > b) \\
 \text{Gaussian well } V(r) &= -s b^{-2} (229.37) \exp \left[-2.0604 (r/b)^2 \right] \\
 \text{Exponential well } V(r) &= -s b^{-2} (752.06) \exp(-3.5412 r/b) \\
 \text{Yukawa well } V(r) &= -s b^{-2} (147.69) (b/r) \exp(-2.1196 r/b)
 \end{aligned} \tag{9.2}$$

The conversion factor used was $\hbar^2/M_p = 41.480 \times 10^{-26} \text{ Mev} \times \text{cm}^2$. For the Yukawa well, the equivalent meson mass is $\mu = 818.57 b^{-1} m_e$.

In the calculations the Coulomb potential was assumed to be valid right down to $r=0$ i.e. equation (7.1) was used, with $W(r)$ given by (9.1). Present concepts about the nature of the nucleons themselves makes such an assumption questionable. Deviations from the purely Coulomb form of the electromagnetic interaction most probably occur at distances of the order of, or smaller than, the range of nuclear forces. However, the Coulomb field itself produces little change in the variational parameters^(7,8) except the scattering length a (see Section 6). Consequently, deviations from the Coulomb law at small distances can be assumed to produce no significant changes in the higher coefficients in (1.3), and only slight modifications in a . In any event, when the actual form of these deviations is known, the parameters can be corrected accordingly by the methods of Section 8.

The results of the calculation are collected in Table

(9.1). The first column of the table specifies the potential shape. The second and third columns give the values of the well parameters s and b for which the calculation was carried out. The next four columns give the variational parameters a , r_0 , P , Q . Finally the last four columns give the derivatives $\frac{\partial a}{\partial s}$, $\frac{\partial r_0}{\partial s}$, $\frac{\partial a}{\partial b}$, $\frac{\partial r_0}{\partial b}$ which one needs to compute the effects of small changes in the well parameters.

These numbers can be compared with those obtained by Hatcher, Arfken and Breit⁽³⁷⁾ for the Gaussian and Yukawa well shapes. These authors computed S-wave phase shifts, then evaluated K (1.3), and made a least squares fit with a second-degree polynomial over the energy range up to 10 Mev. The comparison is satisfactory.

They can also be compared with the corresponding parameters for neutron-proton scattering. The scattering lengths differ appreciably, as was shown in Section 6. However, the higher coefficients agree quite well. For the same values of s and b as given in Table (9.1), a comparison with the curves of reference (2) shows that the effective ranges differ by 6 percent at most (the difference is 0.2 percent for the Yukawa well, and 5.6 percent for the square well). Similarly, the values of P in the two cases differ by 10 percent at most for all the well shapes considered. This gives a clear indication that the Coulomb potential can be treated as a small perturbation on the higher parameters in (1.3).⁽⁸⁾

Table 9.1: Calculated values of the variational parameters and their derivatives for various potential well shapes

Well shape	s	b	a	r_0	P	Q
Square	.890	2.626	-7.7930	2.6388	-.03313	..00179
Gaussian	.900	2.540	-7.7797	2.6055	-.01936	-.00073
Exponential	.900	2.500	-7.4235	2.6776	.00907	.00089
Yukawa	.924	2.400	-7.6512	2-6756	.05540	.019

Well shape	$\partial a / \partial s$	$\partial r_0 / \partial s$	$\partial a / \partial b$	$\partial r_0 / \partial b$
Square	-33.521	-1.5300	-2.0824	.94975
Gaussian	-34.654	-1.8553	-2.0966	.98193
Exponential	-33.813	-2.5690	-2.0510	1.0439
Yukawa	-39.399	-3.6387	-2.1002	1.1157

All lengths are in units of 10^{-13} cm.

The first thing to note in the comparison with experiment is the very small value of P for all four well shapes. In view of the fact that the present experimental data are not in disagreement with values of P anywhere in the range $+ 0.15$ to $- 0.8$, one can conclude that all four commonly assumed well shapes give equally good fits to the Van de Graaff data, the fits being quite excellent compared to the experimental errors. Conversely, the disagreement of the DOP point at 7 Mev cannot be used as an indication of well shape since this point is in disagreement no matter which well shape is assumed. The excellence of the fits to the Van de Graaff data is shown in Figure (9.1) where the best least-squares fits for the square and Yukawa well shapes (the extremes of the four well shapes) are given along with the best shape-independent fit.

The present results are in essential agreement with the results of BTE⁽¹⁾. However, they disagree with the results of Hoisington, Share and Breit⁽³⁸⁾ concerning the exponential well shape. These authors claim that the exponential well provides a significantly poorer fit to the then available data than the Yukawa well. They attribute this difference to the longer tail of the exponential well, claiming that the $1/r$ singularity at the origin in the Yukawa well compensates for its tail. Their fit to the data with the exponential well was made using the well parameters determined by Rarita and Present⁽³⁹⁾ ($s = .885$, $b = 3.08 \times 10^{-13}$ cm).

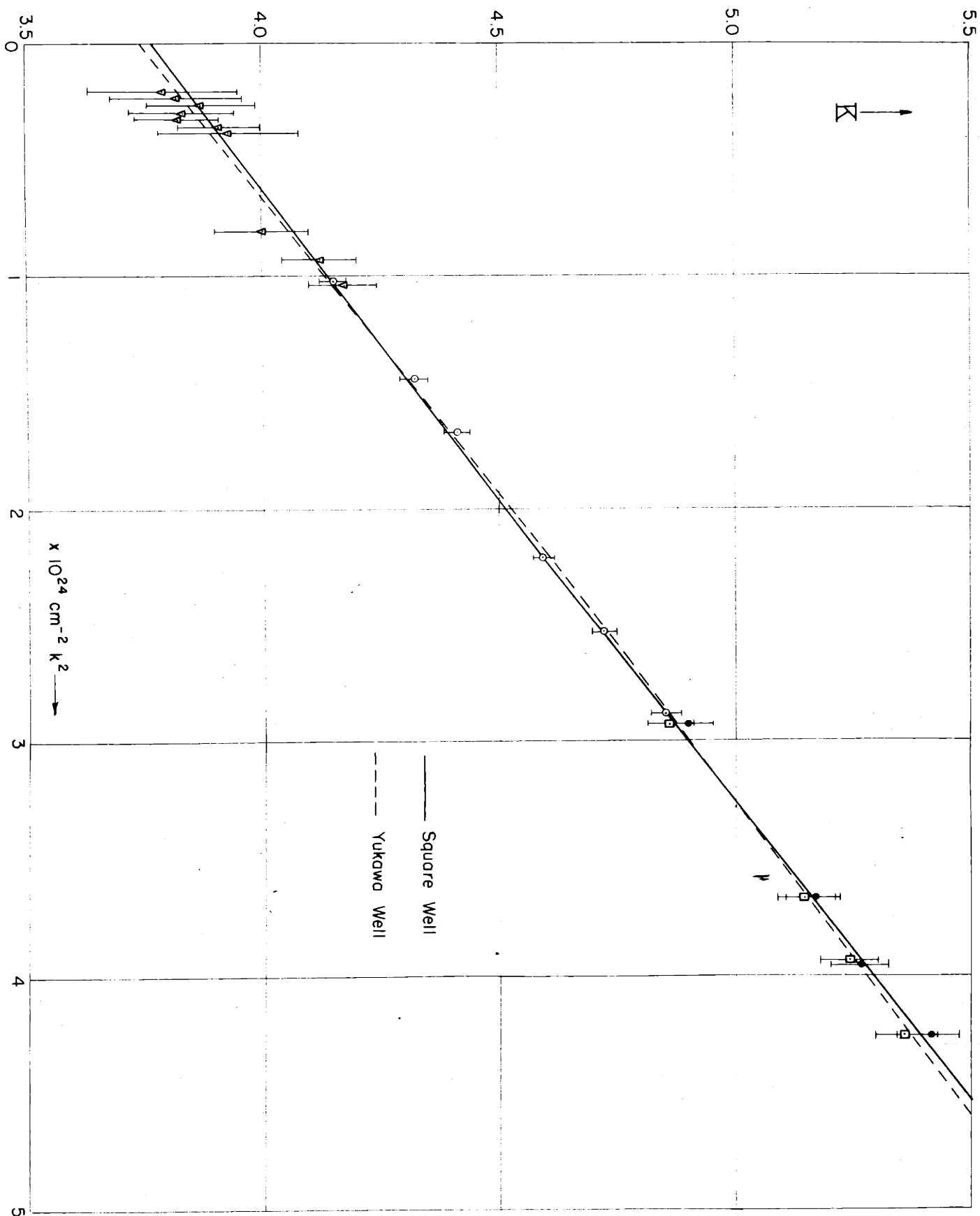


Figure 9.1: Experimental values of K plotted against k^2 for the Van de Graaff data, with the best weighted least-squares fit to the data for the square and Yukawa well shapes. Both potential shapes give equally good fits to the data.

These well parameters give too large (absolute) values for both a ($\sim -8.10 \times 10^{-13}$ cm.) and r_0 , ($\sim 3.32 \times 10^{-13}$ cm.) so that a plot of δ vs. k^2 would lie across the best linear fit shown in Figure (5.3), passing below the lower energy points and above the higher energy points of HKPP. But it just happens that the Rarita-Present well predicts the same value for the phase shift as determined from the HHT data at 670 Kev. This point will be seen to lie considerably below the best fit in Figure (5.3). Hoisington, Share and Breit remark that their comparison may be unfair since they choose to fit their theoretical curve exactly to the HHT point at 670 Kev. However, they go on to argue that this really should make no difference since the curvature of the δ_0 vs. E curve for the exponential well is too great to be in agreement with the experimental data no matter at what energy it was fitted, and that a change in the range of the potential primarily affects the slope, not the curvature of such a plot. It is clear that, since the present data do not discriminate between well shapes, the earlier data (which covered a narrower energy range) certainly discriminate even less. With the proper choice of range and depth (see Table (9.2)), the exponential well gives as good a fit to the data (either as it was then, or as it is now) as any of the other usually assumed shapes. The conclusion to be drawn from the work of Hoisington, Share and Breit is that

the Rarita-Present exponential well gives a poor fit to the data, but not that the exponential well per se gives a poorer fit than any other well shape. This situation illustrates the difficulties involved in deciding what is a "good fit" if one does not have a simple functional form such as (1.3) with which to fit the data.

The results in Table (9.1) are not in the most convenient form for comparison with experiment since one wishes to find s and b from the measured a and r_0 , rather than the other way around. The quantities in Table (9.1) are used as follows:

$$a = a_0 + \frac{\partial a}{\partial s}(s - s_0) + \frac{\partial a}{\partial b}(b - b_0) + \dots$$

$$r = r_0 + \frac{\partial r_0}{\partial s}(s - s_0) + \frac{\partial r_0}{\partial b}(b - b_0) + \dots$$

These equations can be treated as a pair of linear simultaneous equations in two unknowns (s and b), and can be solved for these unknowns in terms of $(a - a_0)$ and $(r - r_0)$. The resulting expressions, given below, correspond to the linear terms in a Taylor series around the computed points.

Square well

$$\begin{aligned} s &= .890 - .02712 (a + 7.793) - .05946 (r_0 - 2.639) \\ b &= 2.626 - .04369 (a + 7.793) + .95716 (r_0 - 2.639) \end{aligned} \quad (9.3S)$$

Gaussian well

$$\begin{aligned} s &= .900 - .02590 (a + 7.780) - .05529 (r_0 - 2.606) \\ b &= 2.540 - .04893 (a + 7.780) + .91395 (r_0 - 2.606) \end{aligned} \quad (9.3G)$$

Exponential well

$$s = .900 - .02573 (a + 7.424) - .05056 (r_0 - 2.678) \quad (9.3E)$$

$$b = 2.500 - .06333 (a + 7.424) + .83354 (r_0 - 2.678)$$

Yukawa well

$$s = .924 - .02162 (a + 7.651) - .04070 (r_0 - 2.676) \quad (9.3Y)$$

$$b = 2.400 - .07051 (a + 7.651) + .76353 (r_0 - 2.676)$$

All lengths in these formulae are in 10^{-13} cm.

Using the results of the weighted least squares fitting to the Van de Graaff data for arbitrary values of P which are summarized in Figures (5.5) and (5.6) it is possible to determine the best values of a and r_0 for each well shape. Then use of equations (9.3) allows the determination of the best well parameters s and b in each case. These results are given in Table (9.2). The first column of the table gives the well shape, the second column the value of P for that well. The third and fourth columns give the corresponding values of a and r_0 with their probable errors, while the next two columns give the implied values of the well parameters s and b with their probable errors. The potentials corresponding to these values of s and b can be found by reference to equations (9.2). For the Yukawa well the "meson" mass turns out to be 332 ± 8 electron masses. The values of b are seen to be determined to within 2.5 percent, while the values of s are determined to within 0.3 percent.

The results summarized in Table (9.2) are in essential

Table 9.2: The variational parameters and well parameters which give the best weighted least-squares fit to the experimental data below 3.6 Mev

Well shape	P	a (10^{-13} cm)	r_0 (10^{-13} cm)	s	b (10^{-13} cm)
Square	-.033	-7.66 ± .05	2.60 ± .07	.889 ± .003	2.58 ± .06
Gaussian	-.019	-7.66(5) ± .05	2.62 ± .07	.896 ± .003	2.55 ± .06
Exponential	+.009	-7.68 ± .05	2.67 ± .07	.907 ± .003	2.51 ± .06
Yukawa	+.055	-7.70 ± .05	2.76 ± .07	.922 ± .003	2.47 ± .06

agreement with the results of Breit, Thaxton and Eisenbud⁽¹⁾ for the square and Gaussian well shapes (they obtained $s = .872$, $b = 2.81$ for the square well; $s = .887$, $b = 2.78$ for the Gaussian well), and those of Hoisington, Share and Breit⁽³⁸⁾ for the Yukawa well (they got $s = .920$, $b = 2.51$). The differences can be accounted for by the fact that Breit et al. had only the data of HHT and HKPP available for their analysis at that time. As pointed out by Bethe⁽⁷⁾, the errors can now be narrowed down somewhat, both because the data extend to higher energies and because the simple functional form (1.3) allows one to make a reasonable estimate of error by simple inspection rather than by complicated computations.

Bethe⁽⁷⁾ has given a discussion of the assumption of charge-independence of the specifically nuclear forces. He has shown that the recent data for the epithermal neutron-proton cross section definitely imply a neutron-proton potential in the singlet state with a bigger value of s than the proton-proton force. It is interesting to see how such a conclusion can be reached by means of the approximate relation between neutron-proton and proton-proton scattering lengths obtained in Section 6, and to see how well this agrees with a more detailed accurate determination. The recent measurements of the epithermal neutron-proton scattering cross section⁽⁴⁰⁾ give:

$$\sigma_0 \equiv 4\pi \left(\frac{3}{4} a_t^2 + \frac{1}{4} a_s^2 \right) = 20.36 \text{ barns}$$

The measurements of the coherent neutron-proton scattering amplitude⁽⁴¹⁾ yield:

$$r \equiv 2 \left(\frac{3}{4} a_t + \frac{1}{4} a_s \right) = -3.95 \times 10^{-13} \text{ cm.}$$

From these two measurements the singlet neutron-proton scattering length is found to be:

$$a_s \approx - (2.376 \pm .010) \times 10^{-12} \text{ cm} \quad (9.4)$$

Now equation (6.14) gives the proton-proton scattering length a_p in terms of the corresponding neutron-proton quantity.

$$a_p^{-1} \approx a_n^{-1} + \frac{1}{R} \left[\ln\left(\frac{b}{R}\right) + 0.330 \right] \quad (6.14)$$

Using the values of b in Table (9.2) and the value of a_s given in (9.4), one obtains the value of a_p implied by the neutron-proton singlet potential which has the same shape and range as, but perhaps different depth from the proton-proton potential.

$$a_p \approx - 8.75 \times 10^{-13} \text{ cm.} \quad (\text{square well})$$

$$a_p \approx - 8.63 \times 10^{-13} \text{ cm.} \quad (\text{Yukawa well})$$

These values do not agree with the best values given in Table (9.2). To find the difference in depth (assuming the same range and shape) necessary to account for this disagreement one can use the derivatives in Table (9.1) i.e.

$$a = a_0 + \frac{\partial a}{\partial s} (s - s_0)$$

where a_0 and s_0 are the values given in Table (9.2). By this means, one finds that the singlet neutron-proton potential is stronger than the proton-proton potential by about 3 percent for the square well shape, and stronger by about 2 percent for the Yukawa well shape.

A more exact comparison can be made by means of the curves in reference (2) and the value of a_s in (9.4). The values of s for the neutron-proton potentials with the same shape and range as the proton-proton potentials giving a_s (9.4) can be read directly off Figure (4.4) of reference (2). In this way, one finds that the neutron-proton 1S potential is stronger, by 3.3 percent for the square well, and 1.6 percent for the Yukawa well, than the corresponding proton-proton potential, assuming the same shape and range. These differences are small, but are definitely outside the limits of experimental error, so that the hypothesis of charge-independence of nuclear forces is not exactly satisfied (although very nearly so). One might argue that the presence of the nuclear force distorts the Coulomb field.

for values of r less than the nuclear range. If so, the distortion has to be in such a way that the effective Coulomb potential is increased. One of the other aspects of charge-independence, namely the charge-independence of the intrinsic range of the nuclear potential, has no direct experimental verification at present. The neutron-proton scattering data are not accurate enough to settle this point (see reference (2)). And, of course, the question of potential shape is completely unanswered by present experimental data of any sort. The closer equality of the neutron-proton and proton-proton forces found by Breit and collaborators⁽⁴²⁾ was due to the use of Simon's⁽⁴³⁾ value of the epithermal neutron-proton scattering cross section, which has since been shown to be considerably too low. Their calculations with $\sigma_0 = 20$ barns are in accord with the results given here.

In conclusion some considerations will be given about the accuracy necessary for a hypothetical experiment at 10 Mev to discriminate between the Yukawa and square well shapes (these being the two extremes in well shapes usually employed). As a basis for comparison, the square and Yukawa potentials which give equivalently good fits to the Van de Graaff data will be considered. The values of K (1.3) at 10 Mev for these two potentials can be found by means of the values of a , r_0 , P , Q given in Table (9.2). They are $K = 8.20$ for the Yukawa well, $K = 8.53$ for the square well, the difference being $\Delta K \approx .33$. From Figures (5.7) and

(5.8) it is found that $E\left(\frac{\partial K}{\partial E}\right)_\sigma \approx -4$, and $\sigma\left(\frac{\partial K}{\partial \sigma}\right)_E \approx -8$. Since the signs of the experimental errors are presumably unknown, it is necessary to consider the worst possible case i.e.

$$4 \left| \frac{\Delta E}{E} \right| + 8 \left| \frac{\Delta \sigma}{\sigma} \right| = \Delta K$$

It is seen that the uncertainty in cross section is twice as important as the uncertainty in beam energy as far as errors in K are concerned. If ΔK is put equal to one half of the difference of the K's for the two potential shapes, a lower limit will be set on the accuracy needed to discriminate between the two shapes. The table given below shows how the uncertainties go.

$\Delta \sigma / \sigma$	0	.01	.02
$\Delta E / E$.04	.02	0

It is seen that even to begin to discriminate between the extremes in potential shapes, the measurements in cross section must have less than 2 percent overall uncertainty, assuming the energy is known exactly. In view of the cyclotron measurements at 7 and 8 Mev, an energy accuracy of around one percent seems feasible with such machines, and by careful work the cross section measurement can be made accurate to within 2 percent or less. Hence, a measurement

in the neighborhood of 10 Mev that would discriminate between extremes in well shapes appears possible with existing equipment and techniques. In any event, it is recommended that careful measurements be made at energies considerably above 3.5 Mev, and that particular attention be paid to the elimination of systematic errors (which might, for example, account for the peculiar DOP point at 7 Mev.).

(10) A rough estimate of the phase shifts for higher angular momenta

It is an easy matter to write the generalization of the variation principle (7.5) for orbital angular momenta $l \neq 0$ different from zero. Indeed, all one has to do is to replace $F(r) = F_0(r)$ and $G(r) = G_0(r)$ by the appropriate Coulomb wave function for orbital angular momentum l , i.e. by the $F_l(r)$ and $G_l(r)$ given in Yost, Wheeler and Breit.⁽³³⁾ (The replacement must be made also in the definition of the Green's function $K_l(r, r')$ (7.4), of course). The derivation of an expansion similar to (1.3) presents no difficulties. Indeed, the result has been derived by Chew and Goldberger⁽⁸⁾ for $l = 1$. The generalization of (1.3) to arbitrary l was given by Landau and Smorodinsky⁽⁵⁾ for the zero-range approximation.

However, such a detailed treatment for higher angular momenta is unreasonable at this time. As was seen in Section 4, the experimental evidence for P or D-wave contributions to the scattering is only of a qualitative nature. All that is necessary at present is a rough, order of magnitude, estimate of these higher phase shifts. Breit, Thaxton and Eisenbud⁽¹⁾ give estimates for the Gaussian and exponential well shapes. Estimates for the four usual well shapes will be given here in terms of the well-depth parameter s and the intrinsic range b .

For a first orientation, it is sufficient to use the Born approximation for the phase shifts⁽⁴⁴⁾

$$\delta_l \approx k^{-1} \int_0^{\infty} F_l^2(r) W(r) dr \quad (10.1)$$

Furthermore, the regular Coulomb wave function will be approximated by its behavior near the origin (see reference (33)):

$$F_l(r) \approx C_l (kr)^{l+1} \quad (10.2)$$

Here C_l is the penetration factor for the combined centrifugal and Coulomb barriers, given by

$$C_l^2 = \frac{2^{2l}}{[(2l+1)!]^2} (l^2 + \eta^2)(l-1)^2 + \eta^2 \dots (1 + \eta^2) \frac{2\pi\eta}{l^{2\pi\eta - 1}} \quad (10.3)$$

The potential $W(r)$ is written in the standard form (8.7).

Then the estimate for the phase shift δ_l becomes:

$$\delta_l \approx C_l^2 s (kb)^{2l+1} f_{2l+2} \quad (10.4)$$

where f_n is the n 'th moment of the shape function $f(r/b)$ defined in (8.7):

$$f_n = \int_0^{\infty} x^n f(x) dx \quad (10.5)$$

Formula (10.4) shows that δ_l is proportional to (1) the barrier penetration factor (which is a function of energy), (2) the well-depth parameter s , (3) the $(l + \frac{1}{2})$ power of the energy, (4) the $(2l + 1)$ power of the intrinsic range, (5) a pure number depending only upon the shape of the well and increasing rapidly as the well gets to be more "long-tailed". δ_l will be positive for attractive potentials (positive s) and negative for repulsive potentials (negative s).

In Table (10.1) the values of f_{2l+2} are given for the four commonly assumed well shapes and for the first few values of l .

Table (10.1): Values of f_{2l+2}

	Square well	Gaussian well	Exponential well	Yukawa well
$l = 1$.4935	.6031	.7814	1.058
$l = 2$.3525	.7318	1.869	4.712
$l = 3$.2742	1.243	8.348	44.05

In Table (10.2) the values of δ_l at a few representative energies are given under the assumption that $W(r)$ for the

higher angular momenta has the same intrinsic range b as the best fit (see Table (9.2)) for the S-wave phase shifts, and a well-depth parameter $s=1$. In order to get δ_l for different assumptions about s or b , it is only necessary to remember the proportionality of δ_l to s and b^{2l+1} .

It should be emphasized that the numbers in Table (10.2) are very rough estimates, and are to be used only in that sense. The possibility of a tensor force contribution in the states of odd angular momentum has not been included, since detailed considerations of this type seem premature. The absolute value of δ_l in higher approximation for a given potential depends on whether the force is attractive or repulsive (see, for example, Thaxton and Hoisington⁽⁴⁵⁾ for calculations of δ_1 for a square well). The values in Table (10.2) are approximately the mean of the absolute values for attractive and repulsive potentials, the attractive potential giving a somewhat larger value for δ_l , and the repulsive potential, a smaller (absolute) value.

The following preliminary conclusions can be drawn from the estimates summarized in Table (10.2). (1) A P-wave phase shift of the order of half a degree at an energy around 3 Mev is not unreasonable, (2) A D-wave phase shift of the order of magnitude 0.1 degree at that same energy is considerably higher (by a factor of 5 to 50) than the expected values, (3) At energies of the order of 8 or 10 Mev the P-wave phase shifts (assuming that they exist at all,

Table 10.2: Estimates of δ_0

The sets of three numbers at each energy are the estimated values of δ_1 , δ_2 , and δ_3 in degrees for $s = 1$, and b given in Table (9.2).

Energy (Mev)	Square well	Gaussian well	Exponential well	Yukawa well
2	.14	.17	.21	.27
	.00065	.0013	.0030	.0070
	.000002	.000007	.000042	.00020
4	.44	.52	.65	.84
	.0041	.0080	.019	.044
	.000021	.000087	.00052	.0025
6	.85	1.01	1.25	1.61
	.012	.023	.054	.13
	.000090	.00038	.0023	.011
8	1.35	1.60	1.97	2.54
	.025	.049	.12	.27
	.00025	.0011	.0064	.030
10	1.93	2.27	2.81	3.62
	.044	.087	.20	.48
	.00056	.0024	.014	.067

cf. reference (15)) are likely to become large enough so that the linear approximation of Section 4 will be invalid. If this turns out to be the case, one will also have to include tensor force effects more carefully at those energies (i.e. the replacement (4.8) will no longer be valid). As was mentioned in Section 4, while small values of $\delta(^3P_0)$, $\delta(^3P_1)$, and $\delta(^3P_2)$ imply a small value of δ_1 (4.8), this is not true the other way around. Indeed, some estimates show that the weighted average of the phase shifts (4.8) may well be considerably smaller than any one of the phase shifts taken separately. At present the evidence for P-wave phase shifts is not sufficiently precise to worry about these finer details, however. (4) It is clear from (10.4) that the phase shift estimates depend quite strongly upon the shape of the well; hence, one can always get larger estimates by using longer-tailed wells. However, the evidence summarized in Section 5 limits the value of P (the amount of tailing of the well) that one can permit for the force in the 1S state. At present it is a matter of taste whether one is willing to assume a potential with a very long tail in the states of higher angular momentum. In this connection, it should be recalled that the analysis of the experiments given in Section 4 indicated that the P-wave phase shifts, if real, were of the order of, or less than, one degree even up to 10 Mev. Hence there is no need to postulate long-tailed potentials in the states of higher angular momentum to give agreement with the present uncer-

tain experimental evidence.

Appendix 1: Formulae relating phase shifts to experimental cross sections

The general expression for the proton-proton scattering cross section including all higher angular momentum terms is given by Breit, Condon, and Present.⁽¹⁾ If the nuclear phase shifts δ_l beyond δ_2 vanish, then the cross section in the center of mass system can be written as:

$$\sigma(\theta) = \sigma_M(\theta) + \Delta_0(\theta) + \Delta_1(\theta) + \Delta_2(\theta) \quad (\text{A1.1})$$

where $\sigma_M(\theta)$ is the Mott formula (2.15) given by:

$$\sigma_M(\theta) = \left(\frac{e^2}{M_N^2}\right)^2 \left[\operatorname{cosec}^2 \frac{\theta}{2} + \sec^2 \frac{\theta}{2} - \frac{\cos(\eta \ln \tan^2 \frac{\theta}{2})}{\sin^2 \frac{\theta}{2} \cos^2 \frac{\theta}{2}} \right] \quad (\text{A1.2})$$

and the other terms are:

$$\begin{aligned} \left(\frac{M_N^2}{e^2}\right)^2 \Delta_0(\theta) = & -\frac{2}{\eta} \left(\frac{\cos \alpha_0}{\sin^2 \frac{\theta}{2}} + \frac{\cos \beta_0}{\cos^2 \frac{\theta}{2}} \right) \sin \delta_0 \cos \delta_0 + \\ & + \left(\frac{4}{\eta^2} + \frac{2}{\eta} \frac{\sin \alpha_0}{\sin^2 \frac{\theta}{2}} + \frac{2}{\eta} \frac{\sin \beta_0}{\cos^2 \frac{\theta}{2}} \right) \sin^2 \delta_0 \end{aligned} \quad (\text{A1.3})$$

$$\begin{aligned} \left(\frac{M_N^2}{e^2}\right)^2 \Delta_1(\theta) = & -\frac{18}{\eta} P_1(\cos \theta) \left(\frac{\cos \alpha_1}{\sin^2 \frac{\theta}{2}} - \frac{\cos \beta_1}{\cos^2 \frac{\theta}{2}} \right) \sin \delta_1 \cos \delta_1 + \\ & + \left[\frac{108}{\eta^2} P_1^2(\cos \theta) + \frac{18}{\eta} \left(\frac{\sin \alpha_1}{\sin^2 \frac{\theta}{2}} - \frac{\sin \beta_1}{\cos^2 \frac{\theta}{2}} \right) P_1(\cos \theta) \right] \sin^2 \delta_1 \end{aligned} \quad (\text{A1.4})$$

$$\begin{aligned}
\left(\frac{Mv^2}{\hbar^2}\right)^2 \Delta_2(\theta) &= -\frac{10}{\eta} P_2(\cos\theta) \left(\frac{\cos\alpha_2}{\sin^2\frac{\theta}{2}} + \frac{\cos\beta_2}{\cos^2\frac{\theta}{2}} \right) \sin\delta_2 \cos\delta_2 + \\
&+ \left[\frac{100}{\eta^2} P_2^2(\cos\theta) + \frac{10}{\eta} P_2(\cos\theta) \left(\frac{\sin\alpha_2}{\sin^2\frac{\theta}{2}} + \frac{\sin\beta_2}{\cos^2\frac{\theta}{2}} \right) \right] \sin^2\delta_2 + \quad (\text{A1.5}) \\
&+ \frac{40}{\eta^2} \sin\delta_0 \sin\delta_2 \cos(\delta_2 - \delta_0 + 2\sigma_2 - 2\sigma_0) P_2(\cos\theta)
\end{aligned}$$

where $\eta = e^2/\hbar v = 0.15806/\sqrt{E}$
 $(e^2/Mv^2)^2 = 5.1824 \times 10^{-3} E^{-2}$ barns (10^{-24} cm^2).
 $\alpha_0 = \eta \ln \sin^2\frac{\theta}{2}$ $\beta_0 = \eta \ln \cos^2\frac{\theta}{2}$
 $\alpha_2 = \alpha_0 + 2(\sigma_2 - \sigma_0)$ $\beta_2 = \beta_0 + 2(\sigma_2 - \sigma_0)$
 $\sigma_2 - \sigma_{2-1} = \tan^{-1}(\eta/2)$

For the $l=0$ case, Breit, Thaxton, and Eisenbud⁽¹⁾ (denoted by BTE from now on) define:

$$X \equiv \frac{\cos\alpha_0}{\sin^2\frac{\theta}{2}} + \frac{\cos\beta_0}{\cos^2\frac{\theta}{2}} \quad (\text{A1.6})$$

$$Y \equiv \frac{\sin\alpha_0}{\sin^2\frac{\theta}{2}} + \frac{\sin\beta_0}{\cos^2\frac{\theta}{2}} \quad (\text{A1.7})$$

Then the S-wave anomaly $\Delta_0(\theta)$ can be written as:

$$\left(\frac{Mv^2}{\hbar^2}\right)^2 \Delta_0(\theta) = -\frac{2X}{\eta} \sin\delta_0 \cos\delta_0 + \left(\frac{4}{\eta^2} + \frac{2Y}{\eta}\right) \sin^2\delta_0 \quad (\text{A1.8})$$

BTE also define:

$$m = \left(\frac{M_N^2}{E^2}\right)^2 \sigma_M(\theta) = \cos \sec^4 \frac{\theta}{2} + \sec^4 \frac{\theta}{2} - \frac{\cos(\eta \ln \tan^2 \frac{\theta}{2})}{\sin^2 \frac{\theta}{2} \cos^2 \frac{\theta}{2}} \quad (\text{A1.9})$$

If there is only S-wave scattering, the cross section can be written (using (A1.1), (A1.8), (A1.9)) as:

$$\sigma(\theta) = \sigma_M(\theta) \left[1 - \frac{2X}{\eta m} \sin \delta_0 \cos \delta_0 + \left(\frac{4}{\eta^2 m} + \frac{2Y}{\eta m} \right) \sin^2 \delta_0 \right] \quad (\text{A1.10})$$

BTE give tables of $\frac{2X}{\eta m}$, $\left(\frac{4}{\eta^2 m} + \frac{2Y}{\eta m} \right)$, X , $-\frac{2Y}{\eta}$, and m as functions of angle and energy, as well as expansions for X , $-\frac{2Y}{\eta}$, and m in powers of E^{-1} .

If one defines the angle ω through:

$$\tan \omega \equiv \frac{2/\eta + Y}{X} \quad (\text{A1.11})$$

and the quantity q^{-1} as the positive square root of:

$$q^{-2} \equiv \frac{1}{\eta^2 m^2} \left[X^2 + (2/\eta + Y)^2 \right] \quad (\text{A1.12})$$

then the formula (A1.10) can be rewritten in the simpler form:

$$\sigma(\theta) = \sigma_M(\theta) \left[1 + \frac{1}{q} (\sin \omega - \sin(2\delta_0 + \omega)) \right] \quad (\text{A1.13})$$

solving for $2\delta_0$, the result is:

$$\text{where } 2\delta_0 = \sin^{-1} \left(\sin \omega - q(R-1) \right) - \omega ; R = \frac{\sigma(\theta)}{\sigma_M(\theta)} \quad (\text{A1.14})$$

In Table (A1.1) expansions of q , $\sin \omega$, and $\sigma_M(\theta)$ in

powers of E^{-1} (energy in the laboratory system) are given for angles from 40 degrees to 90 degrees (in the center of mass system). The table is almost self-explanatory. The leading term given in column 3 is to be multiplied by the corresponding correction term involving C_1 and C_2 . For example, the value in barns of σ_M at $\theta = 40$ degrees is given by:

$$\sigma_M(40^\circ) = .3352 E^{-2} (1 + .00764/E - .000065/E^2 + \dots)$$

By means of these expansions and formula (A1.14) the phase shifts can be found from the experimental cross sections with a minimum of effort. Of course, at very low energies the expansions become inaccurate. Then one must resort to the exact formulae, or make use of the tables of numerical values given in BTE. At small angles of scattering the expansions for $\sin \omega$ and q are inconvenient due to slow convergence even at energies above 1 Mev. It has been found that the quantity Q defined by:

$$Q \equiv \frac{\pi m}{X} = \frac{q}{\cos \omega} \quad (\text{A1.15})$$

and $\tan \omega$ yield useful expansions for small angles. With this definition of Q the formula (A1.14) for δ_0 is replaced by:

$$2\delta_0 = \sin^{-1}(\sin \omega - Q \cos \omega (R-1)) - \omega \quad (\text{A1.16})$$

Table (A1.2) gives expansions for Q , $\tan \omega$, and $\sigma_M(\theta)$ for angles from 16 to 40 degrees. It is seen from Table (A1.2) that the convergence of the expansions, especially those of $\tan \omega$, is rather poor especially at the smallest angles of scattering. A rough criterion is that the expansion is valid if the second correction term ($C_2 E^{-2}$) does not amount to more than one or two percent. Thus, for example, the expansion for $\tan \omega$ at $\theta = 16$ degrees should not be trusted for E much less than 4 Mev. The low energy limit decreases as θ increases, as can be readily seen; and $\theta = 16$ degrees (a scattering angle of 8 degrees in the laboratory!) is an extreme case.

In connection with the breakdown of the expansions at low energies and the necessity of using the tables of BTE, it is useful to note that $\tan \omega$ is just the ratio of the quantity $(4/\pi^2 \mu + 2Y/\pi \mu)$ given by Table II of BTE to the quantity $2X/\pi \mu$ given by Table I of BTE. Similarly, Q is just n times the ratio of μ (Table V of BTE) to X (Table III of BTE) by definition. Once $\tan \omega$ and Q are known, formula (A1.16) can be applied in the usual way.

Table A1.1: Expansions of $\sin \omega$, q , and σ_M

E = energy in laboratory in MEV

 σ_M is in 10^{-24}cm^2

Scattering angle	Quantity	Leading term	Corrections $1 + C_1 E^{-1} + C_2 E^{-2}$	
			C_1	C_2
40°	$\sin \omega$	1	-.2927	.0230
	q	.8084 E^{-1}	-.05414	.00390
	σ_M	.3352 E^{-2}	.00764	-.000065
50°	$\sin \omega$	1	-.1451	.00461
	q	.3249 E^{-1}	-.01400	.000254
	σ_M	.13479 E^{-2}	.00761	-.000037
60°	$\sin \omega$	1	-.08882	.00192
	q	.1554 E^{-1}	-.00828	.000168
	σ_M	.06447 E^{-2}	.00645	-.000016
70°	$\sin \omega$	1	-.06408	.00121
	q	.08658 E^{-1}	-.01027	.000209
	σ_M	.03591 E^{-2}	.00416	-.000004
80°	$\sin \omega$	1	-.05311	.000954
	q	.05794 E^{-1}	-.01368	.000256
	σ_M	.02404 E^{-2}	.00137	0
85°	$\sin \omega$	1	-.05074	-.000902
	q	.05189 E^{-1}	-.01490	.000279
	σ_M	.02153 E^{-2}	.000368	0
90°	$\sin \omega$	1	-.04997	.000885
	q	.04997 E^{-1}	-.01533	.000283
	σ_M	.02073 E^{-2}	0	0

Table A1.2: Expansions of $\tan \omega$, Q , and σ_M

E = energy in laboratory in MEV

 σ_M is in 10^{-24} cm^2

Scattering angle	Quantity	Leading term	Corrections $1 + C_1 E^{-1} + C_2 E^{-2}$	
			C_1	C_2
16°	$\tan \omega$	$.24031 E^{1/2}$	-2.3533	-.2901
	Q	$7.8480 E^{-1/2}$.19457	.03080
	σ_M	$13.548 E^{-2}$.003878	-.000124
20°	$\tan \omega$	$.37005 E^{1/2}$	-1.3023	-.12327
	Q	$4.9308 E^{-1/2}$.15346	.01889
	σ_M	$5.5281 E^{-2}$.004827	-.000121
25°	$\tan \omega$	$.56499 E^{1/2}$	-.70519	-.04904
	Q	$3.0657 E^{-1/2}$.11748	.01083
	σ_M	$2.2512 E^{-2}$.005850	-.000111
30°	$\tan \omega$	$.79084 E^{1/2}$	-.41977	-.02175
	Q	$2.0548 E^{-1/2}$.09192	.006443
	σ_M	$1.0779 E^{-2}$.006668	-.000096
35°	$\tan \omega$	$1.0408 E^{1/2}$	-.26760	-.01038
	Q	$1.4476 E^{-1/2}$.07295	.003920
	σ_M	$.57706 E^{-2}$.007273	-.000081
40°	$\tan \omega$	$1.3070 E^{1/2}$	-.18008	-.005241
	Q	$1.0560 E^{-1/2}$.05846	.002418
	σ_M	$.33520 E^{-2}$.007638	-.000065

Appendix 2: Formulae and Tables for the determination of
higher phase shifts

The functions $p_n(E, \theta, \delta_0)$ defined by:

$$p_n(E, \theta, \delta_0) = \frac{\left(\frac{\partial \sigma}{\partial \delta_n}\right)}{\left(\frac{\partial \sigma}{\partial \delta_0}\right)} \quad (4.7)$$

can be readily found by means of the formulae (A1.3), (A1.4), (A1.5) for $n=1, 2$. Thus

$$\left(\frac{Mv^2}{R^2}\right)^2 \frac{\partial \sigma}{\partial \delta_0} = \left[-\frac{2X}{\eta} \cos(2\delta_0) + \left(\frac{4}{\eta^2} + \frac{2Y}{\eta}\right) \sin(2\delta_0) \right] \quad (A2.1)$$

where X and Y are defined by (A1.6) and (A1.7). Similarly

$$\left(\frac{Mv^2}{R^2}\right)^2 \frac{\partial \sigma}{\partial \delta_1} = -\frac{18}{\eta} \left(\frac{\cos \alpha_1}{\sin^2 \frac{\theta}{2}} - \frac{\cos \beta_1}{\cos^2 \frac{\theta}{2}} \right) P_1(\cos \theta) \quad (A2.2)$$

and

$$\begin{aligned} \left(\frac{Mv^2}{R^2}\right)^2 \frac{\partial \sigma}{\partial \delta_2} = & \left[\frac{40}{\eta^2} \sin \delta_0 \cos(\delta_0 - 2\sigma_2 + 2\sigma_0) - \right. \\ & \left. - \frac{10}{\eta} \left(\frac{\cos \alpha_2}{\sin^2 \frac{\theta}{2}} + \frac{\cos \beta_2}{\cos^2 \frac{\theta}{2}} \right) \right] P_2(\cos \theta) \end{aligned} \quad (A2.3)$$

It should be noted that while (A2.1) and (A2.3) involve δ_0 , they are relatively insensitive to variations in δ_0 over the energy range of interest. The higher phase shifts are certainly negligible for energies below 2 Mev while the assumption that δ_1 and δ_2 are small probably is not valid above 8 or 10 Mev. In this energy range of 2 - 10 Mev where the functions p_n are presumably useful, the value of δ_0 is in the neighborhood of 50 degrees. Thus $\sin(2\delta_0)$ is near unity, and a slowly varying function of δ_0 , while $\cos(2\delta_0)$ is small. From this it is seen that (A2.1) and (A2.3) are insensitive to δ_0 . Of course, (A2.2) does not involve δ_0 at all.

Of some interest, as far as the general behavior of $p_1(\theta)$ and $p_2(\theta)$ is concerned, are the limiting forms for p_1 and p_2 as E becomes very large. It is easily seen from examination of (A2.1) and (A2.2) that:

$$\lim_{E \rightarrow \infty} p_1(\theta) = \frac{-18\pi}{\sin(2\delta_0)} \cot^2 \theta \quad (\text{A2.4})$$

Similarly, the limiting form of $p_2(\theta)$, from (A2.1) and (A2.3) is:

$$\lim_{E \rightarrow \infty} p_2(\theta) = 5P_2(\cos \theta) \quad (\text{A2.5})$$

It is interesting to note that the limiting form of $p_1(\theta)$ is proportional to η , so that $p_1(\theta)$ vanishes in the limit of very high energy (or when the electric charge is made to vanish). This is because $p_1(\theta)$ arises from an interference between the 3P nuclear scattering and the Coulomb scattering in all the higher odd angular momentum states (the Pauli principle prevents interference effects between states of even and odd angular momentum). In the transition to neutron-proton scattering (electric charge to zero) such a term must vanish if it is assumed that higher odd angular momentum states do not contribute to the nuclear scattering. In consequence, the P-wave phase shift first appears quadratically in neutron-proton scattering, but appears linearly in proton-proton scattering if all δ 's above δ_2 vanish in both cases. On the other hand, the limiting form of $p_2(\theta)$ does not depend on the Coulomb scattering in the even angular momentum states, but involves only an interference effect between 1S and 1D nuclear scattering. Hence the D-wave phase shift appears linearly in both neutron-proton and proton-proton scattering.

The values of $p_1(E, \theta)$ and $p_2(E, \theta)$ which were computed using (A2.1), (A2.2), and (A2.3) are given in Tables (A2.1) and (A2.2) for energies from 2 to 10 Mev in the laboratory and angles from 16 to 90 degrees (the functions are symmetrical about $\theta = 90$ degrees). In Figures (A2.1) and (A2.2) the graphical representations of $p_1(E, \theta)$ and $p_2(E, \theta)$ are

Table A2.1: $p_1(\theta)$ Values of $p_1(\theta)$ in the Laboratory, Energy are in Mev

E	θ	16°	20°	24°	30°	40°	50°	60°	70°	80°	90°
2.0		137.0	-45.29	-17.31	-7.831	-3.196	-1.504	-.6958	-.2734	-.06381	0
2.5		-67.40	-21.22	-11.51	-6.057	-2.665	-1.290	-.6047	-.2392	-.05603	0
3.0		-31.52	-15.07	-9.140	-5.127	-2.356	-1.159	-.5473	-.2174	-.05101	0
3.5		-22.40	-12.31	-7.868	-4.572	-2.150	-1.068	-.5067	-.2017	-.04740	0
4.0		-18.24	-10.73	-7.062	-4.191	-2.000	-.999	-.4755	-.1896	-.04458	0
4.5		-15.88	-9.70	-6.50	-3.91	-1.883	-.944	-.450	-.180	-.0423	0
5.0		-14.32	-8.97	-6.08	-3.69	-1.787	-.898	-.429	-.171	-.0403	0
6.0		-12.41	-7.98	-5.53	-3.36	-1.64	-.825	-.394	-.158	-.0371	0
7.0		-11.26	-7.32	-5.13	-3.11	-1.52	-.767	-.367	-.147	-.0345	0
8.0		-10.47	-6.84	-4.82	-2.92	-1.43	-.719	-.344	-.137	-.0323	0
9.0		-9.89	-6.47	-4.56	-2.76	-1.35	-.679	-.324	-.130	-.0305	0
10.0		-9.44	-6.17	-4.35	-2.62	-1.28	-.644	-.308	-.123	-.0289	0

Values of the energy E are Mev in the laboratory. The values of the scattering angles θ are angles in the center of mass system.

Table A2.2: $p_2(\theta)$

E \ θ	16°	20°	24°	30°	40°	50°	60°	70°	80°	90°
2.0	41.77	-7.795	-4.221	1.580	1.577	.5726	-.6374	-1.711	-2.437	-2.693
2.5	-18.61	-2.767	+3.542	1.695	1.582	.5733	-.6389	-1.717	-2.447	-2.704
3.0	-7.984	-1.464	.6918	1.756	1.587	.5739	-.6398	-1.719	-2.451	-2.709
3.5	-5.252	-.8532	.8918	1.805	1.594	.5747	-.6402	-1.720	-2.452	-2.711
4.0	-3.974	-.4822	1.0339	1.848	1.601	.5754	-.6403	-1.720	-2.451	-2.709
4.5	-3.224	-.2215	1.1476	1.889	1.609	.5761	-.6400	-1.718	-2.448	-2.706
5.0	-2.71	-.0206	1.243	1.925	1.617	.577	-.640	-1.717	-2.45	-2.70
6.0	+2.03	+.284	1.38	1.99	1.63	.578	-.640	-1.71	-2.44	-2.69
7.0	-1.58	.519	1.51	2.06	1.65	.580	-.639	-1.71	-2.43	-2.68
8.0	-1.23	.712	1.62	2.11	1.66	.581	-.638	-1.70	-2.42	-2.67
9.0	-.954	.879	1.72	2.16	1.67	.582	-.638	-1.70	-2.41	-2.66
10.0	-.717	1.028	1.81	2.21	1.69	.583	-.637	-1.70	-2.41	-2.66

Values of the energy E are in Mev in the laboratory. Values of the scattering angle θ are angles in the center of mass system.

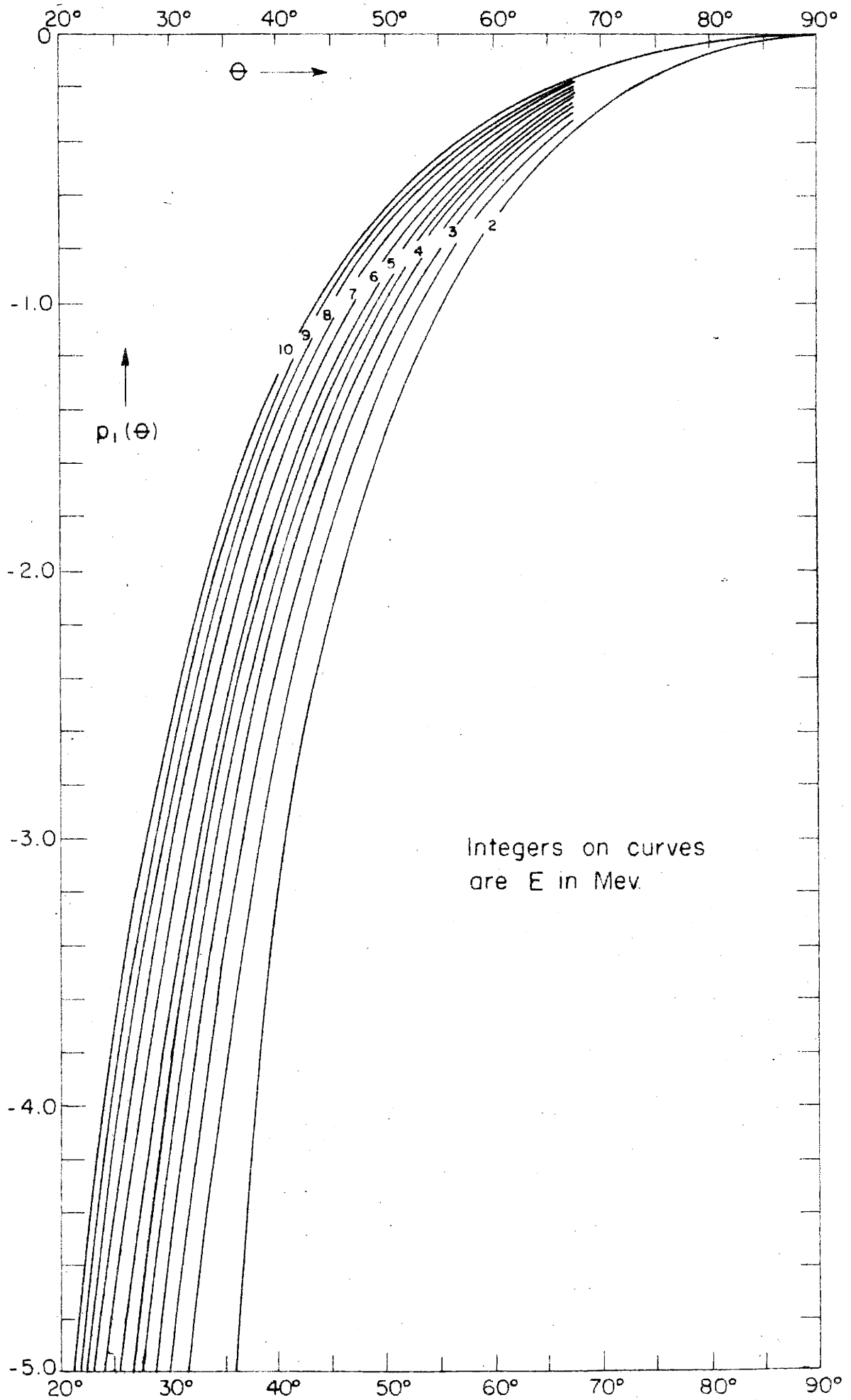


Figure A2.1: $p_1(\theta)$ as a function of scattering angle in the center of mass system for various values of the energy in the laboratory.

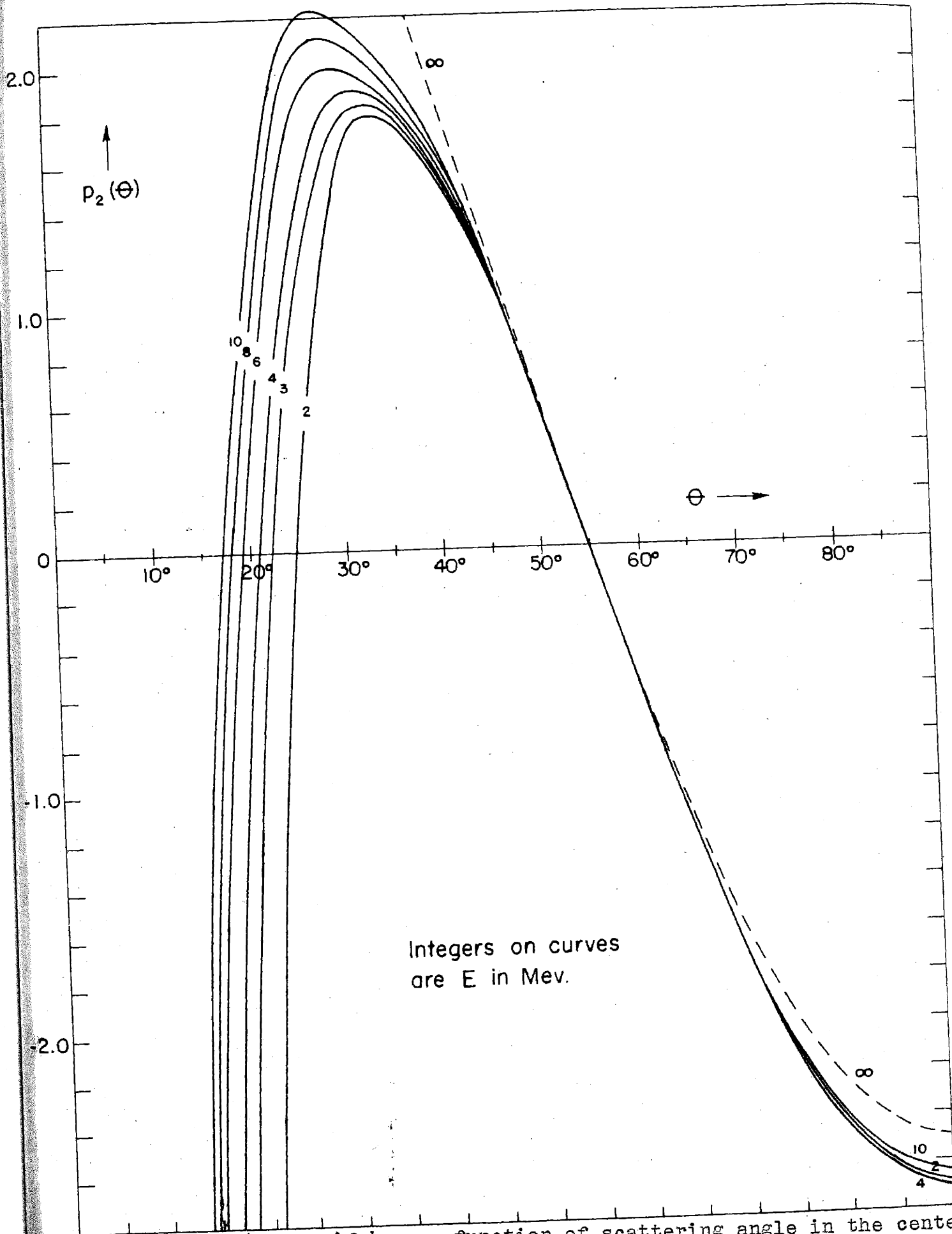


Figure A2.2: $p_2(\theta)$ as a function of scattering angle in the center of mass system for various values of the energy in the laboratory.

given as functions of θ for various energy values. The general behavior of $p_1(\theta)$ is seen to be similar to $\cot^2 \theta$, as predicted by (A2.4). But the behavior of $p_2(\theta)$ shown in Figure (A2.2) is more striking; for angles greater than 40 degrees (20 degrees in the laboratory) $p_2(\theta)$ is given very closely by the asymptotic form (A2.5), independent of energy. The curves all pass through zero in the neighborhood of 55 degrees because of the root of $P_2(\cos \theta)$ in (A2.3). The angular dependence of $p_1(\theta)$ and $p_2(\theta)$ at small angles is conditioned by the "Coulomb" factors in (A2.3), and deviates from the asymptotic forms (A2.4) and (A2.5).

Since the need for interpolation in energy occurs more often than the need for interpolation in angle, plots of $p_1(E, \theta)$ and $p_2(E, \theta)$ as functions of the energy E for various scattering angles θ are quite useful. Such plots are shown in Figures (A2.3) and (A2.4). It is seen from Figure (A2.4) that $p_2(E)$ is almost constant at any given value of θ over the whole energy range, for θ 's between 40 and 90 degrees, as was seen in Figure (A2.2). In this angular range, the asymptotic form (A2.5) yields very good values of p_2 independent of energy.

It should be pointed out that numerical interpolation in angle for $p_1(\theta)$ from Table (A2.1) can be made quite accurate if the asymptotic behavior (A2.4) is divided out before interpolation. That is, the interpolation should be carried out between values of $p_1(\theta) \tan^2 \theta$, rather than between

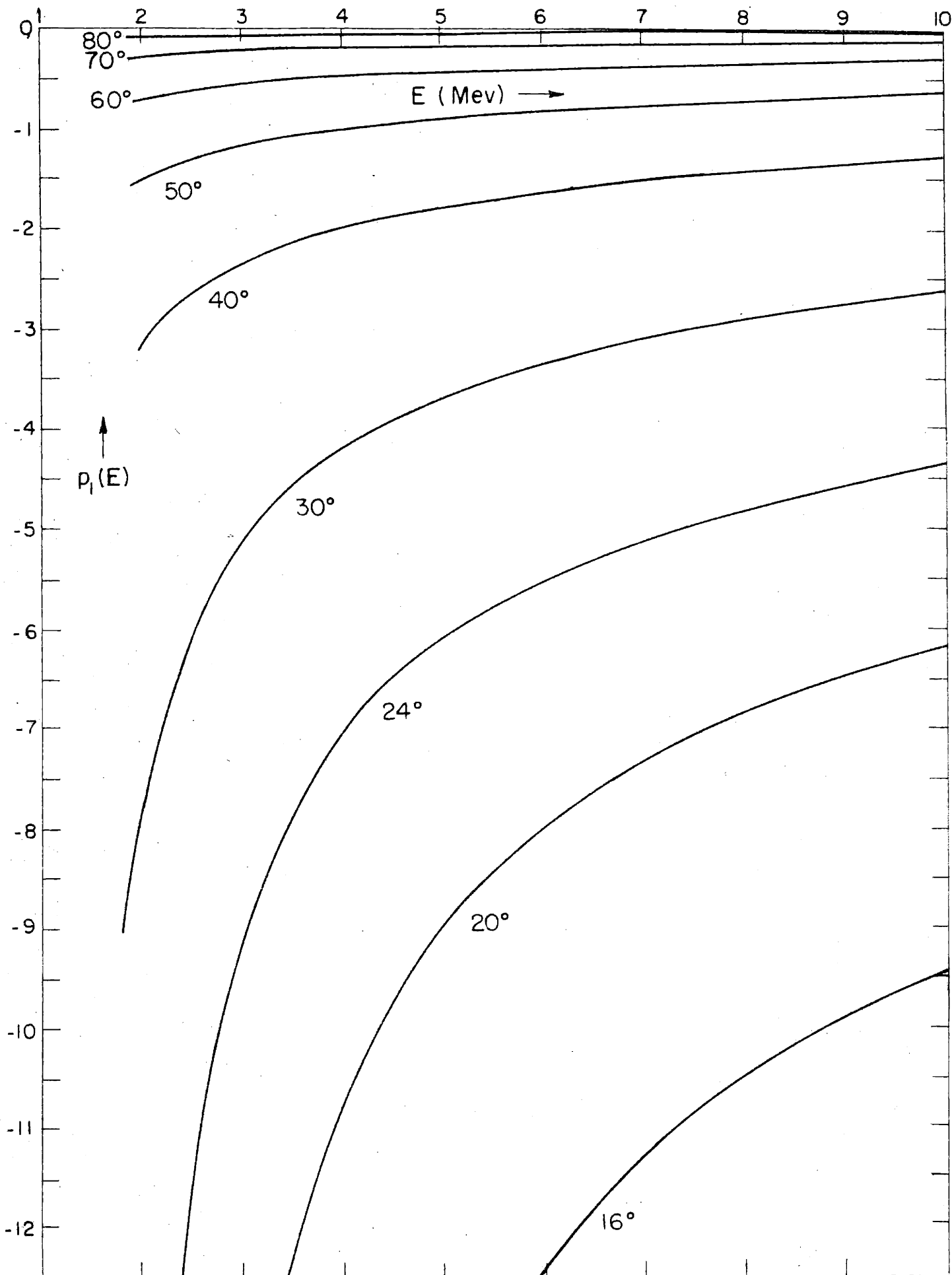


Figure A2.3: $p_1(E)$ as a function of energy in the laboratory for various scattering angles in the center of mass system.

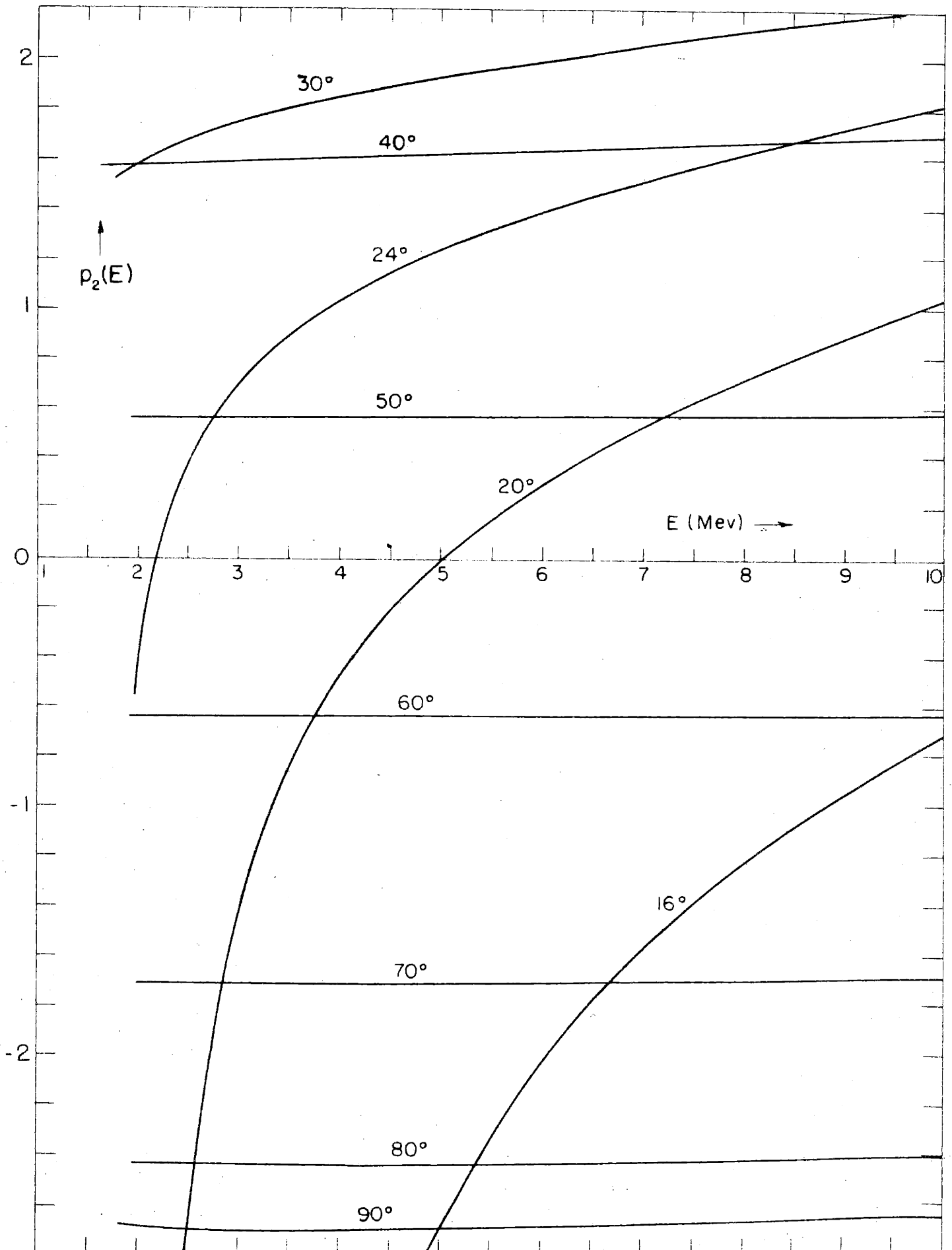


Figure A2.4: $p_2(E)$ as a function of energy in the laboratory for various scattering angles in the center of mass system.

values of $p_1(\theta)$, because $p_1(\theta) \tan^2 \theta$ is a much more slowly-varying function of angle than is $p_1(\theta)$ itself.

The values of δ_0 used to compute p_1 and p_2 were obtained by using the shape-independent approximation to the Schwinger function given by (1.3). The parameters a and r_0 were taken to be those yielding the best fit to the experimental data below 3.5 Mev (see Section 5). The values used were:

$$a = -7.66 \times 10^{-13} \text{ cm.}$$

$$r_0 = 2.62 \times 10^{-13} \text{ cm.}$$

Use of (1.2) and (1.3) with these parameters yields the following values of δ_0 as a function of energy:

E (MEV)	2	3	4	5	6	7	8	9	10
δ_0°	45.6	50.9	53.5	54.8	55.5	55.7	55.7	55.6	55.3

The values of δ_0 above 4 Mev should be considered as approximate since they are based on an extrapolation of the shape-independent fit of K to the low energy data. The values of $p_1(E, \theta)$ and $p_2(E, \theta)$ in Tables (A2.1) and (A2.2) for energies above 4 Mev are tabulated to fewer significant figures to indicate their approximate character as compared to the more reliable values from 2 to 4 Mev.

Appendix 3: Apparent S-wave phase shifts from experiment

The values of the apparent S-wave phase shifts for the experimental data cited in Section 4 are tabulated below. The manner in which the S-wave phase shift given in Table (4.1) was determined is also stated.

(1) Ragan, Kanne, Taschek⁽¹⁸⁾

The values quoted in Table (4.1) were computed from the experimental cross sections at $\theta = 90$ degrees (center of mass).

(2) Heydenburg, Hafstad, Tuve⁽¹⁹⁾

The numbers given in Table (4.1) were determined from the data by Creutz⁽²⁰⁾.

(3) Herb, Kerst, Parkinson, Plain⁽²¹⁾

This data was analyzed by Breit, Thaxton, and Eisenbud⁽¹⁾. The values of δ_a (shown in Figure (4.2) for $E = 2.39$ Mev) from $\theta = 40$ degrees to $\theta = 90$ degrees are given by them. The S-wave phase shifts in Table(4.1) are averages of the four values of δ_a from $\theta = 60$ degrees to $\theta = 90$ degrees in each case.

(4) Blair, Freier, Lampi, Sleator, Williams⁽²²⁾

Critchfield⁽¹⁴⁾ has published values of δ_a for $\theta = 50$ degrees to 90 degrees from these data. Values of δ_a have been computed for a wider range of scattering angles than given by Critchfield. These numbers are tabulated below. They have been corrected for the second-order geometry effect discussed by Critchfield.

θ (degrees)	E(MEV) 2.42	3.04	3.27	3.53
25		51.28	53.30	53.54
30	48.75	51.18	52.91	53.16
35	48.78	51.63	52.50	52.54
40	48.47	50.96	52.11	53.30
50	48.22	51.26	52.59	52.66
60	48.65	50.91	51.67	52.27
70	48.20	50.70	52.08	52.62
80	47.95	50.62	51.57	52.77
90	48.20	51.25	51.55	52.58

The apparent S-wave phase shifts for 3.53 Mev are plotted vs. $p_1(\theta)$ in Figure (4.3). The S-wave phase shifts given in Table (4.1) are averages over the five values of

δ_a from $\theta = 50$ degrees to $\theta = 90$ degrees.

(5) Ralph, Worthington, Herb (17)

The apparent S-wave phase shifts implied by these data have been computed, and are tabulated below.

θ (degrees)	E (MEV)			
	2.42	3.04	3.28	3.53
40	48.76	51.32	52.07	52.86
50	48.54	51.24	52.00	52.68
60	48.31	51.01	51.90	52.45
70	48.09	51.01	51.85	52.30
80	47.99	50.88	51.79	52.20
90	47.64	50.74	51.74	52.21

The values of the S-wave phase shift quoted in Table (4.1) were found by making a reasonable linear fit to the points on a δ_a vs. $p_1(\theta)$ diagram, and taking the intercept to be the S-wave phase shift. An example of this procedure for the 3.53 Mev data is shown in Figure (4.4).

(6) May, Powell⁽²³⁾

May and Powell determined the ratio of proton-proton scattering to Mott scattering at $\theta = 90$ degrees to be 94 ± 6 at $E = 4.2$ Mev by photographic plate techniques. This ratio leads to the value of S-wave phase shift given in Table (4.1). May and Powell incorrectly state $\delta_0 = 54.0 \pm 2.5^\circ$.

(7) Meagher⁽²⁵⁾

Meagher made measurements at an energy $E = 4.93 \pm .05$ Mev with the Illinois cyclotron, using photographic plate techniques. The apparent S-wave phase shifts from these

data are given below.

θ	25	30	40	50	60	70
δ_a	53.29	53.43	54.04	53.56	53.87	54.20

θ	75	80	81	90	100	110
δ_a	54.22	54.06	54.04	54.06	54.02	53.75

The value given in Table (4.1) is an average of the eight values of δ_a from 60 to 110 degrees. Figure (4.6) shows a plot of δ_a vs. $p_1(\theta)$ for these data.

(8) Dearnley, Oxley, Ferry ⁽²⁶⁾

The apparent S-wave phase shifts implied by these data are tabulated below. $E = 7.03 \pm .06$ Mev.

θ	21.02	25.18	30.12	39.90	49.98
δ_a	53.28	53.26	53.33	52.21	52.12

θ	60.00	69.66	79.74	89.24
δ_a	52.17	51.87	52.03	51.79

The S-wave phase shift given in Table (4.1) was determined by Oxley from a least squares fit to the cross section,

assuming S- and P-wave anomalies. Figure (4.7) (where δ_a is plotted vs. $p_1(\theta)$) shows that this is a reasonable value of the S-wave phase shift.

(9) Wilson, Creutz⁽²⁷⁾

These data, taken at $E = 8$ Mev, involved a series of comparative measurements at different angles based on the average of two absolute measurements at $\theta = 90$ degrees. The apparent S-wave phase shifts computed from these data are:

θ	30	40	50	60	70
δ_a	51.51	53.13	53.61	54.00	53.61

θ	80	90	96	100
δ_a	53.13	52.72	54.09	51.79

The S-wave phase shift in Table (4.1) is just the value of δ_a at $\theta = 90$ degrees (from the absolute measurement).

(10) Wilson⁽²⁸⁾

These data consist of relative measurements on angular distribution at $E = 10$ Mev. In order to examine the data for P-wave effects, and to determine the sensitivity of such effects, to changes in the absolute value of the cross section, three values of the differential cross section (center of mass system) at $\theta = 90$ degrees were assumed, and the apparent

S-wave phase shifts determined in each case. The three normalizing values of $\sigma(90^\circ)$ were (1) .0490 barns (2) .0515 barns (3) .0540 barns. These lead to reasonable values of the function K, namely (1) $K=8.87$ (2) $K=8.47$ (3) $K=8.08$ (see Figure (5.4)). The values of the apparent S-wave phase shifts for each case are:

θ°	$\sigma(90^\circ) = .0490$	$\sigma(90^\circ) = .0515$	$\sigma(90^\circ) = .0540$
24	54.74	56.48	58.27
28	54.63	56.28	57.93
32	54.23	55.85	57.46
36	54.06	55.69	57.34
38	53.37	54.94	56.59
40	53.40	55.04	56.63
44	53.69	55.34	57.01
50	53.41	55.07	56.82
52	53.58	55.32	57.01
56	52.59	54.26	55.94
90	52.83	54.58	56.35

The differences $\delta_a - \delta_a(90^\circ)$ are plotted vs. $p_1(\theta)$ in Figure (4.8), since the actual magnitude of δ_a is meaningless for these data. The errors in Figure (4.8) are statistical only, and are hence lower bounds to the actual uncer-

tainties.

(11) Wilson, Lofgren, Richardson, Wright, Shankland (31)

These data consist of absolute measurements taken at $E = 14.5 \text{ Mev} \pm$ "a few percent". The apparent S-wave phase shifts implied by these data are:

θ	20	24	28	36	90
δ_a	58.64	50.90	57.42	51.42	52.16

The uncertainties in these measurements are rather large. The value of the cross section at $\theta = 90$ degrees was determined with the greatest precision. Accordingly, the S-wave phase shift quoted in Table (4.1) is the value of δ_a for $\theta = 90$ degrees.

The probable errors for the phase shifts shown on the points in the various figures in Section 4 and given in Table (4.1) were determined from the experimental uncertainties in cross section and in energy as they were evaluated in the original experimental papers. In order to convert probable errors in cross section and energy into probable errors in apparent S-wave phase shifts, use was made of the quantities, $\sigma \left(\frac{\partial \delta_a}{\partial \sigma} \right)_E$ and $E \left(\frac{\partial \delta_a}{\partial E} \right)_\sigma$, that is, the variation in δ_a due to a change in cross section with energy kept constant, and the variation in δ_a due to a change in the energy keeping cross section fixed. These quantities

are, of course, dependent upon scattering angle and energy, and upon the actual value of the scattering cross section at that angle and energy. In order to tabulate these functions, one must assume, effectively, the functional dependence of δ_a on energy (as was done in Appendix 2 in order to tabulate $p_1(\theta)$ and $p_2(\theta)$), since that is the only unknown in the formula for the scattering cross section (2.18). Breit, Thaxton and Eisenbud⁽¹⁾ give tables (Tables VI and VIII in their paper) of these quantities for energies from .175 Mev to 2.4 Mev and angles from $\theta = 30$ to 90 degrees, under a reasonable assumption as to the dependence of δ_a on energy. These tables have been extended to smaller angles and energies up to 10 Mev, assuming the same energy dependence of δ_a as was used in Appendix 2. In the energy range up to 2.4 Mev, the values of δ_a used here agree closely with those employed by BTE. In Tables (A3.1) and (A3.2), the quantities $\sigma \left(\frac{\partial \delta_a}{\partial \sigma} \right)_E$ and $E \left(\frac{\partial \delta_a}{\partial E} \right)_\sigma$ in degrees are listed. Part of the tables are taken directly from BTE, and only quoted here for completeness. The rest of the tables are the extensions to smaller angles and higher energies made here.

It should be noted that $\sigma \left(\frac{\partial \delta_a}{\partial \sigma} \right)_E$ and $E \left(\frac{\partial \delta_a}{\partial E} \right)_\sigma$ are approximately equal for energies above 2 Mev, and are almost constant in angle at any one energy, except at small scattering angles. This corresponds to the fact that the scattering is predominantly nuclear except at small angles, and

is therefore almost isotropic in the center of mass system
(see Figure 3.2).

Table A3.1: $\sigma\left(\frac{\partial\delta_a}{\partial\sigma}\right)_E$ in degrees

E \ θ	16°	20°	30°	40°	50°	60°	70°	80°	90°
.175	-1954.	-819.	-230.	-97.	-51.	-28.	-16.	-10.	-8.2
.275	-682.	-382.	-140.	-71.	-40.	-23.	-12.	-6.1	-3.9
.375	-453.	-276.	-120.	-64.	-42.	-29.	-19.	-9.1	-1.3
.450	-382.	-240.	-110.	-67.	-55.	-85.	+34.	+4.9	+1.7
.550	-332.	-216.	-110.	-85.	-310.	+29.	8.8	4.7	3.9
.650	-307.	-207.	-120.	-220.	+50.	14.	8.3	6.8	6.4
.750	-296.	-206.	-150.	+310.	27.	12.	9.4	8.5	8.3
.850	-294.	-213.	-220.	85.	21.	12.	11.	10.2	10.1
1.21	-349.	-319.	+180.	30.	18.	16.	15.	15.	15.
1.60	-562.	-1650.	66.	25.	20.	19.	19.	19.	20.
2.0	-2186.	+453.	46.	25.	22.	22.	22.	23.	23.
3.0	+410.	128.	35.1	27.6		28.2		29.2	29.3
4.0	207.	84.2	33.5	30.0		31.7		32.8	32.9
5.0	148.	67.6	33.2	31.6		33.8		35.0	35.1
6.0	119.	55.8	33.2	32.7		35.1		36.3	36.4
7.0	103.	53.5	33.1	33.3		35.8		37.0	37.0
8.0	91.1	49.6	33.0	33.6		36.2		37.3	37.4
9.0	83.7	46.8	32.9	33.7		36.4		37.3	37.4
10.0	76.8	44.7	32.8	33.8		36.2		37.2	37.3

Values of the energy E are in Mev in the laboratory.

Values of the scattering angle θ are angles in the center of mass system.

Table A3.2: $E\left(\frac{\partial \delta_a}{\partial E}\right)_\theta$ in degrees

$E \backslash \theta$	16°	20°	30°	40°	50°	60°	70°	80°	90°
.175	-3930.	-1650.	-460.	-200.	-105.	-60.	-36.	-23.	-19.
.275	-1380.	-774.	-290.	-150.	-86.	-51.	-30.	-17.	-13.
.375	-917.	-563.	-240.	-140.	-91.	-65.	-46.	-26.	-10.
.450	-888.	-492.	-230.	-150.	-119.	-180.	+63.	+2.7	-4.5
.550	-676.	-445.	-230.	-180.	-65.	+51.	8.1	-0.4	-1.8
.650	-625.	-429.	-260.	-460.	+90.	17.	4.9	+1.8	+1.2
.750	-607.	-426.	-320.	+610.	41.	12.	5.5	3.8	3.4
.850	-607.	-441.	-470.	160.	27.	10.	6.7	5.6	5.5
1.21	-722.	-661.	+360.	43.	17.	12.	11.4	11.3	11.4
1.60	-1160.	-3370.	110.	29.	18.	16.	16.	16.	16.
2.0	-4480.	+911.	71.	26.	20.	19.	19.	20.	20.
3.0	+825.	242.	45.4	26.9		25.5		26.7	26.9
4.0	406.	151.	39.3	28.7		29.3		30.6	30.8
5.0	285.	115.	37.0	30.1		31.6		33.1	33.2
6.0	225.	90.0	35.6	31.0		33.1		34.5	34.6
7.0	190.	84.2	35.4	31.6		33.9		35.3	35.4
8.0	166.	75.6	34.1	31.9		34.4		35.8	35.8
9.0	150.	69.3	33.5	32.0		35.4		35.8	36.0
10.0	136.	64.7	33.1	32.0		34.6		35.8	35.9

Values of the energy E are in Mev in the laboratory.

Values of the scattering angle θ are angles in the center of mass system.

Appendix 4: S-state Coulomb wave functions

The wave equation for the partial wave of zero angular momentum in a repulsive Coulomb field is:

$$\left[-\frac{d^2}{dr^2} + \frac{1}{Rr} \right] \Phi(r) = k^2 \Phi(r) \quad (\text{A4.1})$$

where $R = \hbar^2/2me^2$, $k^2 = 2mE/\hbar^2$, m is the mass of the particle (the reduced mass), and E is the kinetic energy of relative motion. $\Phi(r)$ is r times the radial factor of the wave function.

This equation is a special case of the confluent hypergeometric equation⁽⁴⁶⁾, the solutions of which are well known. The regular solution (bounded at the origin) can be shown to be⁽⁴⁷⁾:

$$F(r) = C kr e^{ikr} F(1+i\eta; 2; -2ikr) \quad (\text{A4.2})$$

where $\eta = e^2/\hbar v = (2kR)^{-1}$, and

$$C^2 = e^{-\pi\eta} |\Gamma(1+i\eta)|^2 = \frac{2\pi\eta}{e^{2\pi\eta} - 1} \quad (\text{A4.3})$$

and

$$F(a; b; z) = 1 + \frac{a}{b-1} z + \frac{a(a+1)}{b(b+1) \cdot 1 \cdot 2} z^2 + \dots$$

$F(r)$ is normalized asymptotically ($k^2 Rr \gg 1$) to the form:

$$F(r) \sim \sin(kr - \eta \ln(2kr) + \sigma_0) \quad (A4.4)$$

where $\sigma_0 = \arg \Gamma(1 + i\eta)$. The irregular solutions are known⁽¹²⁾ to differ from $F(r)$ asymptotically only by the insertion of an arbitrary phase in the argument of the sine. The usual choice for the irregular solution $G(r)$ is that solution which asymptotically ($k^2 Rr \gg 1$) has the form:

$$G(r) \sim \cos(kr - \eta \ln(2kr) + \sigma_0) \quad (A4.5)$$

Sexl⁽⁴⁸⁾ has examined the behavior of the irregular solution near the origin. He found that $G(r)$ can be written as:

$$G(r) = \operatorname{Re} [y(r)] \quad (A4.6)$$

where

$$y(r) = \frac{1}{c} e^{-ikr} \left[1 + \sum_{m=1}^{\infty} (2ikr)^m c_m \{ \ln(2ikr) + d_m \} \right]$$

$$c_n = \frac{\Gamma(n-i\eta)}{\Gamma(n)\Gamma(n+1)\Gamma(-i\eta)}$$

$$d_n = \frac{1}{-i\eta} + \frac{1}{1-i\eta} + \dots + \frac{1}{n-1-i\eta} + \frac{\Gamma'(-i\eta)}{\Gamma(-i\eta)} + \frac{1}{n} - 2 \left(1 + \frac{1}{2} + \dots + \frac{1}{n} \right) + 2\gamma$$

$\gamma = 0.5772\dots$ is Euler's constant. The function $y(r) = -C y_k^{(2)}(kr)$ in Sexl's notation.

The behavior of $F(r)$ and $G(r)$ for $kr \ll 1$ and $r \ll R$ can be found by expanding (A4.2) and (A4.6). The results are:

$$F(r) = C kr \left[1 + \frac{r}{2R} + \dots \right] \quad (\text{A4.7})$$

$$G(r) = \frac{1}{C} \left[1 + \frac{r}{R} \left(\ln \frac{r}{R} + 2\gamma - 1 + h(\eta) \right) + \dots \right]$$

where

$$\begin{aligned} h(\eta) &= \text{Re} \frac{\Gamma'(-i\eta)}{\Gamma(-i\eta)} - \ln \eta \\ &= \eta^2 \sum_{\nu=1}^{\infty} \frac{1}{\nu(\nu^2 + \eta^2)} - \ln \eta - \gamma \end{aligned} \quad (\text{A4.8})$$

$h(\eta)$ was also defined in (5.1) and (5.2), with a graph of $h(\eta)$ given in Figure (5.1) and a graph of the summation,

$$\sum_{\nu=1}^{\infty} \frac{1}{\nu(\nu^2 + \eta^2)}, \quad \text{given in Figure (5.2).}$$

The expansions (A4.2) and (A4.6) are inconvenient since they involve real and imaginary quantities while the result is real. Yost, Wheeler, and Breit⁽³³⁾ have given power series expansions of $F(r)$ and $G(r)$ in terms of real quantities only. They also give an expansion for the regular solution $F(r)$ in powers of the energy, involving Bessel functions of argument $2(r/R)^{\frac{1}{2}}$. The expansion of $F(r)$ in powers of k^2 has been treated in more detail by Beckerley⁽³⁴⁾.

Several combinations of Bessel functions arise in the expansions of $F(r)$ and $G(r)$. To be consistent, the following convention will be adopted: all the auxiliary functions defined below approach unity at $r = 0$. Furthermore, in the limit $R \rightarrow \infty$ and $\eta \rightarrow 0$ (i.e. in the limit of vanishing Coulomb field), all these functions can be replaced by unity. Since the expansions for $F(r)$ and $G(r)$ go over in that limit to the well-known power series expansions for $\sin(kr)$ and $\cos(kr)$, this gives a simple method of checking these more complicated expansions. The following auxiliary functions are needed:

$$L_n(r) = n! \left(\frac{r}{R}\right)^{-\frac{1}{2}n} I_n \left(2\sqrt{\frac{r}{R}}\right) \quad (\text{A4.9})$$

$$H_n(r) = \frac{2}{(n-1)!} \left(\frac{r}{R}\right)^{\frac{1}{2}n} K_n \left(2\sqrt{\frac{r}{R}}\right) \quad (\text{A4.10})$$

where $I_n(z)$ and $K_n(z)$ are the modified Bessel functions defined in Watson(35). The expansions of $L_n(r)$ and $H_n(r)$ for the first few values of n are:

$$\begin{aligned} L_1(r) &= 1 + \frac{r}{2R} + \frac{r^2}{12R^2} + \frac{r^3}{144R^3} + \frac{r^4}{2880R^4} + \dots \\ L_2(r) &= 1 + \frac{r}{3R} + \frac{r^2}{24R^2} + \frac{r^3}{360R^3} + \dots \\ L_3(r) &= 1 + \frac{r}{4R} + \frac{r^2}{40R^2} + \frac{r^3}{720R^3} + \dots \end{aligned} \quad (\text{A4.11})$$

$$\begin{aligned}
 H_1(r) = & 1 + \frac{r}{R} \left(\ln \frac{r}{R} + 2\gamma - 1 \right) + \frac{r^2}{2R^2} \left(\ln \frac{r}{R} + 2\gamma - \frac{5}{2} \right) + \\
 & + \frac{r^3}{12R^3} \left(\ln \frac{r}{R} + 2\gamma - \frac{10}{3} \right) + \dots
 \end{aligned}
 \tag{A4.12}$$

$$\begin{aligned}
 H_2(r) = & 1 - \frac{r}{R} - \frac{r^2}{2R^2} \left(\ln \frac{r}{R} + 2\gamma - \frac{3}{2} \right) - \\
 & - \frac{r^3}{6R^3} \left(\ln \frac{r}{R} + 2\gamma - \frac{17}{6} \right) - \dots
 \end{aligned}$$

$$\begin{aligned}
 H_3(r) = & 1 - \frac{r}{2R} + \frac{r^2}{4R^2} + \frac{r^3}{12R^3} \left(\ln \frac{r}{R} + 2\gamma - \frac{11}{6} \right) + \\
 & + \frac{r^4}{48R^4} \left(\ln \frac{r}{R} + 2\gamma - \frac{37}{12} \right) + \dots
 \end{aligned}$$

In terms of the auxiliary functions (A4.9), Beckerley's (Yost, Wheeler, and Breit's) expansion for $F(r)$ can be written as:

$$\begin{aligned}
 F(r) = & C \, kr \left[L_1(r) - \frac{(kr)^2}{6} L_2(r) + \right. \\
 & \left. + \frac{(kr)^4}{108} \left(L_3(r) - \frac{1}{10} L_4(r) \right) - \dots \right]
 \end{aligned}
 \tag{A4.13}$$

In the limit of vanishing Coulomb field, (A4.13) obviously reduces to the expansion of $\sin(kr)$.

The expansion for the irregular function $G(r)$ (to be derived below) can be written as:

$$\begin{aligned}
 G(r) = & \frac{1}{c} \left[H_1(r) - \frac{(kr)^2}{2} M(r) + \frac{(kr)^4}{24} N(r) - \dots \right] + \\
 & + \frac{1}{c} h(\eta) \frac{r}{R} \left[L_1(r) - \frac{(kr)^2}{6} L_2(r) + \right. \\
 & \left. + \frac{(kr)^4}{108} \left(L_3(r) - \frac{1}{10} L_4(r) \right) - \dots \right] \quad (A4.14)
 \end{aligned}$$

where

$$M(r) = \frac{2}{3} \frac{R}{r} \left[L_1(r) - H_2(r) \right] \quad (A4.15)$$

From the expansions (A4.11) and (A4.12) it is readily seen that $M(r)$ has the expansion:

$$\begin{aligned}
 M(r) = & 1 - \frac{4r}{9R} - \frac{67 r^2}{216 R^2} - \frac{107 r^3}{2160 R^3} - \dots + \\
 & + \left(\ln \frac{r}{R} + 2 \gamma \right) \left(\frac{r}{3R} + \frac{r^2}{9R^2} + \frac{r^3}{72R^3} + \dots \right) \quad (A4.16)
 \end{aligned}$$

The function $N(r)$ is:

$$N(r) = \frac{4}{3} \frac{R}{r} \left[L_2(r) + \frac{2R}{r} H_3(r) + \right. \\ \left. + \frac{12}{5} \frac{R^2}{r^2} (H_4(r) - L_1(r)) \right] \quad (A4.17)$$

$N(r)$ can be expanded in a power series, similarly to $M(r)$
i.e.

$$N(r) = 1 + \frac{r}{5R} \left(\ln \frac{r}{R} + 2\gamma - \frac{23}{15} \right) + \dots \quad (A4.18)$$

The expansion (A4.14) for $G(r)$ reduces properly to the expansion of $\cos(kr)$ in the limit of vanishing Coulomb field; the first line becomes the expansion of $\cos(kr)$, while the coefficient $h(\eta)/R$ of the second line vanishes in that limit.

An alternative expansion for $G(r)$ has been stated recently by Breit and Bouricius⁽⁶⁾. Their result can be obtained from (A4.14) by the additional (more restrictive) assumption that $\eta \gg 1$. For $\eta \gg 1$, $h(\eta)$ (A4.8) can be approximated by:

$$h(\eta) \approx \frac{1}{3} k^2 R^2 + \frac{2}{15} k^4 R^4 + \dots \quad (A4.19)$$

With this substitution in (A4.14), the result is:

$$G(\kappa) = \frac{1}{c} \left[H_1(\kappa) + \frac{1}{3} k^2 R \kappa H_2(\kappa) + \right. \\ \left. + \frac{k^4 R^2 \kappa^2}{9} (H_3(\kappa) + \frac{6R}{5\kappa} H_4(\kappa)) + \dots \right] \quad (A4.20)$$

which is equivalent to equation (7.26) of Breit and Bouri-
cius⁽⁶⁾.

The expansion (A4.14) for $G(r)$ can be obtained in straightforward (although tedious) manner from the power series expansions given by Sexl⁽⁴⁸⁾ or Yost, Wheeler and Breit⁽³³⁾. Alternatively, it may be obtained by examining the representation of $G(r)$ as a contour integral.⁽⁴⁹⁾ The expansion (A4.13) for $F(r)$ can also be derived readily in this manner. Still another method, to be outlined here, is the use of Green's functions. The differential equation (A4.1) is decomposed into a set of differential equations by the substitution,

$$\begin{aligned} CG(r) = & \Psi_0(r) + k^2 \Psi_1(r) + k^4 \Psi_2(r) + \dots \\ & + \frac{1}{c} 2\eta h(\eta) F(r) \end{aligned} \quad (\text{A4.21})$$

where $F(r)$ is given by (A4.13). The form of (A4.21) can be justified when one looks at the expansions of Sexl and Yost, Wheeler and Breit in the limit of $k^2 = 0$. The function $G(r)$ is then given by:

$$CG(r) = H_1(\nu) + R(\nu) \frac{\nu}{R} L_1(\nu) + O(k^2) \quad (\text{A4.22})$$

The first term is the truly irregular part, while the second term is that amount of the regular solution necessary

to give the asymptotic form (A4.5).

The set of differential equations obtained by the substitution (A4.21) into (A4.1) is:

$$\left(-\frac{d^2}{d\kappa^2} + \frac{1}{R\kappa}\right)\Psi_n(\kappa) = \Psi_{n-1}(\kappa) \quad (\text{A4.23})$$

For $n=0$, the right hand side is zero (i.e. just equation (A4.1) with $k^2=0$); and the solutions are known to be $H_1(r)$ and $rL_1(r)$ ⁽⁵⁰⁾. The form of (A4.21) together with (A4.22) shows that:

$$\Psi_0(\kappa) = H_1(\kappa) \quad (\text{A4.24})$$

To obtain the next term $\Psi_1(r)$ in the expansion (A4.21), one writes (A4.23) for $n=1$:

$$\left(-\frac{d^2}{d\kappa^2} + \frac{1}{R\kappa}\right)\Psi_1(\kappa) = H_1(\kappa) \quad (\text{A4.25})$$

A Green's function $\xi(r,r')$ appropriate to the operator on the left side of (A4.25) is:

$$\xi(\kappa,\kappa') = \kappa_{<} L_1(\kappa_{<}) H_1(\kappa_{>}) \quad (\text{A4.26})$$

where $r_{<}$ means the smaller of r and r' , $r_{>}$ means the larger of r and r' . $\xi(r, r')$ satisfies the required Wronskian condition i.e. $(rL_1)'H_1 - (rL_1)H_1' = 1$. An arbitrary multiple of $rL_1(r)r'L_1(r')$ or of $H_1(r)H_1(r')$ could be added to $\xi(r, r')$ without destroying its properties as a Green's function. Indeed, to be consistent with the definition of the Green's function $K(r, r')$ (7.4), such an addition would be necessary since:

$$K(r, r') \approx r_{<} L_1(r_{<}) H_1(r_{>}) + \frac{k(\eta)}{R} r r' L_1(r) L_1(r') + O(k^2)$$

However, the form (A4.26) for $\xi(r, r')$ will be retained. The solution for (A4.25) can be written as:

$$\psi_1(r) = A H_1(r) + B r L_1(r) + \int_0^{\infty} \xi(r, r') H_1(r') dr' \quad (\text{A4.27})$$

The constants A and B can be determined from the fact that in the limit of $\eta \rightarrow 0$, $R \rightarrow \infty$, $\psi_1 \rightarrow -r^2/2$, since $G(r) \rightarrow \cos(kr)$. The Green's function integral involves well-known integrals over Bessel functions⁽³⁵⁾. The result is:

$$\begin{aligned}
 \int_0^{\infty} \xi(r, r') H_1(r') dr' &= -\frac{1}{3} r R \left[L_1(r) - H_2(r) \right] + \\
 &\quad + r L_1(r) \int_0^{\infty} H_1^2(r') dr' \quad (A4.28) \\
 &= -\frac{r^2}{2} M(r) + r L_1(r) \int_0^{\infty} H_1^2(r') dr'
 \end{aligned}$$

where $M(r)$ was defined in (A4.15). In the limit of $R \rightarrow \infty$, $\eta \rightarrow 0$, (A4.27) reduces to:

$$\Psi_1(r) \rightarrow A + B r - \frac{r^2}{2} + r \int_0^{\infty} H_1^2(r') dr'$$

Therefore $A = 0$, $B = -\int_0^{\infty} H_1^2(r') dr'$.

Thus the solution for $\Psi_1(r)$ is:

$$\Psi_1(r) = -\frac{r^2}{2} M(r) \quad (A4.29)$$

In a completely equivalent manner $\Psi_2(r)$ can be determined by writing (A4.23) for $n=2$ with $\Psi_1(r)$ given by (A4.29). The Green's function $\xi(r, r')$ is employed to write a form equivalent to (A4.27). The integrations involved are simple, but tedious. The final result for $\Psi_2(r)$ is:

$$\Psi_2(r) = -\frac{r^4}{24} N(r) \quad (A4.30)$$

where $N(r)$ is defined by (A4.17). Thus

$$\begin{aligned}
 c G(r) = & H_1(\kappa) - \frac{(k\kappa)^2}{2} M(\kappa) + \frac{(k\kappa)^4}{24} N(\kappa) - \dots \\
 & + \frac{1}{c} 2\pi h(\pi) F(\kappa)
 \end{aligned}
 \tag{A4.31}$$

which to terms in k^4 inclusive is equal to the expansion (A4.14). If terms higher than k^4 are desired, it is only necessary to repeat the procedure used to obtain $\Psi_1(r)$ and $\Psi_2(r)$ until the required number of terms is obtained.

REFERENCES

- (1) Breit, Condon, Present, *Phy. Rev.*, 50, 825 (1936)
Breit, Thaxton, Eisenbud, *Phy. Rev.*, 55, 1018 (1939)
- (2) Blatt, Jackson, *Phy. Rev.*, 75, 341A (1949); also
June 15, 1949 issue of *Phy. Rev.*
- (3) Fermi, Marshall, *Phy. Rev.*, 71, 66 (1947)
- (4) Schwinger, *Phy. Rev.*, 72, 742A (1947); also
hetrographed notes on nuclear physics, Harvard, 1947
- (5) Landau, Smorodinsky, *Journal Physics USSR*, 8, 154 (1944)
- (6) Breit, Bouricius, *Phy. Rev.*, 75, 1029 (1949)
- (7) Bethe, June 15, 1949 issue of *Phy. Rev.*
- (8) Chew, Goldberger, *Phy. Rev.*, 75, 1466A (1949); also
forthcoming paper in *Phy. Rev.*
- (9) Jackson, Blatt, *Phy. Rev.*, 75, 1296A (1949)
- (10) Mott, Massey, "Theory of Atomic Collisions", Oxford (1933)
- (11) Reference (10), p. 22
- (12) Gordon, *Zeit. f. Phy.*, 48, 180 (1928)
- (13) Mott, *Proc. Roy. Soc.*, A126, 259 (1930)
- (14) Critchfield, *Phy. Rev.*, 75, 419 (1949)
- (15) cf. Hadley et al., *Phy. Rev.*, 75, 351 (1949)
- (16) Breit, Kittel, Thaxton, *Phy. Rev.*, 57, 255 (1940)
- (17) Ralph, Worthington, Herb, private communication.
- (18) Ragan, Kanne, Taschek, *Phy. Rev.*, 60, 628 (1941)
- (19) Heydenburg, Hafstad, Tuve, *Phy. Rev.*, 56, 1078 (1939)

- (20) Creutz, *Phy. Rev.*, 56, 893 (1939)
- (21) Herb, Kerst, Parkinson, Plain, *Phy. Rev.*, 55, 247 (1939)
- (22) Blair, Freier, Lampi, Sleator, Williams, *Phy. Rev.*,
74, 553 (1948)
- (23) May, Powell, *Proc. Roy. Soc.*, A190, 170 (1947)
- (24) Lubanski, deJager, *Physica*, 14, 8 (1948)
- (25) Meagher, Ph.D. thesis, Dept. of Physics, U. of Illinois,
1948
- (26) Dearnley, Oxley, Perry, *Phy. Rev.*, 73, 1290 (1948)
- (27) Wilson, Creutz, *Phy. Rev.*, 71, 339 (1947)
- (28) Wilson, *Phy. Rev.*, 71, 384 (1947); see also
Reference (31)
- (29) Peierls, Preston, *Phy. Rev.*, 72, 250 (1947)
- (30) Foldy, *Phy. Rev.*, 72, 125, 731, (1947)
- (31) Wilson, Lofgren, Richardson, Wright, Shankland,
Phy. Rev., 72, 1131 (1947)
- (32) Breit, Broyles, Hull, *Phy. Rev.*, 73, 869 (1948)
- (33) Yost, Wheeler, Breit, *Phy. Rev.*, 49, 174 (1936)
- (34) Beckerley, *Phy. Rev.*, 67, 11 (1945)
- (35) Watson, "Theory of Bessel Functions", Cambridge (1941)
- (36) Wheeler, *Phy. Rev.*, 50, 643 (1936)
- (37) Hatcher, Arfken, Breit, *Phy. Rev.*, 75, 1389 (1949)
- (38) Hoisington, Share, Breit, *Phy. Rev.*, 56, 884 (1939)
- (39) Rarita, Present, *Phy. Rev.*, 51, 793 (1937)
- (40) Melkonian, Rainwater, Havens, *Phy. Rev.*, 75, 1295A (1949)

- (41) Sutton et al., Phy. Rev., 72, 1147 (1947)
Shull et al., Phy. Rev., 73, 842 (1948)
- (42) Breit, Hoisington, Share, Thaxton, Phy. Rev., 55,
1103 (1939)
- (43) Simon, Phy. Rev., 55, 792 (1939)
- (44) Reference (10), p. 28, 90.
- (45) Thaxton, Hoisington, Phy. Rev., 56, 1194 (1939)
- (46) Whittaker, Watson, "Modern Analysis", Cambridge
(1945), Chap. 16
- (47) Reference (10), p. 39
- (48) Sexl, Zeit. f. Phy., 56, 72 (1929)
- (49) Reference (10), p. 38
- (50) Jahnke, Emde, "Tables of Functions", Dover (1945), p. 147

BIOGRAPHY

John David Jackson was born on January 19, 1925 in London, Ontario, Canada. He received his primary and secondary education in that city, and entered the University of Western Ontario in 1942. He graduated with the degree B.Sc. in Honour Physics and Mathematics in 1946. He entered the Graduate School at the Massachusetts Institute of Technology in June, 1946 as a Research Assistant in Physics assigned to the Research Laboratory of Electronics. During the following year, he had the pleasure to work under Dr. L. J. Chu on electromagnetic problems associated with the theory of traveling wave tubes. In the fall of 1947, he transferred to the theoretical group in the Laboratory of Nuclear Science and Engineering under Professor V. F. Weisskopf.